UNIVERSITY OF SOUTHAMPTON

School of Physics and Astronomy

Polarisation Properties of Exciton-Polaritons in Semiconductor Microcavities

by

Dean Read

A thesis submitted for the degree of

Doctor of Philosophy

July 2010

UNIVERSITY OF SOUTHAMPTON

ABSTRACT

FACULTY OF ENGINEERING, SCIENCE & MATHEMATICS

SCHOOL OF PHYSICS & ASTRONOMY

Doctor of Philosophy

Polarisation Properties of Exciton-Polaritons in Semiconductor Microcavities

Dean Read

Interactions of exciton-polaritons in semiconductor microcavities and the resulting polarisation dynamics are investigated theoretically. Within the coboson framework of polariton-polariton scattering, it is shown that the matrix element of direct Coulomb scattering is proportional to the transferred momentum, q, cubed in the limit of small q. In the same limit, the magnitude of superexchange/exchange interactions can be considered constant. These results are applied to the elastic circle geometry, where a system of equations describing the steady-state pseudospin components is derived. It is shown, that for this geometry, polariton-polariton scattering can account for the generation of circularly/linearly polarised final states from linearly/circularly polarised initial states, depolarisation and the generation of spin currents. In the low density regime polaritons are good bosons and the dynamics of polariton Bose-Einstein condensation (BEC) are investigated. A stochastic model is derived, resulting in a Langevin type equation describing the time dynamics of the condensate spinor order parameter. The build up in condensate polarisation degree is shown to evidence macroscopic ground state population, while the stochastic choice of polarisation vector evidences the symmetry breaking nature of the phase transition. The decrease of polarisation degree above threshold is demonstrated to be a consequence of polariton-polariton interactions, a result which is complemented by recent experimental work. The stochastic model is extended to include Josephson coupling of spatially separate condensates. The coupling results in polarisation and phase correlations between the condensates, explaining the polarisation locking and spatial coherence seen experimentally. Finally, the effect of polarisation pinning by local effective fields is examined.

Contents

Aknowledgements

I would first like to thank the people who have made the undertaking of my PhD seem like fun rather than work. I have been privelaged to share an office with Tim Liew, Tomas Ostatnicky, Fabrice Laussy, Elena del Valle and Tom Tayler. All of whom have helped me in one way or another. From the other end of the building; Dave English, Alastair Grundy and Maria Maragkou are responsible for many spirited conversations during breaks and good memories from conferences.

For giving me the opportunity to do something I've very much enjoyed, I thank my supervisor, Alexey Kavokin. I am also grateful for the interesing research problems he has provided and the time/support he has given me to solve them, especially when things weren't going so well. My research would have been much less productive without the collaborations he organised and so I would particularly like to thank Henni Ouerdane and Jacques Levrat. I specially thank Yura Rubo, whose intuition and patience has on numerous occasions put my research back on track.

Finally, I thank Charlotte Dee, for putting up with the lifestyle of a PhD student and providing somewhere physics free when I needed it.

Chapter 1

Introduction

The prevailing direction of current solid state physics research is to reduce dimensionality and observe previously exotic quantum effects under increasingly less exotic conditions. This trend is nowhere more visible than in the evolution of semiconductor structures. The process of decreasing the number of degrees of translational freedom began with the production of the first quantum well (QW) [1] and continued with quantum wires (QWR) [2] and quantum dots (QD) [3]. The emission spectra produced by these structures is a direct look at the discretisation of energy levels due to confinement of the electron/hole states. These forays into the quantum scale developed in tandem with the realisation of collective phenomena in semiconductor devices, the most notable and widely distributed of which being the light emitting diode (LED) [4]. The synergy of collective effects and confinement was first demonstrated in the quantum well diode laser [5] which benefited from increased efficiency due to the modified density of states and the ability to tune the wavelength by changing the thickness of the QW, rather than modifying the band structure through composition alterations, as was previously necessary. The QW laser and its derivatives are edge emitting devices, i.e.,

the light emission is perpendicular to the current flow through the device. There are a number of benefits to producing a structure with emission parallel to the flow of current, i.e., surface emitting, not least of which being the ability to produce numerous devices on a single semiconductor wafer. This practical desire led to the creation of the vertical cavity surface emitting laser (VCSEL) [6]. Although itself interesting, this thesis will discuss the implications of the VCSEL design taken into the strong coupling regime; the exciton-polariton[1] and the interesting effects associated with it.

A semiconductor is a material with electrical conductance between that of a metal and an insulator. This rather simple definition encapsulates a sizable amount of physics which underlies these fundamental materials. The properties of solids are determined by their lattice structure and the energy bands formed because of it. The defining characteristic of a semiconductor is that the band gap (difference between the top of the valence band and bottom of the conduction band) is non-zero at 0K but allows for thermal excitation at some point below the melting point of the material. The origin of this band gap can be explained intuitively through the nearly free electron model. Here we imagine a crystal as a set of fixed ion cores producing a potential weakly perturbing the free electron wave function, given by

$$\psi_k = \exp(i\mathbf{k} \cdot \mathbf{r}), \tag{1.1}$$

where $\mathbf{k}$ is the electron wave vector and $\mathbf{r}$ is the spatial coordinate. Assuming a simple 1D periodic lattice the Bragg condition determining the allowed reflections of electron from ion is $k = \pm G/2 = \pm n\pi/a$ where a is the lattice spacing and therefore G is a reciprocal lattice vector. The first reflections occur at $k = \pm\pi/a$ and at these points a wave traveling to the right is reflected to the left and vice versa resulting in a wave function with equal parts traveling to the right and left. This represents a time-independent wave

[1] In the remainder of the text they will be referred to only as polaritons as this variant is the only form which will be discussed.

function as the wave is stationary. Symmetric and anti-symmetric waves can be formed from the two traveling waves,

$$\begin{aligned}\psi(+) &= \exp(i\pi x/a) + \exp(-i\pi x/a) = 2\cos(\pi x/a)\\ \psi(-) &= \exp(i\pi x/a) - \exp(-i\pi x/a) = 2i\sin(\pi x/a).\end{aligned} \tag{1.2}$$

The probability density of a particle is $\psi^*\psi = |\psi|^2$. For the standing waves in Eq. 1.2 these are

$$|\psi(+)|^2 \propto \cos^2(\pi x/a) \tag{1.3a}$$

$$|\psi(-)|^2 \propto \sin^2(\pi x/a) \tag{1.3b}$$

By examination we see that the symmetric wave function concentrates electrons at the positively charged lattice points whereas the antisymmetric wave function concentrates electrons at the points between the positive ions. These distributions are shown in Fig. 1.1 along with the constant electron distribution associated with a free electron wave and the attractive potential seen by the electrons due to the ion cores. From inspection it can be seen that the

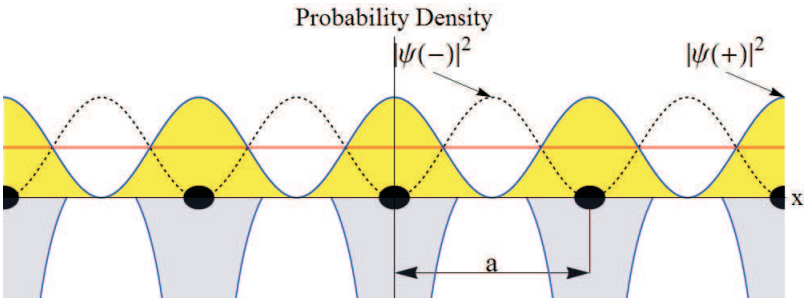

Figure 1.1: Probability density for symmetric and antisymmetric standing waves in the lattice. Also shown is the charge distribution for the free electron (red line) and the potential energy variation (filled blue) of a conduction band electron in the field of the positively charged ion cores (black dots) comprising the 1D lattice

expectation value of the potential energy for $\psi(+)$ and $\psi(-)$ is greater than and lower than that of the stationary wave respectively. It is the difference between these two expectations which produces the energy gap. In this sim-

plified case it is therefore possible to define the first order energy difference between the two standing waves as

$$E_g = \int U(x)[|\psi(+)|^2 - |\psi(-)|^2]dx \tag{1.4}$$

Where $U(x)$ is the potential energy of an electron in the crystal at a point x. This idealised model, although highly simplified, presents a solid conceptual introduction to the idea of energy bands in crystalline solids which are the first steps in polariton physics.

In semiconductors the bands either side of the Fermi level are the valence and conduction bands, which at 0 K are full and empty respectively. As the temperature is increased an electron from the valence band can be excited to the conduction band leaving a localised hole of opposite charge in the valence band. Due to the opposing charges the two bind to form excitons, the semiconductor equivalent of a hydrogen atom. This bound electron-hole pair can be thought of as the fundamental excitation of a semiconductor and as such can be created through a range of mechanisms, the most notable of which for polariton physics being optical excitation. As we are interested in the efficient creation of excitons, direct band gap semiconductors are considered i.e., the top of the valence and bottom of the conduction bands occur at the same value of k and a transition can occur with purely photonic excitation, Fig. 1.2(a). In the case of indirect band gap semiconductors the transition requires a photon and phonon to provide both energy and momentum to the electron, Fig. 1.2(b). The process of exciton creation in an indirect semiconductor is significantly less probable than in the direct case and therefore only direct band gap semiconductors are discussed from this point as the efficient optical excitation of excitons is essential to polaritonic systems.

Excitons are classified within two different theoretical frameworks named for their progenitors: Frenkel [7] and Wannier-Mott [8, 9]. Frenkel excitons

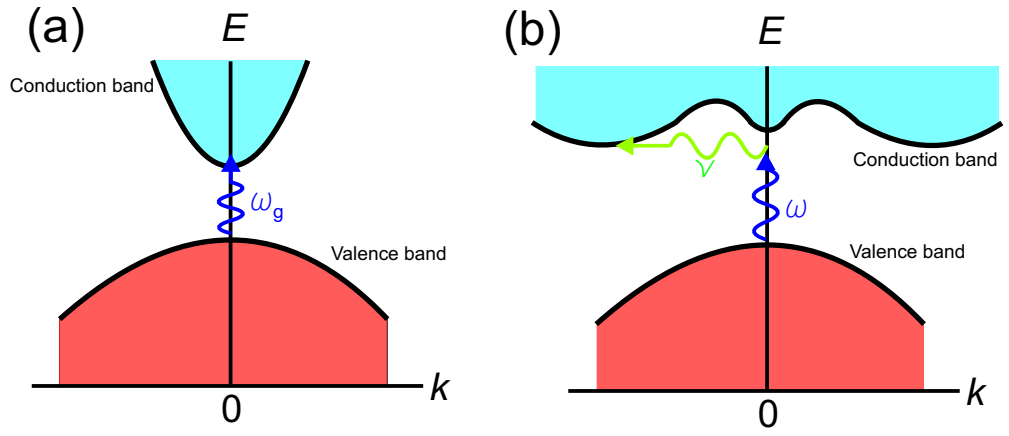

Figure 1.2: (a) shows a direct band gap semiconductor where the electron is excited by a photon with frequency ω_g, where $E_g = \hbar\omega_g$, whereas an electron in the indirect semiconductor shown in (b) requires a photon to traverse the energy gap and a phonon of frequency ν to conserve momentum.

prevail in materials with a small dielectric constant and as a consequence large binding energies of the order 100-300 meV. They can be considered as essentially an excited state of an individual atom in the lattice, however this excitation can hop to its neighbours due to the coupling afforded by the crystalline structure. This transmission of excitation between neighbouring atoms results in wave-like eigenstates of the system. Frenkel excitons are widely studied in organic materials where they are the dominant factor in optical spectra.

Wanner-Mott excitons present the opposite case, where the dielectric constant is large and consequently the Coulomb interaction is strongly screened, resulting in Bohr radii on the order of tens of lattice constants and binding energies of a few meV. The delocalised nature of Wannier-Mott excitons allows for the approximation of the periodic potential of the crystal by a change in the effective mass of the excitons constituent particles (electrons and holes). This approximation can be validated by looking at the effect of an electric field on a semiconductor electron with dispersion $E(k)$. The work done by an electric field χ in time δt is $\delta E = -e\chi v_g \delta t$, where $v_g = \hbar^{-1} dE/dk$

is the group velocity. A small change in energy is equivalent to

$$\delta E = \frac{dE}{dk}\delta k = \hbar v_g \delta k \tag{1.5}$$

using the definition of group velocity. From Eq. 1.5 we can write $\delta k = -(e\chi/\hbar)\delta t$ which when combined with $\hbar dk/dt = -e\chi$ (the same as for free electrons) produces a fundamental relation for crystals

$$\hbar\frac{d\mathbf{k}}{dt} = \mathbf{F} \tag{1.6}$$

where $\mathbf{F}$ is the external force on the electron. To determine the effective mass of electrons in semiconductors we recast the relation into a structure which coincides with the Newtonian form $\mathbf{F} = m\mathbf{a}$. The acceleration is the time differential of the group velocity

$$\frac{dv_g}{dt} = \hbar^{-1}\frac{d^2E}{dkdt} = \hbar^{-1}\left(\frac{d^2E}{dk^2}\frac{dk}{dt}\right), \tag{1.7}$$

using Eq. 1.6 and rearranging we obtain the result:

$$F = \frac{\hbar^2}{d^2E/dk^2}\frac{dv_g}{dt}. \tag{1.8}$$

This leads naturally to a definition of the effective mass, m^* as

$$\frac{1}{m^*} = \frac{1}{\hbar^2}\frac{d^2E(k)}{dk^2}, \tag{1.9}$$

demonstrating the direct link between the electron dispersion (a similar derivation can be carried out for the holes), determined by the crystal potential and the electron effective mass. Within the Wannier-Mott framework electrons and holes are considered as free particles characterised by this effective mass. For the remainder of this thesis discussion of excitons will always relate to the Wannier-Mott type as their delocalised nature provides greater opportunity for observation of interesting collective effects.

The model of an exciton as a bound pair of free particles invites direct comparison to the Hydrogen atom and as such the wave function of relative electron-hole motion f_{EX} is calculable from the Schrödinger equation

$$-\frac{\hbar^2}{2\mu}\nabla^2 f_{EX} - \frac{e^2}{4\pi\epsilon\epsilon_0 r} f_{EX} = E f_{EX}. \tag{1.10}$$

Where $\mu = m_e m_h/(m_e + m_h)$ is the reduced mass and $r = \sqrt{x^2 + y^2 + z^2}$ is the absolute distance between the electron and hole. Eq. (1.10) is a direct analogue of the Schrödinger equation describing a Hydrogen atom electron state. The solutions are well known;

$$f_{EX}^{1s} = \frac{1}{\sqrt{\pi a_B^3}} e^{-r/a_B} \tag{1.11}$$

where

$$a_B = \frac{4\pi\hbar^2\epsilon\epsilon_0}{\mu e^2} \tag{1.12}$$

is the Bohr radius. The results are identical to the Hydrogen case but with the renormalisations $m_0 \rightarrow \mu$ and $e^2 \rightarrow e^2/\epsilon$. The ground state binding energy is defined in a similar fashion

$$E_B = \frac{\hbar^2}{2\mu a_B^2}. \tag{1.13}$$

For a wide range of applications the interaction of excitons with light (light-matter coupling) is an important area of interest. The possibility to create new quasiparticles based on this interaction, so called exciton-polaritons, was postulated in the 1950s by Hopfield [10] (although not yet named polaritons).A fundamental difference between Hopfield's theory and previous theories of light absorption by excitonic states can be understood qualitatively. Previous to Hopfield it was believed that light propagating through a semiconductor crystal directly created excitons with the energy flux of the incident beam reduced by the amount of energy given to the exci-

ton. The viewpoint espoused in [10] views light as mixing with the excitonic mode in the crystal, producing a propagating mode of mixed exciton and photon - an exciton polariton. In this case absorption only occurs when other crystal states are excited by the exciton part of the propagating mode and not in the exciton modes to which the light is directly coupled. Excitons created in bulk inorganic semiconductors have a weak light-matter interaction and therefore the effects can be treated as a perturbation to the lone exciton. The requirement to study polaritons is to restrict the dimensionality of the exciton and increase the interaction strength. The experimental ability to do this was not available for many years after the postulation of the new quasiparticles. After an evolution of semiconductor structures as discussed earlier, researchers were ultimately able to fabricate a device which incorporated a semiconductor QW within a Fabry-Perot cavity. A schematic of this device is shown in Fig. 1.3 and known as a microcavity. The structure consists of

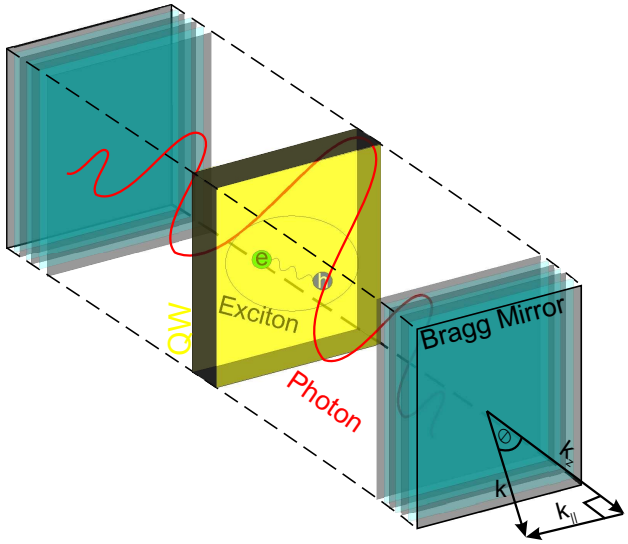

Figure 1.3: Schematic diagram of a typical semiconductor microcavity. The red line shows the cavity electric field profile, which decays inside the Bragg reflectors.

a pair of Bragg mirrors sandwiching a semiconductor QW, itself created by sandwiching a semiconductor material with a small band gap in between two with large band gaps. A Bragg reflector is a stack of alternating high and

low refractive index materials satisfying the condition that the optical path length in each layer is $\lambda_c/4$ where λ_c is the desired wavelength of light the cavity is intended to trap. When this condition is satisfied an incoming light wave is partially reflected at each layer boundary and due to constructive interference a very high reflectivity is achieved. This reflectivity reaches values of $\approx 99\%$ as standard, meaning the photon makes nearly 100 round trips of the cavity before escaping through the mirror. The reflection spectrum of a Bragg mirror shows a high degree of reflectivity around the chosen wavelength, a feature known as the stop band. Fabrication of microcavities is a precise process usually carried out through molecular beam epitaxy which allows the build up of single crystal layers on a substrate. Due to the high requirements placed on the light-matter coupling strength in a microcavity the location and thickness of all the component parts must be exact. The QW is generally placed at the anti-node of the light field within the cavity, maximising coupling strength, while it is also critical that the frequency of the light at the centre of the stop band matches the resonant excitation frequency of the exciton and the frequency of the Fabry-Perot mode. Clearly this is a non-trivial procedure and explains the long gap between theory and experiment.

Obtaining a clear mental picture of the true quantum processes occurring inside a microcavity is a difficult hurdle to overcome, however a conceptual shortcut can be used to get an intuitive feel for the system. We can imagine a new photon in the cavity from an external laser source, this photon will be absorbed by the semiconductor QW and an exciton produced. After a short period of time the electron and hole constituents will recombine[2] emitting a photon with the same wave vector and energy as the original exciting photon. The new photon, identical to the original, will reflect from a Bragg mirror and again be absorbed by the QW, restarting the process. Due to the high reflectivity of the Bragg mirrors this process will occur many times before the

[2]Unlike their atomic analogue (Hydrogen) excitons have a finite lifetime.

photon leaves the cavity, providing us with a strong light-matter interaction between the photon and exciton. In physical systems the strong coupling regime is defined as a correlation between two objects strong enough for the interaction not to be dealt with perturbatively (e.g., the strong force in particle physics). The picture of polaritons as coupled oscillators periodically exchanging energy provides a basis for understanding the criteria for strong coupling in microcavities

$$V > \left| \frac{\gamma_x - \gamma_c}{2} \right| \tag{1.14}$$

Where γ_x is the exciton broadening caused by their interactions (non radiative decay processes), γ_c is the photon broadening due to the finite reflectivity of the mirrors and V is the photon-exciton interaction strength. A longer cavity photon lifetime[3] $\propto \gamma_c^{-1}$ and shorter exciton lifetime $\propto \gamma_x^{-1}$ will both lead to a greater amount of energy exchange between the two oscillators. Strong coupling manifests itself in a significant change to the dispersion, with a distinct upper and lower branch, split in energy at $k = 0$ by $2V$ known as the vacuum field Rabi splitting[4], Fig. 1.4. The detuning is defined as the energy mismatch between the cavity and exciton modes $\Delta(k) = E_C(k) - E_X(k)$ and samples are engineered so that a range of detunings are available by scanning in real space[5].

Experimental observation of strong coupling did not occur until 1992 [14] where the characteristic anti-crossing of the exciton and photon modes as a function of detuning was observed. This experiment evidenced a benefit of studying polariton physics, the ability to directly access polariton dynamics by measuring the cavity emission. As the excitons and photons are strongly coupled they cannot be considered as separate entities, as such when a photon escapes the cavity (due to the finite reflectivity of the mirrors) its

[3]This relation appears due to the Heisenberg uncertainty principle

[4]A term adopted from atomic physics [11].

[5]In practice the cavity spacer is grown inhomogeneously allowing for different cavity lengths and therefore modes at different points on the sample.

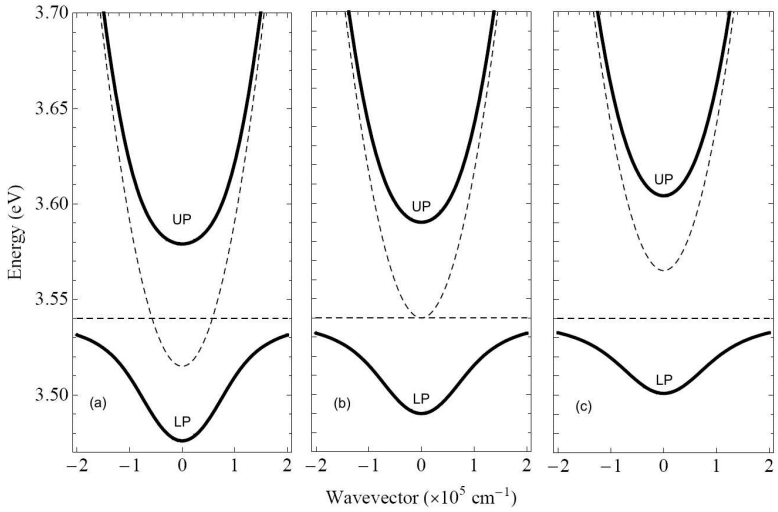

Figure 1.4: Dispersion of polaritons for (a) negative, (b) zero and (c) positive detuning between the bare photon and exciton modes. The upper polariton (UP) and lower polariton (LP) branches are labeled. Results are based on a GaN microcavity with typical parameters from [12, 13].

measurement provides the properties of what is occurring inside the cavity. As alluded to in Fig. 1.3 it is possible to couple a laser or detector to any polariton wave vector by altering the angle of incidence θ, allowing for excitation/measurement of chosen regions of the dispersion. This ability was taken advantage of to prove the bosonic nature of polaritons in the low density limit (where the density is low enough that the exciton wave function overlap integrals are negligible). Until the work of Savvidis [15] the statistics obeyed by polaritons was still a debated question. Although the polariton constituents were both bosons it was unclear whether the electron and hole interactions would supersede the bosonic nature. Numerous theoretical and experimental work had addressed this issue previously [16, 17, 18, 19, 20, 21, 22] without a definitive answer[6]. The experimental setup of Savvidis exploited the effect of bosonic stimulation[7] to show significant gain in a parametric scat-

[6]The experimental work was carried out at high powers producing many excited states in the QW. Such high powers lead to polariton bleaching, where the electrons and holes in the semiconductor begin to act as plasmas rather than bound pairs, destroying polaritonic effects

[7]Bosonic stimulation is the increased probability of scattering to an occupied final

tering process. This involves pumping the sample at the so called 'magic angle'(equivalent to the correct point on the dispersion) where a polariton-polariton scattering event will scatter one polariton to a point with high k near the bare exciton energy and the other to $k = 0$, conserving energy and momentum Fig. 1.5[8]. The bosonic nature of polaritons was established through the use of a probe pulse at $k = 0$. For the case of no pumping at the magic angle the spectra from $k = 0$ showed the standard normal mode splitting. The effect of exciting polaritons at the magic angle is a gain of 2 orders of magnitude in the emission from the lower polariton $k = 0$ state, demonstrating stimulated scattering. If the cavity was not in the strong coupling regime and excitons were the interaction participants this scattering process is forbidden by energy and momentum conservation. Conclusive proof was finally obtained that within certain limits polaritons act as good bosons, beginning the push to observe more exotic collective effects within an already interesting confined system.

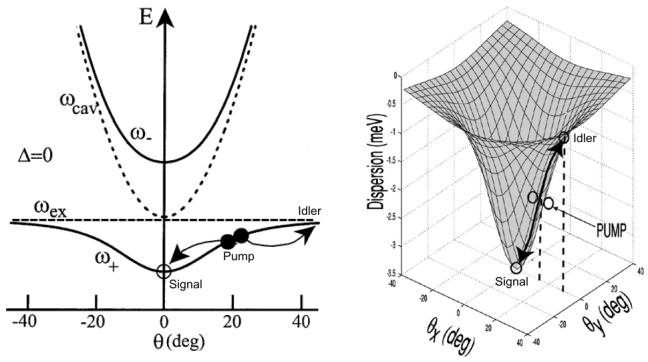

Figure 1.5: Parametric oscillator dispersions from [15] and [23], showing the scattering of pumped states to signal and idler.

The field of polariton physics is now an established and continually expanding area of study with numerous theoretical [24, 25, 26, 27, 28, 29, 30]

state proportional to its current occupancy: $\frac{dN_{final}}{dt} \propto (1 + N_{final})N_{pump}$. This is in stark contrast to fermions where indistinguishable particles may not occupy the same state.

[8]In microcavity physics the angle of incidence θ is equivalent to the wave vector and therefore it is common for dispersions to be presented with this replacement

and experimental groups [31, 32, 33, 34, 35, 36]. These quasiparticles garner such international interest due to the rich physics of their dual nature [37]. By diagonalisation of the QW polariton Hamiltonian the superposition of exciton and photon can be shown explicitly. The exciton and photon fractions are given by the Hopfield coefficients X and C respectively, which themselves depend on the coupling strength and polariton dispersion.

$$|X|^2 = \frac{1}{2}\left(1 + \frac{\Delta(k)}{\sqrt{\Delta(k)^2 + 4V^2}}\right) \tag{1.15a}$$

$$|C|^2 = \frac{1}{2}\left(1 - \frac{\Delta(k)}{\sqrt{\Delta(k)^2 + 4V^2}}\right). \tag{1.15b}$$

A photon confined within a microcavity is known to acquire a finite effective mass, $m_{ph} \approx \hbar\bar{n}_c/c\bar{L}_c$, where $\bar{n}_c$ is the effective refractive index of the cavity[9] and $\bar{L}_c$ is the effective cavity length which accounts for the penetration of the mode into the mirrors[10]. The polariton effective mass is the weighted harmonic mean of the mass of its exciton and photon components

$$\frac{1}{m_{LP}} = \frac{|X|^2}{m_{EX}} + \frac{|C|^2}{m_c}, \tag{1.16}$$

$$\frac{1}{m_{UP}} = \frac{|C|^2}{m_{EX}} + \frac{|X|^2}{m_c}. \tag{1.17}$$

Because $m_c \ll m_{EX}$ the lower polariton effective mass at $k = 0$ is very small,

$$m_{LP}(k \sim 0) \simeq m_c/|C|^2 \sim 10^{-4} m_{EX}. \tag{1.18}$$

Such a low mass is an attractive feature of polaritons, making possible the very high critical temperatures of phase transitions in the system. This is exemplified by Bose-Einstein condensation (BEC) where the critical temper-

[9] The effective refractive index of the cavity is a weighted average of the different cavity media's refractive index with the cavity field mode.

[10] $\bar{L}_c = L_c + L_{DBR}$ where L_{DBR} is the mode penetration approximated by $L_{DBR} \approx \frac{\lambda_c}{2\bar{n}_c}\frac{n_1 n_2}{|n_1 - n_2|}$, here n_1 and n_2 are the refractive indices of the two Bragg reflector materials.

ature, T_c, has the following dependence [38]

$$k_B T_c = \frac{2\pi\hbar^2}{m}\left(\frac{n}{2.612}\right)^{2/3}, \tag{1.19}$$

where n is the particle density. Eq. 1.19, while not directly applicable to polaritons still shows the inverse relationship between critical temperature and mass. The inapplicability is founded on the quasiparticles 2D nature. In systems with dimension less than 3 a true BEC cannot be created, instead cavity polaritons can undergo a Berezinski-Kosterlitz-Thouless phase transition [39]. This is a form of local condensation to a superfluid state in terms of topological order that can occur in two-dimensional systems in which no long range order of the conventional type can exist[11]. Although such a phase transition is forbidden for ideal bosons it can take place in systems of weakly interacting bosons such as low density polaritons [40]. This being the case, most literature in the field refers to the macroscopic occupation of the polariton ground state as BEC, because for all practical reasons the definition is apt and this will be adopted for further discussion of polariton BEC. For phase transitions it is the low photon effective mass which discriminates polaritons from other solid state bosonic systems, but the excitonic component means that polariton-polariton interactions are a significant factor in the dynamics of the system, vastly increasing the complexity and richness of polariton physics, demonstrated by further experimental work on parametric scattering [41, 42, 43, 44, 45, 46].

The combination of strong non-linear scattering effects and low effective mass has allowed polaritonic systems to push ahead of atomic and excitonic systems in the field of high temperature BEC. The first experimental consideration of BEC occurred in 1938 with the superfluid transition of helium-4 [47, 48] at $T < 2.17$K, where it was realised that the effect was due to

[11]BEC occurs in the thermodynamic limit where the volume of the system tends to infinity.

partial condensation. The first pure condensate was created in 1995 by cooling dilute Rubidium-87 atoms to temperatures below 170nK [49] followed shortly after by sodium atoms at $T \sim 2\mu K$ [50]. Experimental procedures to produce such low temperatures are a significant barrier to the realisation of BEC, leading to the exploration of BEC in particles with lower mass and therefore higher T_C. Excitons were a suitable candidate for BEC at high temperatures as they have an effective mass much lower than atoms, giving them a critical temperature $\sim$ 1K. Condensation in this medium was initially also difficult due to the finite lifetime of excitons. Photo-excited excitons have a significantly higher temperature than the lattice and therefore thermalisation processes must take place on a timescale shorter than the exciton lifetime for BEC to occur [51]. The solution of the exciton lifetime issue was to use the longer lifetime of indirect excitons, the meaning of which is slightly modified in the 2D case to mean electrons and holes in different coupled QWs. The increased separation results in a decrease of the overlap integrals and therefore lower probability of recombination. Exciton condensation under these new conditions was experimentally achieved [52, 53] and further work has been carried out in this field [54, 55, 56, 57].

Following the relatively high temperature breakthrough of exciton BEC the natural progression to polaritons was envisioned [58, 59, 60, 61]. With an effective mass roughly four orders of magnitude smaller it was expected that BEC could occur at much higher temperatures, even breaching room temperature in some materials. Despite initial realisations only occurring recently [62, 63, 64] the production of polariton condensates is now a widely accepted scientific fact and occurs frequently [36, 65, 66, 26, 67, 68, 69, 70]. Experimental and theoretical investigations are focused on extending the range of observed phenomena, from superfluidity [71, 72, 73, 74, 75, 76, 77, 78, 79] to quantized vortices/half-vortices [80, 32, 81, 82, 83] to superconductivity [84]. For the discussion of this text the seminal work is the experimental demonstration of polariton room temperature condensation in a GaN based

microcavity [85, 86], which fulfilled the potential of the low effective mass polariton. The characteristic macroscopic occupation of the ground state was demonstrated in concert with a build-up in the polarisation degree, Fig. 1.6. The importance of polariton condensation at room temperature lies in its

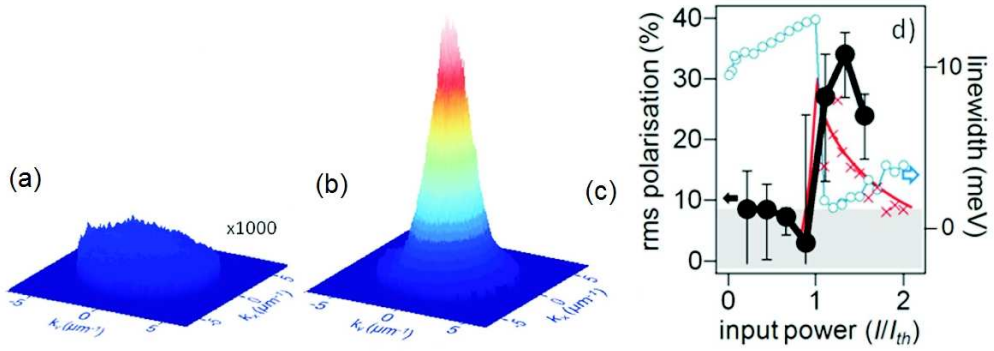

Figure 1.6: Reciprocal space polariton distribution just below (a) and just above threshold (b). (c) shows the jump in polarisation degree at threshold followed by the decrease due to polariton-polariton interactions [86].

practical application as the condensate emits coherent light producing a polariton laser [85, 87, 88, 89]. Such a device is expected to have a much lower threshold as population inversion is not required for optical amplification. The polarisation of emitted light from the condensate provides direct access to its order parameter i.e., the wave function representing the collective state assumed by all particles in the condensate. The behavior of the order parameter and by extension the polarisation is critical to understanding the condensation process in microcavities. As BEC is a symmetry breaking phase transition a comprehensive model of the system must include the stochastic nature of individual condensate realisations. This has been attempted with a stochastic extension of Langevin fluctuations to the Boltzmann equations for the system [89, 90] and through a truncated Wigner approach [91]. These models can determine the first and second order coherence values for the condensates, however experimental measurement is of these values is difficult. In Chapter 3 we discuss a stochastic model which fully takes into account the polarisation of microcavity emission and shows the direct link between polar-

isation degree and macroscopic occupation of the ground state. The model is derived from the master equation and naturally includes the characteristic decrease of polarisation degree above threshold (Fig. 1.6, [36]). Our model has been successfully applied to describe the experimental data on power dependence of polarisation of emission of a GaN-based polariton laser [36]. The richest features of polariton physics come from their strong interactions and unsurprisingly these are the key to condensate dynamics. An understanding of polariton-polariton interactions is necessarily important and Chapter 2 discusses an approach to their calculation and some of the interesting results which can be obtained from studying polariton-polariton scattering.

In one of the original experimental realisations of polariton BEC [62] a fragmented group of condensates was observed within the exciting spot. Despite spatial separation the condensates emitted light of the same polarisation. Chapter 4 extends the stochastic model developed in Chapter 3 to the case of two Josephson coupled [92] condensates. Polarisation and phase locking of the condensates is innate to the model which demonstrates that the build up of a common vector polarisation can be considered as a criterion for a macroscopically coherent state in a system of localised polariton condensates. Similar work in this area [57, 93] has ignored the fundamentally stochastic nature of BEC.

Chapter 2

Polariton-Polariton Interactions

The rich and interesting physics of polaritons is founded upon their strong interactions. Because of their composite nature, the excitonic part of a polariton plays a significant role in the interaction dynamics. It is therefore important to understand how these interactions are modified due to the 2 component form of the excitons themselves i.e., what is the effect of the fermionic nature of the bound electron hole pair which constitutes the exciton. This question gains greater depth from the spin structure of the underlying particles. In the following section we provide an introduction to the spin structure of polaritons, as the effects related to it are critical to the remainder of this text.

When undertaking calculations involving polariton-polariton interactions it is necessary to separate the dynamics into two components; polaritons of the same spin and polaritons of opposite spin, the strength of which is given by the constants α_1 and α_2 respectively. It is standard to approximate these constants in a phenomenological way with $\alpha_1 \approx 6E_B a_B/S$ and $\alpha_2 \approx$

$0.1\alpha_1$ where S is the excitation spot area [94, 24]. It is self-evident that this approximation must simplify significantly the processes occurring when polaritons interact. Most notably any dependence on polariton wave vector is ignored. As such, it is necessary to approach the calculation of these interaction 'constants' from a fundamental basis accounting for the possibility of additional effects from the fermionic nature of the underlying constituents. This is motivated by the fact that some of the greatest breakthroughs in polariton physics are dependent on wave vector specific scattering events (for example the OPO [15] which demonstrated bosonic stimulation) and a more physically sound approach to their modeling and the prediction of further interesting results is a necessity. As such we present calculations of the wave vector dependence of scattering and discuss the results when calculated on the elastic circle.

2.1 Polariton Spin

Strong coupling of excitons with photons ensures the equivalence of the polariton pseudospin and the polarisation of light emitted from the cavity. Experimentally it is possible to measure the polariton pseudospin dynamics through this emitted polarisation and gain significant insight into the physical effects accessed through the spin degree of freedom. An exciton is defined as a Coulomb bound electron and hole, two fermions with total angular momenta projections on the structure-growth axis equal to $J_z^e = \pm 1/2$ for a conduction band electron with S-symmetry and $J_z^h = \pm 1/2, \pm 3/2$ for a valence band hole with P-symmetry[1]. Hole states with $J_z^h = \pm 1/2$ are light holes and form if the hole spin projection is anti-parallel to the projection of its orbital angular momentum. Conversely, parallel spin projection and orbital angular momentum leads to heavy holes with $J_z^h = \pm 3/2$. In the bulk

[1]Here we are only discussing excitons in zinc-blend semiconductors such as GaAs.

semiconductor materials generally used for polariton physics, at $k = 0$ the light and heavy holes are degenerate, however in QW's the confinement lifts this degeneracy and heavy hole energy levels are closer to the band edge than those of light holes. This results in the ground-state exciton being formed by an electron and heavy hole.

The exciton spin is the sum of the contributions from the electron and hole. There are four possible total angular momentum projections on the structure growth axis, $J_z = \pm 1, \pm 2$. States with $J_z = \pm 1$ are split in energy due to the electron-hole exchange interaction [95] and are of most relevance for polariton physics. Due to conservation rules, $J_z = \pm 2$ states cannot be optically excited, so are not directly coupled to the photonic cavity mode (although scattering via these states as intermediaries is a possibility [96]), leading to the label dark states. The obvious extension of this nomenclature is that excitons with $J_z = \pm 1$ are called bright states. The inextricable link between photonic polarisation and polariton spin, combined with conservation of spin in photoabsorbtion means it is possible to spin-orient excitons through the polarisation of the exciting light. Light with $\sigma = +1$ (right circularly polarised) or $\sigma = -1$ (left circularly polarised) excites $J = +1$ and $J = -1$ excitons respectively. As linearly polarised light is a combination of the two circularly polarised modes the same relationship holds in excitons.

For the electrons and holes composing the exciton there are three main spin relaxation mechanisms: Elliott-Yaffet [97], D'yakanov-Perel [98] and Bir-Aronov-Pikus (BAP) [12]. The first involves mixing of different spin wave functions due to the $\mathbf{k} \cdot \mathbf{p}$ interaction with other bands, while the second is caused by spin-orbit interaction induced spin splitting of the conduction band with some asymmetry (either inversion asymmetry [99] or the Rashba term from QW asymmetry). It has been shown that in 2D excitons the BAP mechanism is sufficiently strong for the other two to be neglected [100]. The BAP mechanism involves the spin-flip exchange interaction of electrons and

holes. This mechanism is especially potent in excitons rather than free carriers due to their bound nature. In the general case there are two components to this mechanism the long and short range. The short range couples light and heavy holes whereas the long range causes transitions between $J_z = +1$ and $J_z = -1$. As we are discussing confined excitons the usual degeneracy between light and heavy holes is lifted and therefore the strength of the short range BAP mechanism is reduced and the dark exciton states can generally be neglected in microcavities. This has a very important consequence for the description of exciton-polaritons in microcavities as the exciton can now be considered as a two level system and the pseudospin formalism used. Formally, an exciton is described by a 2×2 spin density matrix:

$$\rho_{\mathbf{k}} = N_{\mathbf{k}} \left[\frac{\mathbf{I}}{2} + \mathbf{s}_{\mathbf{k}} \cdot \boldsymbol{\sigma}_{\boldsymbol{k}} \right]. \tag{2.1}$$

Where $\mathbf{I}$ is the identity matrix, $N_{\mathbf{k}}$ is the number of polaritons, $\mathbf{s}_{\mathbf{k}}$ is the polariton pseudospin and $\boldsymbol{\sigma}_{\boldsymbol{k}}$ is the vector of Pauli matrices.

The pseudospin components of the spin density matrix correspond directly to the Stokes parameters of light emitted from the microcavity in the strong coupling regime [101, 102]. It is generally the convention that states with $s_z = \pm 1/2$ are associated with right or left circular polarisations, the states $s_x = \pm 1/2$ with X and Y linear polarisations and $s_y = \pm 1/2$ with linear diagonal polarisation, with other states corresponding to elliptical polarisation. This equivalence with the polarisation of light allows for the pseudospin to be represented on the Poincaré sphere as shown in Fig. 2.1. This introduction to polariton polarisation and especially the pseudospin vector are relevant to this and following chapters.

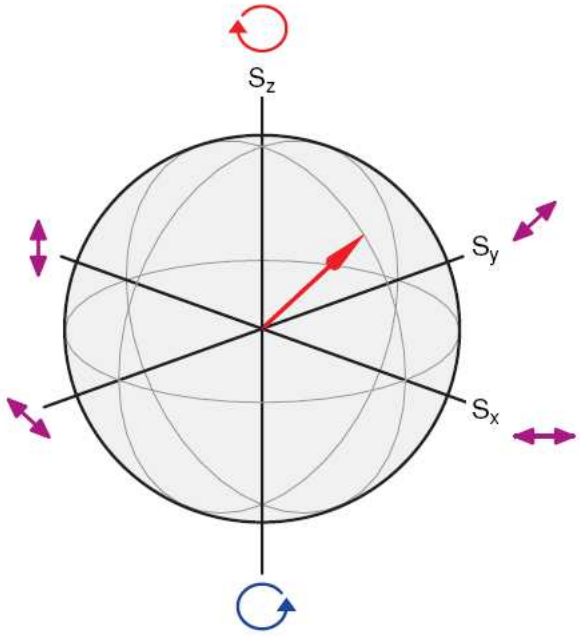

Figure 2.1: The direction of the pseudospin vector represents the polarisation of the polariton state [24].

2.2 Composite Bosons

Throughout most of this text and the majority of work in this field excitons and therefore polaritons are considered as good bosons, however recent work has claimed that in the high density limit this assumption may not be valid [103, 104, 105]. In this case the composite nature of excitons must be accounted for when describing their interactions. The term coined for such a compound particle is a composite boson or coboson in its abbreviated form. Taking into account the composite nature of excitons poses a problem. Although electron-electron and hole-hole Coulomb interactions can be defined unambiguously the same is not true for the electron-hole interaction. Due to the indistinguishable nature of electrons and holes (i.e. an electron/hole in one exciton is indistinguishable from an electron/hole in another exciton) an interaction, $V_{eh'}$, between them is invalid if one of the excitons is composed

of (e, h') rather than (e, h). This problem has led to the introduction of so called "Pauli scatterings" for carrier exchange in the absence of Coulomb interactions. Although this process results in a dimensionless addition to the Hamiltonian, such Paul scatterings are usually linked with a photonic interaction also to obtain an energy-like quantity.

When taking into account the fermionic constituents of the exciton, there are four possible leading order scattering processes, as seen in Fig 2.2. By expressing the exciton creation operator in terms of its fermionic components (as is clearly necessary in the coboson approach), $B_i^\dagger = \sum_{k_e,k_h} \langle k_e, k_h | i \rangle \, e_{k_e}^\dagger h_{k_h}^\dagger$ where $e_{k_e}^\dagger$ and $h_{k_h}^\dagger$ are the free electron and hole creation operators with wave vector k, it is possible to derive the matrix elements for the processes shown in Fig 2.2. The derivations are lengthy and will not be repeated here as they do not add to the discussion, but an interested reader is directed to the appendix of [104]. Considering first the direct term (Fig. 2.2(b)) it is clear that this should be the most analytically tractable scattering to determine. As such we include in Appendix A a derivation which provides the result

$$\xi_{ij,mn}^{\mathrm{dir}} = f(\mathbf{q}, w) V_{2D}(\mathbf{q}) \left(\tilde{\psi}(\gamma_e \mathbf{q}) - \tilde{\psi}(\gamma_h \mathbf{q}) \right)^2, \tag{2.2}$$

for the direct scattering matrix element from $i \to m$ and $j \to n$, where $\mathbf{q} = \mathbf{k}_m - \mathbf{k}_i = \mathbf{k}_j - \mathbf{k}_n$, the transferred exciton center of mass momentum. $f(\mathbf{q}, w)$ is the form factor determined by the electron and hole envelope functions which in the case of an infinitely deep quantum well is

$$f(\mathbf{q}, w) = \frac{2}{w} \left[\frac{1}{q} + \frac{1}{2} \frac{q w^2}{q^2 w^2 + 4\pi^2} + (e^{-qw} - 1) \frac{1}{w} \left(\frac{1}{q} - \frac{q w^2}{q^2 w^2 + 4\pi^2} \right)^2 \right], \tag{2.3}$$

where w is the well width. $V_{2D}(\mathbf{q})$ is the Fourier transform of the ideal Coulomb potential, $V_{2D}(\mathbf{q}) \propto 1/q$ and $\tilde{\psi}(\mathbf{q})$ is the Fourier transform of the

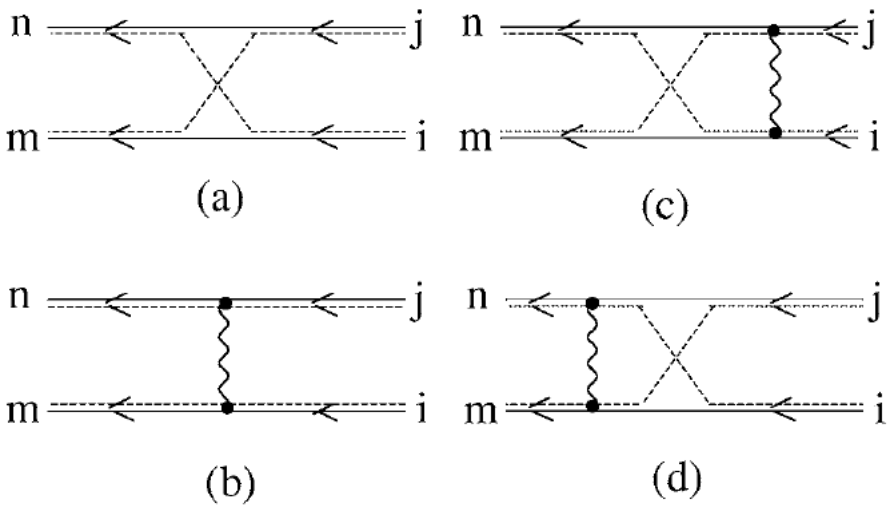

Figure 2.2: (a) Exchange interaction between two in excitons (i, j) to form two out excitons (m, n) where either a hole or electron is swapped. (b) Direct Coulomb scattering. (c) Coulomb exchange scattering where the Coulomb process takes place between the in excitons. (d) Coulomb exchange scattering where the Coulomb process takes place between the out excitons. In all four diagrams the solid line represents the electrons, the dashed line the holes and the wavy line represents the Coulomb interaction. Figure from [104].

relative motion part of the 2D excitonic wave function

$$\tilde{\psi}(\gamma_{\mathbf{h}}\mathbf{q}) = \left(1 + \frac{16(\gamma_h \mathbf{q})^2 a_B^2}{16}\right)^{-3/2}. \tag{2.4}$$

The prefactors $\gamma_{e,h}$ are the ratio of constituent mass to total mass, $\gamma_{e,h} = m_{e,h}/(m_e + m_h)$. Because of the indistinguishability of the exciton constituents the other channel must also be considered, $i \to n$ and $j \to m$ and the result is similar,

$$\xi^{\mathrm{dir}'}_{ij,nm} = f(\mathbf{q}', w) V_{2D}(\mathbf{q}') \left(\tilde{\psi}(\gamma_e \mathbf{q}') - \tilde{\psi}(\gamma_h \mathbf{q}')\right)^2, \tag{2.5}$$

where $\mathbf{q}' = \mathbf{k}_n - \mathbf{k}_i = \mathbf{k}_j - \mathbf{k}_m$. The result is formally the same, but the definition of the transferred exciton momentum has changed. When considering any direct scattering process it is necessary to sum the contributions from

both channels. We carried out calculations of the direct scattering term as a function of both QW width and exchanged momenta, Fig. 2.3. The interpre-

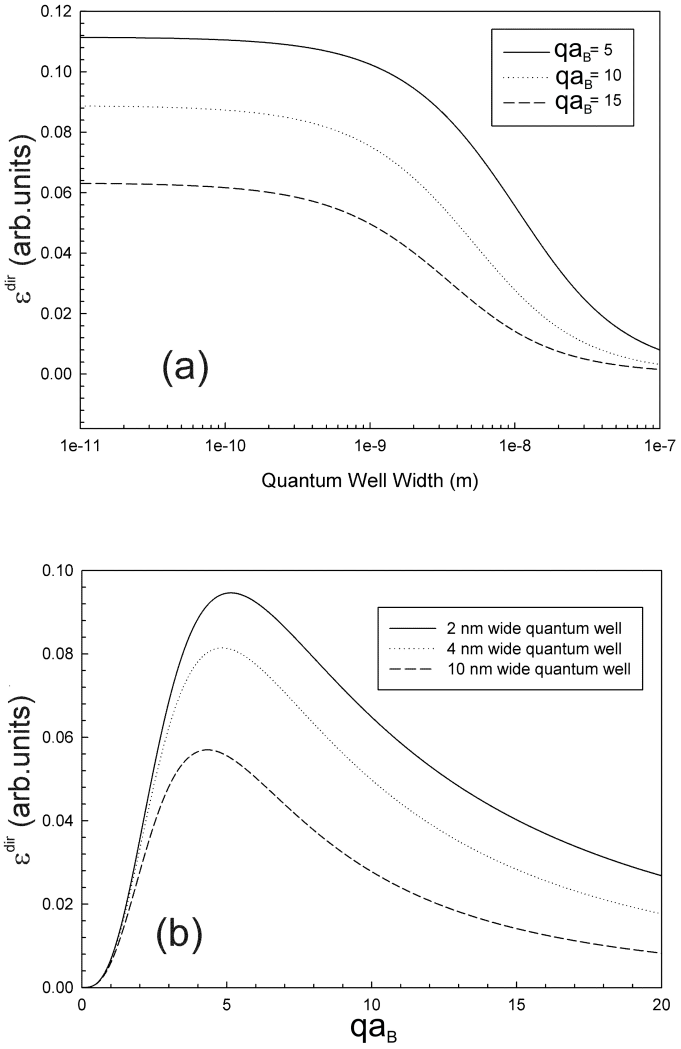

Figure 2.3: (a) Dependence of direct scattering term on width of quantum well for three values of **Q**. (b) Dependence of direct scattering term on transferred exciton center of mass momentum for three values of well width. q is scaled by a_B which in this case is 12nm.

tation of the results for QW width are quite intuitive. Once the QW width begins to exceed the Bohr radius of the exciton the scattering amplitude de-

creases sharply, which is to be expected as we are considering the interaction between fermionic components of the exciton. As the localisation area exceeds the quasiparticles extent they enter the low density regime and begin to act again as good bosons. Excitons are uncharged resulting in negligible Coulomb interaction. The exchanged momentum dependence of the scattering amplitude is more complicated showing a clear peak and significant dependence on the well width even though all widths are below the exciton Bohr radius. The direct Coulomb interaction term in QW's appears due to the different shape of the electron and hole wave functions. From Eq. (2.2) it is evident that an increase in the difference between the electron and hole wave functions results in a square increase in the scattering amplitude. The difference between the wave functions is provided from the γ prefactors which account for the different effective masses of electrons and holes in semiconductors. The lower electron effective mass means that it penetrates further into the QW barrier for narrow QW's and the narrower the well the greater the degree of penetration relative to the hole, explaining the behaviour.

In real world experiments the scattering events considered are at a significantly lower scale than the peak shown in Fig. 2.3(b) and generally $q \ll a_b^{-1}$. To investigate this regime Eq. (2.3) is expanded in this limit, the first three terms are

$$\begin{aligned}
\text{Term 1} &= \left(\frac{3}{32}\right)^2 \left(\gamma_h^2 - \gamma_e^2\right)^2 q^3 \\
\text{Term 2} &= \left(\frac{5}{4\pi^2} - \frac{1}{3}\right)\left(\frac{3}{32}\right)^2 \left(\gamma_h^2 - \gamma_e^2\right)^2 q^4 w \\
\text{Term 3} &= \Bigg[\left(\frac{45}{32768}\right)\left(\gamma_e^4 - \gamma_h^4\right)\left(\gamma_h^2 - \gamma_e^2\right) + \\
&\qquad \left(-\frac{1}{2\pi^2} + \frac{1}{12}\right)\left(\frac{3}{32}\right)^2 \left(\gamma_h^2 - \gamma_e^2\right)^2 w^2\Bigg] q^5. \qquad (2.6)
\end{aligned}$$

Calculating these terms and comparing them with the non-approximate solution, it becomes clear that the q dependence of the direct scattering term

is suitably described by the first term in the expansion for small q i.e., cubic.

The exchange interaction shown in Fig. 2.2(a) has so far not been solved analytically and numerical procedures are necessary. Further elaboration on the work carried out for the exchange term is unnecessary, but we mention the result that in the range of exchanged momenta generally considered in microcavity experiments this term can be considered constant [106]. The remaining scattering events in Fig. 2.2 are combinations of the exchange and direct scattering events and are treated as such formally. These results for the scattering amplitude through the coboson approach can be applied to experimental work and in the following section we consider their impact on the polarisation properties of emission from the elastic circle.

2.3 The Elastic Circle

The nonparabolic form of the lower-polariton dispersion means there are a number configurations available for resonant polariton-polariton scattering [107]. These resonant processes are responsible for operation of the microcavity OPO [43, 45, 108]. Among various geometries of the polariton based OPO studied until now, one of the most attractive implies scattering of two polaritons having equal energies and opposite in-plane wave vectors on a so-called elastic circle. A circle in a 2D reciprocal space characterised by some fixed value of the kinetic energy for the polaritons [109], see Fig. 2.4. The advantage of this geometry is in the fully symmetric final states, which is favourable for realisation of the parametric oscillations [110]. The signal and idler states are characterised by the same polariton lifetime which is not the case in the "magic angle" setup discussed in the introduction. Conversely, the geometry, which involves the simultaneous generation of polaritons with opposite in-plane wave vectors is more complex and harder to

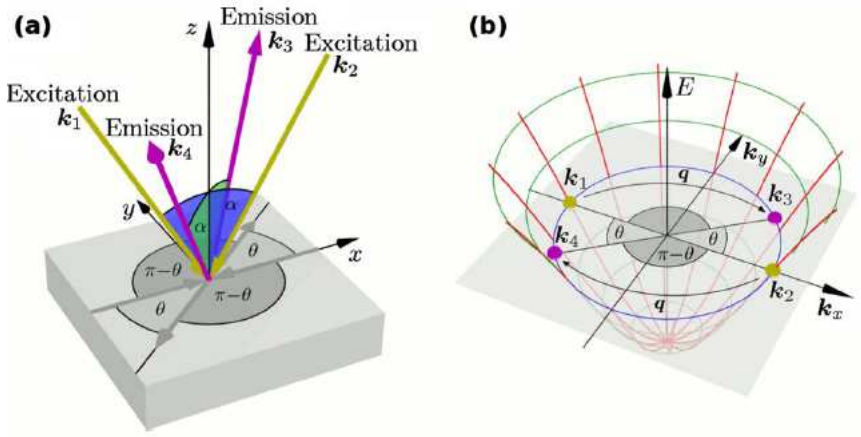

Figure 2.4: (a) Considered geometry of polariton-polariton scattering in real space with α being the angle of incidence and θ being the scattered angle.(b) In reciprocal space, the dispersion of the lower-polariton branch is shown and the elastic circle is highlighted by the blue colour.

model due to the multitude of possible final states, as the scattering to any pair of states belonging to the same diameter of the elastic circle is allowed by energy and wave vector conservation laws. Recent experimental studies revealed a strong angular dependence of the scattering probability on the polar angle along with polarisation selection rules in polariton-polariton scattering [111]. These effects were interpreted in terms of the spin-dependent Gross-Pitaevskii (GP) equations, which assume a single fully coherent state. This method (although powerful and insightful) has two important shortcomings. First, it does not account for the possible depolarisation of the polaritons during the scattering; second, it implies a wave vector independent interaction between the polaritons. We show that applying the results obtained from the coboson approach to polariton-polariton scattering, the formalism allows for the prediction of nontrivial angular polarisation dependence of the scattering amplitude and sheds light on the mechanisms of polarisation relaxation in polariton gases in the elastic circle geometry.

2.4 Scattering Hamiltonian

We consider a planar microcavity pumped with two continuous wave lasers, producing macroscopic occupation of two cavity modes with opposite in-plane wave vectors $\mathbf{k}_1$ and $\mathbf{k}_2 = -\mathbf{k}_1$. The angle of incidence of the two laser beams is the same (angle α in Fig. 2.4). Due to energy and momentum conservation polaritons can scatter only to states on the elastic circle defined by the in-plane momentum $|\mathbf{k}| = |\mathbf{k}_1| = |\mathbf{k}_2|$. The final states are therefore fully defined by the angle θ. We consider all other states to be initially empty and bosonic stimulation can be ignored, we also neglect depletion of the pump states and the longitudinal-transverse splitting of the polariton eigenstates is taken to be zero.

As discussed earlier and pointed out in numerous publications [112, 113, 114, 115], the theoretical treatment of excitons must account for the fermionic nature of their constituents. Because of this polariton-polariton interactions must be considered within the framework of interactions between four fermions, with the different first order processes shown in Fig. 2.2. It is, however, possible and convenient to use an effective scattering Hamiltonian for the bright polaritons and introduce the fermionic scatterings within this formulation. Such an effective Hamiltonian would couple the states on the elastic circle only to the pump states $\mathbf{k}_1$ and $\mathbf{k}_2$

$$H_{SC} = \frac{1}{2}\sum_{s,\mathbf{q}}[\alpha_1(\mathbf{k}_1,\mathbf{k}_2,\mathbf{q})a^\dagger_{s,\mathbf{k}_1+\mathbf{q}}a^\dagger_{s,\mathbf{k}_2-\mathbf{q}}a_{s,\mathbf{k}_1}a_{s,\mathbf{k}_2} + \alpha_2(\mathbf{k}_1,\mathbf{k}_2,\mathbf{q})a^\dagger_{s,\mathbf{k}_1+\mathbf{q}}a^\dagger_{-s,\mathbf{k}_2-\mathbf{q}}a_{s,\mathbf{k}_1}a_{-s,\mathbf{k}_2}]. \quad (2.7)$$

Here, $a_{s,\mathbf{k}}$ is the annihilation operator for a polariton having a wave vector $\mathbf{k}$ and spin s. The amplitudes α_1 and α_2 describe scattering of the polaritons with parallel and antiparallel spins. In general, $\alpha_1 \neq \alpha_2$. This spin dependence of polariton-polariton interactions is at the origin of many in-

teresting effects in polariton dynamics [116], including self-induced Larmor precession [94] and the buildup of linear polarisation in polariton condensates [117]. New results due to these effects will be discussed in more detail in the following chapters.

By defining the final state wave vector as in Fig. 2.4, $\mathbf{k}_3(\theta)$ and $\mathbf{k}_4(\theta)$ and the exchanged momenta $\mathbf{q} = \mathbf{k}_3 - \mathbf{k}_1$ and $\mathbf{q}' = \mathbf{k}_4 - \mathbf{k}_1$ the Hamiltonian can be written

$$H_{SC} = \sum_{s,\theta} (\beta_1(\theta) a^\dagger_{a,\mathbf{k}_3} a^\dagger_{a,\mathbf{k}_4} a_{a,\mathbf{k}_1} a_{a,\mathbf{k}_2} + [\beta_2(\theta) a^\dagger_{s,\mathbf{k}_1+\mathbf{q}} a^\dagger_{-s,\mathbf{k}_2-\mathbf{q}} + \beta_2'(\theta) a^\dagger_{-s,\mathbf{k}_1+\mathbf{q}} a^\dagger_{s,\mathbf{k}_2-\mathbf{q}}] a_{s,\mathbf{k}_1} a_{-s,\mathbf{k}_2}), \tag{2.8}$$

where the summation over θ goes from 0 to π and more convenient scattering amplitudes have been defined

$$\beta_1(\theta) = \frac{1}{2}[\alpha_1(\mathbf{q}) + \alpha_1(\mathbf{q}')], \tag{2.9}$$

$$\beta_2(\theta) = \frac{1}{2}\alpha_2(\mathbf{q}), \tag{2.10}$$

$$\beta_2'(\theta) = \frac{1}{2}\alpha_2(\mathbf{q}') = \beta_2(\pi - \theta). \tag{2.11}$$

The matrix elements of Eq. (2.7) for selected initial and final spin states are shown in Table 2.1. The matrix elements should be interpreted carefully as, for example, the matrix element $\langle XX|H_{SC}|XX\rangle$ squared, expresses the conditional probability of finding the X polarised polariton in the direction $\mathbf{k}_3$ given that we observe another X polarised polariton in $\mathbf{k}_4$, after being pumped by X polarised beams. This does not mean that the final state emission is X polarised as other matrix elements also contribute polaritons of different polarisations i.e., $\langle YY|H_{SC}|XX\rangle$ is non-zero also. Interestingly, if $\beta_2 = \beta_2' = 0$ or $\beta_1 = 0$, because both the aforementioned matrix elements have the same magnitude the emission will be unpolarised and the

final states are in the non-polarised entangled state $(|XX\rangle + |YY\rangle)/\sqrt{2}$. In order to quantitatively characterise the microcavity emission in the limit of spontaneous scattering on the elastic circle, we estimate the amplitudes of the coefficients β_1, β_2 and β_2'. One can expand

$$\alpha_1(\mathbf{q}, \mathbf{k}_1, \mathbf{k}_2)|X_H|^{-4} = \xi^{\text{dir}}(\mathbf{q}, \mathbf{k}_1, \mathbf{k}_2) + \xi^{\text{exch}}(\mathbf{q}, \mathbf{k}_1, \mathbf{k}_2), \tag{2.12}$$

$$\alpha_2(\mathbf{q}, \mathbf{k}_1, \mathbf{k}_2)|X_H|^{-4} = \xi^{\text{dir}}(\mathbf{q}, \mathbf{k}_1, \mathbf{k}_2) + \xi^{\text{super}}. \tag{2.13}$$

With the β coefficients being retrieved from their definition. X_H is the Hopfield coefficient describing the excitonic fraction of polariton states on the elastic circle. As discussed in Section 2.2, the amplitude of ξ^{dir} has a strong dependence on the exchanged momentum when $q \ll a_B^{-1}$ and varies as q^3. The exchange term can be considered constant for scattering on realistic microcavity elastic circles. Intuitively, as the scale on which this term might change is given by the inverse exciton Bohr radius, a_B^{-1}, which is orders of magnitude larger than the radius of the elastic circle which we consider, it is unsurprising that the exchange term is constant. The superexchange, ξ^{super}, is an effective exchange term that comes from a second order process where virtually excited dark exciton states act as intermediaries. This process has been discussed in detail in [118, 24] and we also consider this interaction to be constant around the elastic circle. In the 2D exciton gas limit the magnitude of the direct term is significantly smaller than that of the exchange term because of compensation of the electron-electron and hole-hole repulsion by electron-hole attraction. However, when considering narrows QW's and the different shaped electron and hole wave functions caused by this, the direct term can become orders of magnitude larger than the exchange term. This effect is tunable by application of an external electric field which separates the charges and again modifies the relative shapes of the wave functions. An interested reader is directed to [106] for further details in this area and calculations for a range of structures.

	Final state						
Initial state	$\sigma^+\sigma^+$	$\sigma^+\sigma^-$	$\sigma^-\sigma^-$	XX	XY	YY	$XL(\phi)$
$\sigma^+\sigma^+$	β_1	0	0	$\beta_1/2$	$i\beta_1/2$	$-\beta_1/2$	$\epsilon^*\beta_1/2$
$\sigma^+\sigma^-$	0	β_2	0	$(\beta_1+\beta_2')/2$	$-i(\beta_2-\beta_2')/2$	$(\beta_2+\beta_2')/2$	$(\epsilon\beta_2+\epsilon^*\beta_2')/2$
$\sigma^-\sigma^-$	0	0	β_1	$\beta_1/2$	$-i\beta_1/2$	$-\beta_1/2$	$\epsilon\beta_1/2$
XX	$\beta_1/2$	$(\beta_2+\beta_2')/2$	$\beta_1/2$	$(\beta_1+\beta_2+\beta_2')/2$	0	$(\beta_2+\beta_2'-\beta_1)/2$	$(\beta_1+\beta_2+\beta_2')\cdot(\cos\phi)/2$
YY	$i\beta_1/2$	$i(\beta_2-\beta_2')/2$	$i\beta_1/2$	0	$(\beta_1+\beta_2-\beta_2')/2$	0	$(\beta_1+\beta_2-\beta_2')\cdot(\sin\phi)/2$
YY	$-\beta_1/2$	$(\beta_2+\beta_2')/2$	$-\beta_1/2$	$(\beta_2+\beta_2'-\beta_1)/2$	0	$(\beta_1+\beta_2+\beta_2')/2$	$(\beta_2+\beta_2'-\beta_1)\cdot(\cos\phi)/2$

Table 2.1: Matrix elements of the Hamiltonian Eq. (2.7) for selected spin combinations of the incoming and outgoing polaritons. Polarisation state $L(\phi)$ is defined as the linear polarisation rotated by an angle ϕ with respect to the X-polarised state and we defined $\epsilon = \exp[-i\phi]$. The notation for the table is as follows: $\sigma^+\sigma^-$ for the initial state denotes the $s = 1$ polariton in the state $\mathbf{k}_1$ and $s = -1$ polariton in the state $\mathbf{k}_2$. Same for the final state. The matrix element for the $\sigma^-\sigma^+$ configuration can be retrieved from permutation of β_2 and β_2'.

2.5 Spin and Polarisation of Final States

The Hamiltonian in Eq. (2.8) and its matrix elements do not directly show either the degree of polarisation or the polarisation of the final states. We therefore develop an algebraic procedure for calculation of both these quantities. The system of interacting polaritons is described by the density matrix $\rho(t)$ with an initial condition $\rho(t = 0) = \rho_0$. We assume that dephasing in the system is strong due to interactions between polaritons and phonons which allows one to use the Born-Markov approximation for evaluation of the density matrix dynamics. This yields,

$$\frac{\mathrm{d}\rho(t)}{\mathrm{d}t} = -\frac{2\pi}{\hbar^2}\delta(E_f - E_i)\{H_{SC}, [H_{SC}, \rho(t)]\}, \tag{2.14}$$

where $E_{f,i}$ are the energies of the final and the initial state respectively, and the Dirac delta function is responsible for energy conservation. As we assume the final states are weakly populated and therefore no simulated scattering processes occur, the system response in an arbitrary direction is governed only by the populations of the initial states and scattering angle θ. This allows for the substitution of $\rho(t) = \rho(0)$ in the right hand side of Eq. (2.14). It is clear that we do not need the evolution of the entire density matrix, which is why we fragment it to the submatrices whose evolution is of particular interest.

We define the 2×2 spin-density matrix ρ_k for a state with wave vector $\mathbf{k}$ in the basis of spins $\{\sigma^+, \sigma^-\}$. The 4×4 joint density matrix for the final states is therefore defined as a direct product $\rho_{\mathbf{k}_3(\theta),\mathbf{k}_4(\theta)} = \rho_{\mathbf{k}_3(\theta)} \otimes \rho_{\mathbf{k}_4(\theta)}$ and it fully describes the spin states of the scattered polaritons. The equation of motion for this density matrix can be derived from Eq. (2.14) within the

assumptions made, giving

$$\frac{\mathrm{d}\rho_{\mathbf{k}_3(\theta),\mathbf{k}_4(\theta)}}{\mathrm{d}t} = -\frac{4\pi}{\hbar^2}\delta(E_f - E_i)H_B^\dagger(\theta)\rho_{\mathbf{k}_1,\mathbf{k}_2}H_B(\theta), \tag{2.15}$$

where the joint density matrix for the initial states is $\rho_{\mathbf{k}_1,\mathbf{k}_2} = \rho_{\mathbf{k}_1} \otimes \rho_{\mathbf{k}_2}$ and the Hamiltonian sub-block H_B reads

$$H_B(\theta) = \begin{pmatrix} \beta_1(\theta) & 0 & 0 & 0 \\ 0 & \beta_2(\theta) & \beta_2'(\theta) & 0 \\ 0 & \beta_2'(\theta) & \beta_2(\theta) & 0 \\ 0 & 0 & 0 & \beta_1(\theta) \end{pmatrix} \tag{2.16}$$

We are interested in the polarisation of the radiation emerging in some definite direction denoted by the wave vector $\mathbf{k}_3$. The polarisation properties of the radiation are fully described by the pseudospin vector $\mathbf{S}_{\mathbf{k}3}$. The spin matrix is defined as in Eq. (2.1), $\rho_{\mathbf{k}_3} = \frac{1}{2}N_{\mathbf{k}_3} + \mathbf{S}_{\mathbf{k}3} \cdot \boldsymbol{\sigma}$. The population and pseudospin components of the final state may be retrieved by evaluation of appropriate quantum-mechanical mean values

$$N_{\mathbf{k}_3}(t) = \sum_s \left\langle a_{s,\mathbf{k}_3}^\dagger a_{s,\mathbf{k}_3} \right\rangle = \mathrm{Tr}[(\mathbf{I} \otimes \mathbf{I})\rho_{\mathbf{k}_3(\theta),\mathbf{k}_4(\theta)}(t)], \tag{2.17}$$

$$S_{x,\mathbf{k}_3}(t) = \frac{1}{2}\sum_s \left\langle a_{s,\mathbf{k}_3}^\dagger a_{-s,\mathbf{k}_3} \right\rangle = \mathrm{Tr}[(\boldsymbol{\sigma}_x \otimes \mathbf{I})\rho_{\mathbf{k}_3(\theta),\mathbf{k}_4(\theta)}(t)], \tag{2.18}$$

$$S_{y,\mathbf{k}_3}(t) = \frac{1}{2}\sum_s \left\langle a_{s,\mathbf{k}_3}^\dagger a_{-s,\mathbf{k}_3} \right\rangle = \mathrm{Tr}[(\boldsymbol{\sigma}_y \otimes \mathbf{I})\rho_{\mathbf{k}_3(\theta),\mathbf{k}_4(\theta)}(t)], \tag{2.19}$$

$$S_{z,\mathbf{k}_3}(t) = \frac{1}{2}\sum_s \left\langle a_{s,\mathbf{k}_3}^\dagger a_{s,\mathbf{k}_3} \right\rangle = \mathrm{Tr}[(\boldsymbol{\sigma}_z \otimes \mathbf{I})\rho_{\mathbf{k}_3(\theta),\mathbf{k}_4(\theta)}(t)], \tag{2.20}$$

Considering the finite lifetime of polaritons, τ, and continuous excitation, the steady state pseudospin components may be derived as $S_j^{\mathrm{steady}} = \tau[\mathrm{d}S_j/\mathrm{d}t]_{\mathrm{coh}}$, where 'coh' denotes the coherent temporal evolution according to Eq. (2.15). Using Eqs. (2.15) and (2.17)-(2.20), we obtain the steady-state pseudospin

components

$$N_2^{\text{steady}} \propto (\beta_1^2+|\beta_2|^2+|\beta_2'|^2)N_1N_2 + 8\text{Re}[\beta_2(\beta_2')^*]S_{1x}S_{2x} \\ +8\text{Re}[\beta_2^*\beta_2']S_{1y}S_{2y} + 4(\beta_1^2-|\beta_2|^2-|\beta_2'|^2)S_{1z}S_{2z}, \quad (2.21)$$

$$S_{3x}^{\text{steady}} \propto 2\beta_1\text{Re}(\beta_2')S_{1x}N_2 + 2\beta_1\text{Re}(\beta_2)N_1S_{2x} \\ + 4\beta_1\text{Im}(\beta_2)S_{1z}S_{2y} + 4\beta_1\text{Im}(\beta_2')S_{1y}S_{2z}, \quad (2.22)$$

$$S_{3y}^{\text{steady}} \propto 2\beta_1\text{Re}(\beta_2')S_{1y}N_2 + 2\beta_1\text{Re}(\beta_2)N_1S_{2y} \\ - 4\beta_1\text{Im}(\beta_2)S_{1z}S_{2x} - 4\beta_1\text{Im}(\beta_2')S_{1x}S_{2z}, \quad (2.23)$$

$$S_{3z}^{\text{steady}} \propto (\beta_1^2-|\beta_2|^2+|\beta_2'|^2)S_{1z}N_2 + (\beta_1^2+|\beta_2|^2-|\beta_2'|^2)N_1S_{2z} \\ + 4\text{Im}[\beta_2(\beta_2')^*]S_{1y}S_{2x} + 4\text{Im}[\beta_2^*\beta_2']S_{1x}S_{2y}. \quad (2.24)$$

Eqs. (2.21)-(2.24) allow us to investigate the polarisation selection rules governing polariton-polariton scattering on the elastic circle. The angle dependence of the scattering amplitudes comes from the direct scattering term, while the exchange and superexchange contributions are virtually insensitive to the scattering if the radius of the elastic circle is much less than the inverse Bohr radius.

The total polarisation degree of a polariton quantum state $\mathbf{k}_3$ can be defined as $P = 2|\mathbf{S}_3|/N_3$. This quantity ranges between 1 (fully polarised) and 0 (non-polarised state). We note that Eqs. (2.22)-(2.24) account for the possible depolarisation of the final states with respect to the initial states. For example, if considering fully colinearly polarised initial states, we obtain

for the total polarisation degree of the final states

$$P = \frac{2|\beta_1 \mathrm{Re}(\beta_2 + \beta_2')|}{\beta_1^2 + |\beta_2|^2 + |\beta_2'|^2 + 2\mathrm{Re}(\beta_2^* \beta_2')}. \tag{2.25}$$

P is zero if $\beta_2 = \beta_2' = 0$ or $\beta_1 = 0$ and equals 1 if $\beta_2 = \beta_2' = \pm\beta_1/2$. The ratios β_2/β_1 and β_2'/β_1 determine the degree of polarisation and also the orientation of the pseudospin vector. The exchange interaction couples the initial states with colinear polarisations, to the final states with parallel and perpendicular linear polarisations, with the same probability. This is why, in this configuration, only the superexchange term and the direct interaction term affect the polarisation degree of the final states. The coefficients β_2 and β_2' may be negative if the exchanged momentum is small and therefore the inversion of linear polarisation is often observed in polariton-polariton scattering experiments [94, 119]. This formulation of the pseudospin dynamics demonstrates a new possibility for polarisation conversion as a result of polariton-polariton scattering. To illustrate this, let us consider Eq. (2.24). The last two terms describe creation of the circular polarisation component from two incoming polaritons with linear polarisations rotated by 45° with respect to each other. As the states on the elastic circle with nonzero wave vectors are created, this means creation of spin currents with well defined propagation directions. We recall that polariton spin currents may be generated in microcavities due to the optical spin Hall effect [120, 121] caused by the TE-TM splitting of polaritons [12] and their elastic scattering by a static disorder potential. The effect we propose here does not require either disorder scattering, or TE-TM splitting but exploits the specific selection rules in the polariton-polariton scattering. Note that the total spin is conserved by the process we consider, because the build up of some degree of circular polarisation in one direction is compensated by appearance of an opposite circular polarisation degree in the opposite scattering direction. Equations (2.22) and (2.24) allow for the inverse process: the creation of linear polarisation from one linearly and one circularly polarised initial state.

2.6 Numerical Simulations

Numerical simulations of Eqs. (2.22)-(2.24) are plotted in Fig. 2.5. Curves in (a,e) have nonzero offsets which were removed for clarity; (a) GaAs (0 nm): -52%, GaAs (1 nm): +4%, InGaAs (0 nm): -11%, InGaAs (1 nm): -2%, (e) GaAs (0 nm): -100%, GaAs (1 nm): +60%, InGaAs (0 nm): -100%, InGaAs (1 nm): -35%. Here we consider a microcavity with a 2.5 nm wide $In_{0.04}Ga_{0.96}As$/GaAs or GaAs/$Al_{0.3}Ga_{0.7}As$ QW. We have fixed $\xi^{\rm super}/\xi^{\rm exch} = -0.28 + 0.01i$ following the results in [118]. The linear polarisation degree of the final states defined as $P_x = 2S_{3x}/N_3$ is plotted in Figs. 2.5(a)-2.5(d) in the case of colinear (X polarised) and cross-linear polarisations of the initial states, respectively, as a function of the scattering angle. The curves in Figs. 2.5(a) and 2.5(c) are calculated accounting for the electron and hole spatial separation due to an applied electric field for both types of QW. Figs. 2.5(b) and 2.5(d) illustrate the wave vector dependence of the degree of polarisation in the GaAs/AlGaAs QW.

We observe from Fig. 2.5(a) that the inversion of the linear polarisation degree in the case of scattering of colinearly polarised polaritons takes place unless $\mathrm{Re}(\beta_2) > 0$. Without the strong direct Coulomb interaction, the linear polarisation degree would be $P_x = 2(\xi^{\rm super}/\xi^{\rm exch})/[1 + ((\xi^{\rm super}/\xi^{\rm exch})^2] \approx 52\%$ in the steady-state regime, however the direct interaction compensates the effect of the linear polarisation rotation and the degree of linear polarisation is expected to reach the value of only 11% in narrow InGaAs/GaAs QWs. The contrast of the degree of linear polarisation around the elastic circle is only a few tenths of a percent, with the contrast increased if the wave vector of incident beams (elastic circle radius) is increased as shown in Fig. 2.5(b). Figure 2.5(c) shows nontrivial variations of the degree of linear polarisation as a function of the scattering angle if we consider excitation by cross-polarised beams. The degree depends very strongly on the particular shapes of the

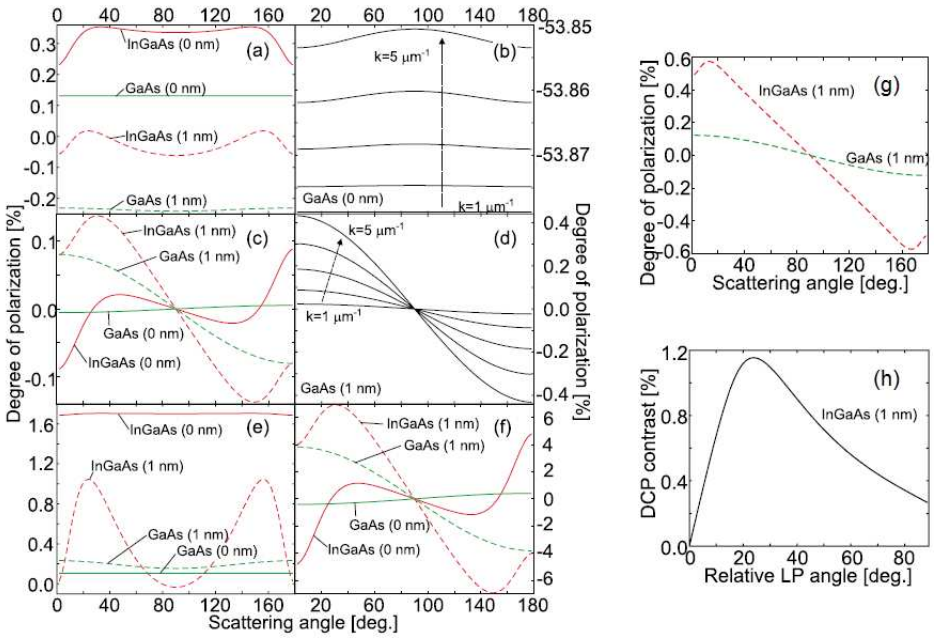

Figure 2.5: Linear polarisation degree P_x in scattering of colinearly (a,b,e) and cross-linearly (c,d,f) polarised pump beams as a function of scattering angle. Spontaneous scattering only is considered in (a-d) while (e-f) display calculations with stimulation accounted for. We compare different QW compositions (a,c,e,f) (circle radius 2 μm^{-1}) and elastic circle radii for "GaAs (0 nm)" QW (b) and "GaAs (1 nm)" QW (d). The numbers in parenthesis denote spatial shift of the particle wave functions due to the applied electric field. (g) Degree of circular polarisation (DCP) around the elastic circle. (h) Dependence of the DCP contrast on the elastic circle on the angle between vectors of linear polarisation of the incident beams.

electron and hole wave functions and obviously the polarisation of the emitted light may be controlled by the applied voltage. The dependence of the polarisation degree on the elastic circle radius for a GaAs/AlGaAs QW subjected to an external bias is shown in Fig. 2.5(d). The elastic circle radius affects the value of the exchanged wave vector, which governs the final state polarisations.

The calculations presented in Figs. 2.5(a)-2.5(d) show only a weak variation of the linear polarisation degree on the elastic circle (below one percent). However, so far we have neglected the final state stimulation of the polariton-polariton scattering, which is expected to magnify the polarisation variation. In order to reveal this effect, we have solved the equations of motion for polariton pseudospin taking into account the stimulated processes in polariton-polariton scattering. The results are plotted in Figs. 2.5(e) and 2.5(f) for the same parameters as in Figs. 2.5(a) and 2.5(c). One can see that the polarisation degree as well as its variations strongly increase. The variations may be as large as several percent in this case. We also observe that depolarisation takes place even in the stimulated regime (polarisation degree is only 35% in InGaAs QW).

The buildup of the circular polarisation and generation of polariton spin currents by linearly polarised optical pumps is demonstrated in Fig. 2.5(g) and 2.5(h). There, the pumps have linear polarisations whose planes are rotated by 22° with respect to each other (at this angle the highest circular polarisation degree is observed, see Fig. 2.5(b)). In this calculation we considered the stimulated scattering regime, in which case the circular polarisation contrast exceeds one percent. This effect, which may be cautiously referred to as the intrinsic optical spin Hall effect, is relatively weak in the model microcavities we have considered. On the other hand its magnitude depends on the spatial separation of the electrons and holes in the QW growth direction so that it can be tuned by applying an external bias.

2.7 Summary

The polariton spin degree of freedom is a critical part of their unique physics. As such, understanding the pseudospin dynamics for different experimental geometries allows us to predict and observe a range of new effects in the strong coupling regime. From a microscopic model, we have calculated the scattering angle dependence of the polariton-polariton scattering amplitudes on the elastic circle. Showing that the amplitude of the direct Coulomb scattering process is strongly angle dependent and reveals pronounced minima and maxima as one goes around the elastic circle because of its cubic dependence on exchanged momentum. The direct terms angular dependence is more pronounced in QWs with spatially separated electron and hole centers of mass because of the different wave function shapes. This offers an opportunity to tune the final state polarisation by the external electric field. On the other hand, contributions from the exchange and superexchange polariton coupling mechanism are virtually independent of the scattering angle.

Using this microscopic formulation for polariton-polariton interactions we have analysed the polarisation selection rules for elastic scattering. We show that the polarisation of scattered polaritons may be different from the polarisation of pumping light. In particular, linear polarisation may be rotated by 90° and circular polarisation may be built up from linearly polarised pumping. Polarisation is lost completely when scattered in particular directions and the polaritons become unpolarised. These properties allow for the generation of spin currents using linearly polarised pump beams. The demonstrated sensitivity of the direct scattering term to the QW geometry and to the applied voltage offers the opportunity to control the polariton-polariton interactions and their spin selection rules via the microcavity design and external fields. This can lead to possible future applications in field-controlled spintronic devices.

Chapter 3

Stochastic Polariton BEC

Recent experimental advances have led to the demonstration of polariton BEC being a regular occurrence [62, 117, 85, 122, 32, 31, 36]. This proliferation requires a reliable and simple to implement experimental criterion for the proof of polariton BEC. From the point of view of the Landau theory of phase transitions [123] BEC requires the build up of an order parameter, ψ, physically associated with the macroscopic wave function of the condensate [124],

$$\psi(\mathbf{r}) = \sqrt{\rho(\mathbf{r})}e^{i\phi(\mathbf{r})}, \tag{3.1}$$

where ρ is the density of the condensate and ϕ is the condensate phase. The order parameters phase is chosen spontaneously by the system undergoing BEC and this spontaneous symmetry breaking is considered the 'smoking gun' for proof of BEC. The spontaneous choice of phase is a symmetry breaking process as all phases result in a system of equal energy and therefore every phase is equivalent. This is akin to a ball balanced at the peak of a perfectly symmetric hill. The ball will remain in this area of increased potential energy forever unless there is some perturbation e.g. the impact of

an air molecule which breaks the symmetry and causes the ball to roll down a given direction. The angle with north that the ball makes can be considered equivalent to the phase chosen by the condensate. It is important to realise that if we were to repeat the test with the ball many times, each time the ball would roll down at a different angle due to a slightly different perturbation and analogously each time a polariton BEC is formed ϕ is chosen randomly. Direct measurement of the BEC order parameter is not possible in polariton physics, however the order parameter build up is accompanied by a decrease in the zero time second order coherence parameter, $g^{(2)}(0)$, which is experimentally observable. Unfortunately, due to the limited time resolution of the Hanbury-Brown and Twiss experimental setup used to measure second order coherence it is very difficult to observe $g^{(2)}(0)$ with a good accuracy [125, 122].

It has been suggested that the order parameter build up can be evidenced by polarisation measurements [126, 127, 86]. Effectively, the polarisation degree of light emitted from the microcavity contains information on the amplitudes and relative phases of both components of the spinor wave function of the condensate. This chapter presents a kinetic model of spontaneous formation of the polariton condensate polarisation vector, accompanying the BEC of polaritons under pulsed excitation. The build up of the polarisation vector is shown to correlate with the decrease in second order coherence of the condensate. Above the threshold pumping power required for BEC the polarisation degree is seen experimentally to decrease [86, 36], this depolarisation appears in the kinetic model as the effect of polariton-polariton interactions.

Because of the symmetry breaking nature of polariton BEC it is a stochastic process. In physical terms this equates to the polaritons entering the condensate with random phase and polarisation. As polaritons interact as good bosons they experience bosonic stimulation i.e., the increased probabil-

ity of scattering to a given final state proportional to that states occupation. Once the average population of the polariton ground state exceeds one, both the stochastic phase and polarisation of the condensate are amplified and stabilise due to the stimulated scattering of polaritons from the incoherent reservoir. Practically this means that the phase and polarisation of the first polariton to enter the ground state stimulate scattering of polaritons to the same state with the same polarisation and phase. The process then becomes more efficient as the scattering is stimulated further by the increased occupancy of the ground state. The polariton interactions with acoustic phonons and themselves produce rich dynamics for the order parameter leading to dephasing and polarisation relaxation, which are accounted for in the kinetic model. These features of polariton BEC are especially noticeable under pulsed excitation and therefore this is the regime focused on in the majority of this chapter[1]. Contrary to the case of continuous wave excitation, where polariton condensation is manifested by spontaneous linear polarisation formation [62, 64, 126, 127], the behaviour of condensate polarisation during the luminescence pulse is much more complex and interesting. This behaviour is characterised by the interplay between the effects of polariton-polariton interactions, polarisaton relaxation and polarisation pinning. As a result, the condensate can exhibit suppression of linear polarisation accompanied with the formation of rings in the polariton distribution, characterised by a fixed circular polarisation component in the case where polarisation relaxation is not effective. It is only the presence of fast relaxation that leads to the suppression of circular polarisation and to the formation of a linearly polarised condensate as in the continuous wave excitation case.

The model put forward in this chapter considers polariton condensation into one spin-degenerate localised state. Neglecting the condensate spatial degrees of freedom is equivalent to assuming spatial coherence across the

[1]The kinetic model has been used to explain the results of a significant experimental work under quasi-continuous pumping and this will be discussed in the final section of the chapter.

whole of the occupied ground state. This is the case in spatially confined systems such as micropillars [128] and is likely to be a feature of localised condensates in planar microcavities, as soon as the polariton lasing threshold is overcome [86]. It is worth noting that although spatial coherence is an experimentally demonstrated feature of BEC [62], it is not a sufficient condition or unambiguous signature. This can be seen from microcavity optical parametric oscillators [129, 130, 76] where spatial coherence has been observed. Here, the spatial coherence is transferred from the laser excitation to the polariton field, but there is not spontaneous symmetry breaking or BEC. The study of polariton BEC spatial coherence formation across several localised states as seen in [62] is taken up in the next chapter where Josephson coupling is introduced into the kinetic model.

There have been two approaches to the modeling of polariton BEC that are most relevant to the kinetic model. The semiclassical Boltzmann approach describes the energy relaxation of polaritons but neglects the phase of the condensate [131, 122]. On the other hand the Gross-Pitaevskii equation [38] and its generalisations assume the existence of a coherent condensate from the beginning [132, 74, 133, 134]. These approaches have included the spin dynamics of polaritons [127, 135] as well. A classical field stochastic approach to polariton BEC has been presented [91] from which the second order coherence can be calculated, however this model ignores the spin degree of freedom and leaves only experimentally difficult methods for the confirmation of BEC. Another recent work has linked the build up of cavity emission polarisation with the condensate order parameter [26] both experimentally and theoretically in the presence of pinning. The kinetic model is an intermediary between the fully coherent spin dependent Gross-Pitaevskii and the spin dependent Boltzmann equations. It allows for the description of the coherent polariton condensate formation from an incoherent reservoir of polaritons, fully accounting for the polariton spin.

3.1 Formalism

The quantum kinetic equation for the condensate density matrix $\hat{\varrho}$ for the case of polariton condensation into one spatially localized state can be written as

$$\frac{d\hat{\varrho}}{dt} = \frac{\mathrm{i}}{\hbar}[\hat{\varrho}, \hat{H}] - \frac{1}{2}\sum_{\sigma=\pm1}\{W(t)(\hat{a}_\sigma\hat{a}_\sigma^\dagger\hat{\varrho} + \hat{\varrho}\hat{a}_\sigma\hat{a}_\sigma^\dagger - 2\hat{a}_\sigma^\dagger\hat{\varrho}\hat{a}_\sigma) + \Gamma_c(\hat{a}_\sigma^\dagger\hat{a}_\sigma\hat{\varrho} + \hat{\varrho}\hat{a}_\sigma^\dagger\hat{a}_\sigma - 2\hat{a}_\sigma\hat{\varrho}\hat{a}_\sigma^\dagger)\}. \tag{3.2}$$

Here $\hat{a}_\sigma^\dagger$ and $\hat{a}_\sigma$ are the bosonic creation and annihilation operators of polaritons with the pseudospin projection $\sigma = \pm1$, where the plus(minus) sign corresponds to the right(left) circular polarization.

The first term in the right-hand side of Eq. (3.2) describes the coherent evolution of the density matrix under the action of the condensate Hamiltonian $\hat{H}$. In what follows we neglect the processes of virtual excitation of polaritons to the other orbital states, which can occur due to the polariton-polariton interaction, assuming the excited states to be far away in energy compared to the value of on-site interaction $\hat{V}$. This approximation is valid, in particular, for localized condensates in planar microcavities and for condensates in pillar microcavities. The condensate Hamiltonian can be written as

$$\hat{H} = \hat{H}_0 + \hat{V}, \tag{3.3a}$$

$$\hat{H}_0 = -\frac{1}{2}\hbar\Omega\sum_{\sigma\sigma'}C_{\sigma\sigma'}\hat{a}_\sigma^\dagger\hat{a}_{\sigma'}, \tag{3.3b}$$

$$\hat{V} = \frac{1}{2}\sum_{\sigma=\pm1}\left\{\alpha_1\hat{a}_\sigma^\dagger\hat{a}_\sigma^\dagger\hat{a}_\sigma\hat{a}_\sigma + \alpha_2\hat{a}_\sigma^\dagger\hat{a}_{-\sigma}^\dagger\hat{a}_\sigma\hat{a}_{-\sigma}\right\}. \tag{3.3c}$$

Here the first term $\hat{H}_0$ describes possible polarization splitting of the single-polariton states, with $\hbar\Omega$ being the splitting energy. The splitting matrix

$C_{\sigma\sigma'}$ can be written as

$$C = \begin{pmatrix} c_z & c_x - \mathrm{i}c_y \\ c_x + \mathrm{i}c_y & -c_z \end{pmatrix}, \tag{3.4}$$

so that the matrix elements of C define the unit 3D vector $\mathbf{c}$. For example, if the splitting of the condensate is because of an external magnetic field applied along the z-direction, $c_z = 1$ and $c_x = c_y = 0$. If there is no Zeeman splitting, $c_z = 0$ and the vector $\mathbf{c}$ defines the linear polarization splitting of the condensate in the xy-plane, which may be caused by the polarisation splitting of exciton or photon modes forming the exciton-polariton. This is a phenomenological addition to the model which can be used to simulate a large range of experimental arrangements.

The polariton-polariton interaction $\hat{V}$ is characterized by two constants, $\alpha_{1,2}$. It should be noted that these interaction constants are inversely proportional to the localization area of the condensate A. The localization area is found from the orbital wave function $\Phi(\mathbf{r})$ of the condensate according to the relation

$$\frac{1}{A} = \int d^2r |\Phi(\mathbf{r})|^4. \tag{3.5}$$

The interaction constant for polaritons with the same pseudospin σ can be estimated as $\alpha_1 \sim E_b a_B^2/A$, where a_B is the exciton Bohr radius and E_b is the exciton binding energy [19]. As we are now considering interactions of polaritons at the same wave vector ($k = 0$) this approximation is valid. One expects a weak attraction between the polaritons with opposite pseudospins [119], so that $\alpha_2 < 0$. The exact value of this parameter depends strongly on the number of quantum wells in the microcavity, their separation, and the detuning between the exciton and photon frequencies that define the exchange scattering of two polaritons.

The two other terms in Eq. (3.2) describe processes of incoherent income

of polaritons into the condensate and the processes of polariton escape from the condensate. The income rate $W(t)$ is time-dependent for the case of pulsed excitation and its value will be defined later in this Section. The outcome rate of polaritons is mainly related to the finite transparency of the distributed Bragg mirrors of the microcavity and, therefore, can be described by a time-independent constant $\Gamma_c = 1/\tau_c$, where τ_c is the lifetime of polaritons in the condensate (typically a few picoseconds).

Quantum kinetic equations of type Eq. (3.2) for spinless polaritons have been studied previously for the *cw* excitation case, i.e., for the time-independent income rate W (see Ref. [136]) and taking into account the time-dependence of W but neglecting polariton-polariton interactions [137, 138]. When both the interactions and the time-dependence of rates are present, an analytical treatment of Eq. (3.2) is not feasible. To analyze the kinetics of polariton condensation numerically we first transform Eq. (3.2) into the partial differential equation of the Fokker-Planck type. This is achieved by the Glauber-Sudarshan representation of the condensate density matrix [139]

$$\hat{\varrho} = \int d^4\psi \, \mathcal{P}(\psi, \psi^*) \, |\psi\rangle\langle\psi| \, . \tag{3.6}$$

Here we denote by ψ two complex numbers, $\psi \equiv \{\psi_{+1}, \psi_{-1}\}$, so that the integration is over two complex planes, $d^4\psi \equiv d^2\psi_{+1} d^2\psi_{-1}$, and the coherent states $|\psi\rangle$ are defined as

$$|\psi\rangle = \prod_{\sigma=\pm 1} \exp\{\psi_\sigma \hat{a}_\sigma^\dagger - \psi_\sigma^* \hat{a}_\sigma\} \, |\mathrm{vac}\rangle \, . \tag{3.7}$$

After substitution of Eq. (3.6) into Eq. (3.2), making use of the relations

$$\hat{a}_\sigma \, |\psi\rangle\langle\psi| = \psi_\sigma \, |\psi\rangle\langle\psi| \, , \tag{3.8a}$$

$$\hat{a}_\sigma^\dagger \, |\psi\rangle\langle\psi| = \left(\psi_\sigma^* + \frac{\partial}{\partial\psi_\sigma}\right) |\psi\rangle\langle\psi| \, , \tag{3.8b}$$

and integration by parts we obtain the equation for the distribution function $\mathcal{P}(\psi, \psi^*)$. This equation reads

$$\frac{\partial \mathcal{P}}{\partial t} = \sum_\sigma \left\{ -\frac{1}{2}\left[\sum_{\sigma'} F_{\sigma\sigma'}(t)\frac{\partial(\psi_{\sigma'}\mathcal{P})}{\partial\psi_\sigma} + \text{c.c.}\right] + W(t)\frac{\partial^2\mathcal{P}}{\partial\psi_\sigma\partial\psi_\sigma^*} \right.$$
$$+ \frac{\mathrm{i}}{\hbar}\left[\alpha_1\frac{\partial(|\psi_\sigma|^2\psi_\sigma\mathcal{P})}{\partial\psi_\sigma} + \alpha_2\frac{\partial(|\psi_{-\sigma}|^2\psi_\sigma\mathcal{P})}{\partial\psi_\sigma} - \text{c.c.}\right]$$
$$\left. - \frac{\mathrm{i}}{2\hbar}\left[\alpha_1\frac{\partial^2(\psi_\sigma^2\mathcal{P})}{\partial\psi_\sigma^2} + \alpha_2\frac{\partial^2(\psi_\sigma\psi_{-\sigma}\mathcal{P})}{\partial\psi_\sigma\partial\psi_{-\sigma}} - \text{c.c.}\right]\right\}, \quad (3.9)$$

where

$$F_{\sigma\sigma'}(t) = [W(t) - \Gamma_c]\,\delta_{\sigma\sigma'} + \mathrm{i}\Omega C_{\sigma\sigma'}. \quad (3.10)$$

The first three terms in Eq. (3.9) are of the usual Fokker-Planck type. The first and the third terms containing the first derivatives are the so-called drift terms, while the second term describes the diffusion in the order-parameter ψ-space. The fourth term in Eq. (3.9) is anomalous. In spite of its similarity to the diffusion term, it is characterized by negative diffusion coefficients. This term describes pure quantum kinetics that do not have a classical analog. A more detailed derivation of Eq. (3.9) can be found in Appendix B.

For polariton condensates in semiconductor microcavities the polariton-polariton interaction starts to play a role only for sufficiently large condensate occupation, namely, in the region $\alpha_{1,2}\langle n\rangle \gtrsim \Gamma_c$. This implies large average occupation of the condensate, $\langle n\rangle \gg 1$, for typical values of $|\alpha_{1,2}| \lesssim 0.1\,\text{meV}$ and $\Gamma_c \sim 1\,\text{ps}^{-1}$. For large occupations the kinetics induced by the polariton-polariton interaction become semiclassical and the last term in Eq. (3.9) can be neglected. This term is small compared to the third by the factor of $\langle n\rangle^{-1}$. In what follows we will assume this limit and will omit the last term in Eq. (3.9). We note that neglecting this term is equivalent to the Gross-Pitaevskii approximation.

In the case of pulsed excitation the initial condition for Eq. (3.9) is $\mathcal{P} = \delta^4(\psi)$ before the arrival of the excitation pulse, implying the absence of polaritons in the condensate. The solution to Eq. (3.9) then gives the distribution function to calculate the statistical averages over many pulses. During each pulse the evolution of the order parameter $\psi_\sigma(t)$ is random and can be described by a stochastic Langevin-type equation. The Langevin stochastic approach will be more convenient for us, and the Langevin equation that is equivalent [140] to Eq. (3.9) with the omitted last term is

$$\frac{d\psi_\sigma}{dt} = \frac{1}{2}\left[W(t) - \Gamma_c\right]\psi_\sigma + \theta_\sigma(t) - \frac{\mathrm{i}}{\hbar}\frac{\delta\mathcal{H}}{\delta\psi_\sigma^*}. \tag{3.11}$$

Here the first term describes evolution of the order parameter due to the pump and decay, the second term is the noise defined below that leads to the diffusive evolution of ψ_σ^* and finally, the third term appears due to the combined effect of the ground state splitting and polariton-polariton interaction. This last term in the right-hand side of Eq. (3.11) has the same form as in the Gross-Pitaevskii equation and we have written it as the functional derivative of the effective Hamiltonian function $\mathcal{H}$ of the order parameter. This function can be found from the condensate Hamiltonian (3.3) by replacing the creation and annihilation operators $\hat{a}_\sigma^\dagger$ and $\hat{a}_\sigma$ with ψ_σ^* and ψ_σ, respectively,

$$\mathcal{H} = -\frac{1}{2}\hbar\Omega\sum_{\sigma\sigma'} C_{\sigma\sigma'}\psi_\sigma^*\psi_{\sigma'} + \frac{1}{2}\sum_\sigma\left[\alpha_1|\psi_\sigma|^4 + \alpha_2|\psi_\sigma|^2|\psi_{-\sigma}|^2\right]. \tag{3.12}$$

The total intensity of the white complex noise, $\theta_\sigma(t)$, is given by the income rate of polaritons into the condensate, $W(t)$, that plays the role of the diffusion coefficient in the Fokker-Planck equation. The correlators of the noise are

$$\langle\theta_\sigma(t)\theta_{\sigma'}(t')\rangle = 0, \tag{3.13a}$$

$$\langle\theta_\sigma(t)\theta_{\sigma'}^*(t')\rangle = \frac{1}{2}W(t)\delta_{\sigma\sigma'}\delta(t-t'). \tag{3.13b}$$

This noise is responsible for the phase and polarization fluctuations in the ground state of the polariton system both below and above the condensation threshold.

It should be noted that the amplitude of the noise depends only on the value of income rate $W(t)$. The outcome rate of polaritons from the condensate, given in our case by Γ_c, does not affect the magnitude of the noise. Physically it happens because the escape of particles from the condensate does not change the condensate coherence.[2] Mathematically, the noise term in the Langevin equation (3.11) appears from the diffusion (second) term in the Fokker-Planck equation (3.9). The easiest way to relate these terms is to consider the case of low condensate occupations ($|\psi_\sigma| \ll 1$), where only the diffusion term and the noise term can be kept in the Fokker-Planck and the Langevin equations, respectively. The amplitude of the noise can be then found by comparison of the time dependence of the average number of polaritons.

In general, the income rate $W(t)$ should be found by solving the semiclassical Boltzmann equation for the polariton relaxation into the condensate [131]. In what follows, however, we adopt a simple model [74] considering all the polaritons that are not in the condensate as a single incoherent reservoir. The reservoir occupation number $N_r(t)$ satisfies the kinetic equation:

$$\frac{dN_r}{dt} = -\Gamma_r N_r - W(t)[n(t)+1] + P(t), \tag{3.14}$$

where $P(t)$ is the incoherent pump rate, Γ_r^{-1} is the lifetime of polaritons in the reservoir (usually $\Gamma_r \ll \Gamma_c$), and $n(t) = |\psi_{+1}(t)|^2 + |\psi_{-1}(t)|^2$ is the instantaneous condensate occupation. The exact dependence of the income

[2]For example, without the polariton-polariton interaction and for zero income rate, the solution to Eq. (3.9) would be given by the coherent state with decreasing amplitude (due to the escape of polaritons), if initially the condensate is put into a coherent state. So, the escape of polaritons defined by the rate Γ_c does not change the coherence of the condensate.

rate $W(t)$ on N_r is defined by the relaxation mechanism. In the simplest case of polariton-phonon relaxation they are proportional to each other, $W(t) = rN_r(t)$.

In the case of very short pulsed excitation, with pulse duration much less then Γ_c^{-1}, the pump is reduced to the initial condition $N_r(0) = \int P(t)dt$ for the reservoir concentration. Eq. (3.14) with $P = 0$ is then solved simultaneously with Eq. (3.11) considering that the condensate is not initially populated, i.e., $\psi_\sigma(t = 0) = 0$. These equations were solved numerically using a (fifth-order) Adams-Bashforth-Moulton predictor-corrector method [141] and standard Monte Carlo methods. The results are presented in the next Section.

3.2 Formation and Dynamics of the Order Parameter

The complex order parameter of the condensate $\psi_\sigma(t)$ cannot be observed directly in a photoluminescence (PL) experiment. On the other hand, the polarization resolved PL gives access to the components of the condensate pseudospin (Stokes) vector:

$$S_x = (1/2)(\psi^*_{-1}\psi_{+1} + \psi^*_{+1}\psi_{-1}), \tag{3.15a}$$

$$S_y = (\mathrm{i}/2)(\psi^*_{-1}\psi_{+1} - \psi^*_{+1}\psi_{-1}), \tag{3.15b}$$

$$S_z = (1/2)(|\psi_{+1}|^2 - |\psi_{-1}|^2). \tag{3.15c}$$

Note that the condensate occupation, n, can be calculated from

$$n^2 = 4(S_x^2 + S_y^2 + S_z^2). \tag{3.16}$$

Averaged values and statistics of different experimentally observable quantities are presented in this section. In what follows we will be interested mostly in time-integrated quantities which will be denoted by a bar, e.g., $\int \psi_\sigma dt = \overline{\psi_\sigma}$. The averaging over multiple pulses (i.e., over realizations of noise) will be denoted by angular brackets as in Eq. (3.13).

From the definition, the time averaged value of the pseudospin $\overline{\mathbf{S}}$ provides direct information about the order parameter of the condensate (except for the phase). It should be noted that fluctuations in the direction of the vector $\overline{\mathbf{S}}$ appear due to the same physical reasons as fluctuations of the condensate phase, namely due to the income of polaritons into the condensate with random polarizations and phases. Therefore, suppression of fluctuations of $\overline{\mathbf{S}}$ indicates suppression of fluctuations of the phase of the condensate as well and manifests itself in the build-up of the order parameter.

When describing experiments on polariton Bose-Einstein condensation in microcavities, one may be able to neglect the effects of polariton-polariton interactions and/or polarization splitting of the ground state of the condensate depending on the sample, geometry of the experiment and pumping intensity. The polarization splitting typically depends on the position of the excitation spot and the polariton-polariton interaction decreases with the increase of the condensate localization radius (for constant occupation number of the condensate). For this reason, in what follows, we present first the results obtained neglecting both these effects (i.e., setting $\mathcal{H} = 0$ in Eq. (3.11)), then we include the effect of polariton-polariton interactions, and finally we study the role of polarization splitting. In numerical calculations we used the parameters $\Gamma_c = 0.5\,\mathrm{ps}^{-1}$, $\Gamma_r/\Gamma_c = 0.01$, $r = 10^{-4}\,\mathrm{ps}^{-1}$, and, when the polariton-polariton interaction is taken into account, $\alpha_1 = 1.8\,\mu\mathrm{eV}$ and $\alpha_2/\alpha_1 = -0.1$[3].

[3]The interaction constant values correspond to a condensate localised within a micron sized area.

Noninteracting BEC without Polarisation Splitting

To evidence the order parameter formation it is convenient to study the total polarization degree of the condensate (TPDC), defined as

$$\rho = \frac{2}{\overline{n}} \left[\left(\overline{S_x}\right)^2 + \left(\overline{S_y}\right)^2 + \left(\overline{S_z}\right)^2 \right]^{1/2}. \tag{3.17}$$

The TPDC changes from 0 for a chaotic state to 1 for the case of a well-defined order parameter with suppressed fluctuations in time. It can be calculated numerically for different realizations of the noise as Fig. 3.1 shows. One can see that the solutions to Eqs. (3.11) and (3.14) exhibit a well pronounced threshold behavior. The dynamical threshold [137] is defined by the balance of the polariton income and outcome rates for the condensate: $W(0) = rN_r(0) = \Gamma_c$, so that the threshold pump intensity is given by $\int P_{th} dt = \Gamma_c / r$.

Below threshold, the average occupation of the condensate is less than unity (see Fig. 3.2) and the order parameter fluctuates extensively during the reservoir lifetime, Γ_r^{-1}, which defines the duration of the PL signal in this case. The pseudospin also fluctuates strongly both in amplitude and direction, so that the TPDC is close to zero. Because of the finite duration of the PL signal (also given by Γ_r^{-1}) the TPDC is not averaged to zero exactly, and it can be shown that $\langle \rho \rangle \sim (\Gamma_r / \Gamma_c)^{1/2}$ for $\Gamma_r \ll \Gamma_c$ and $P \ll P_{th}$.

Above threshold the condensate is formed during the formation time t_f such that $W(t) \geq \Gamma_c$ for $0 < t \leq t_f$, and disappears afterwards on the scale of Γ_c^{-1}. This leads to a drastic increase in the condensate occupancy and narrowing of the emission peak (see Fig. 3.2). At the same time, there is a strong increase in the total polarization degree of the condensate. The TPDC reaches unity, as the dashed curve in Fig. 3.1 shows. The fluctuations of the order parameter become fully suppressed for $P \gg P_{th}$, so that apparently

the fluctuations of ρ are most pronounced in the vicinity of the threshold. It should be noted that while the build-up of TPDC indicates the formation of an order parameter for each excitation pulse, the values of the order parameter and the corresponding values of pseudospin change randomly from pulse to pulse.

Formation of the coherent polariton state at $P > P_{th}$ can be observed also by measuring the second-order coherence in a Hanbury-Brown and Twiss set-up [125, 122]. The second-order coherence parameter $g^{(2)}(0)$,

$$g^{(2)}(0) = \frac{\overline{\langle n^2 \rangle}}{\overline{\langle n \rangle}^2}, \tag{3.18}$$

is also shown in Fig. 3.1. Note that in contrast to the TPDC, $g^{(2)}(0)$ is not a direct measure of the order parameter, whilst its power dependence is sensitive to the build-up of the order parameter. The increase of the pumping power brings the polariton condensate from the thermal (chaotic) state with $g^{(2)}(0) = 3/2$ for $P \ll P_{th}$ [4] to the coherent state for $P \gg P_{th}$, where the fluctuations are suppressed and the order parameter is well-defined for each pulse.

[4]The value of 3/2, instead of the usual 2, appears due to the two component order parameter, $\psi_{\pm 1}$ of the polariton condensate wave function, with each component having a thermal distribution far below threshold. See Appendix C for more details.

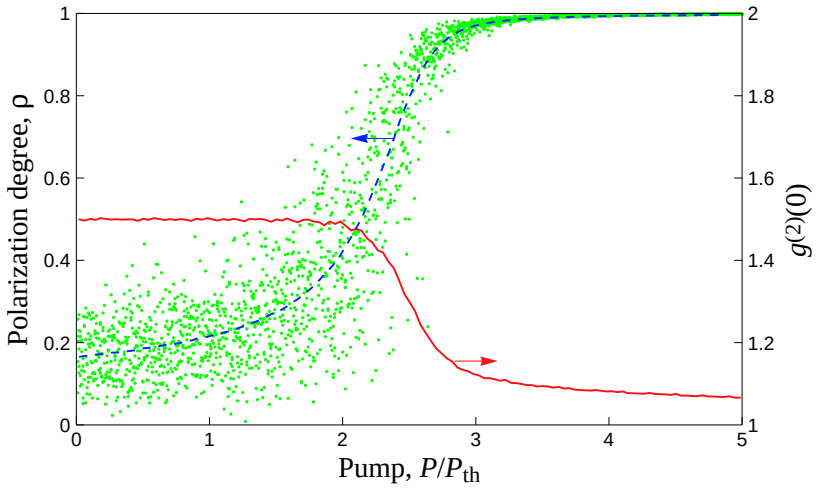

Figure 3.1: The total polarization degree ρ of a polariton condensate as a function of pump intensity for the case of noninteracting polaritons. Dots show the random values of ρ for different pulses, while the average $\langle\rho\rangle$ is shown by the dashed line. The solid line shows the second-order coherence parameter (see text).

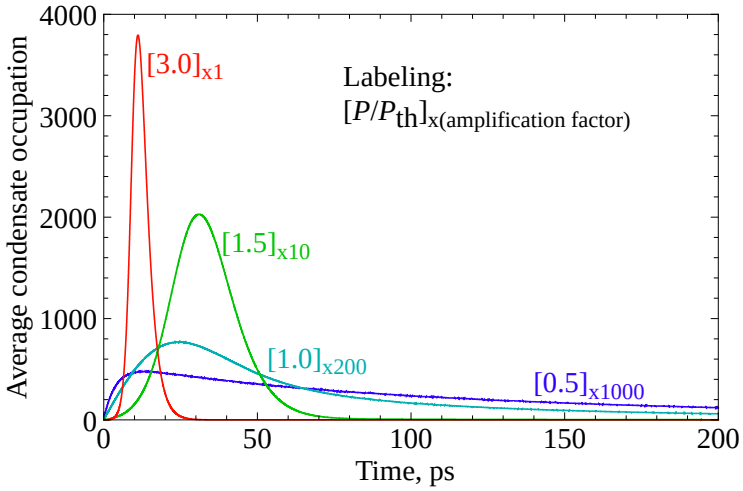

Figure 3.2: The time dependence of the average condensate occupation number $\langle n\rangle$ is shown for the same values of P/P_{th}. The curves are scaled according to the subindex in the labels.

Effects of Polariton-Polariton Interactions

Strong polariton-polariton interactions modify drastically the dependence of the TPDC on the pump as shown in Fig. 3.3. They induce a substantial increase in fluctuations of the polarization degree. Another important effect of polariton-polariton interactions is the nonuniform distribution of the total polarization degree for $P > P_{th}$. Apart from strong fluctuations of the polarization degree from 0 to 1, its distribution exhibits sharp and approximately equidistant peaks that appear far above threshold as shown in Fig. 3.4. The origin of these peaks can be understood if one examines the condensate polariton distribution function in pseudospin space. This distribution function is shown in Fig. 3.5 for four values of the pump power.

One can see that the in-plane component of pseudospin $\left(S_x^2 + S_y^2\right)^{1/2}$ is strongly suppressed for several values of S_z (see Fig. 3.5(d) for $P = 3P_{th}$). This happens as a result of the spin-anisotropy of polariton-polariton interactions. This anisotropy produces the self-induced Larmor precession [135] of the pseudospin vector around the $\hat{z}$-axis. The frequency of this precession is proportional to S_z (see Appendix D for more details). For a fixed n, the in-plane component of pseudospin is averaged to zero for the values of S_z that give a full 2π rotation. In reality the condensate occupation is not fixed and n also fluctuates, so that the in-plane pseudospin never averages to zero exactly. Nevertheless this effect gives rise to a sequence of "Larmor rings" seen at strong pump intensity. An important consequence of the suppression of the average in-plane component of the pseudospin is the non-monotonous dependence of the TPDC on the pump intensity. The TPDC exhibits a peak close to the threshold value of the pump. The non-monotonic behavior of the TPDC as a function of pump intensity with a characteristic peak near the threshold pump intensity has been observed experimentally in GaN-based microcavities [86] and this effect will be discussed relative to further experi-

mental work in the final section of this Chapter.

The polariton-polariton interactions that caused a decrease in the average polarization degree for higher pump powers do not prevent $g^{(2)}$ from approaching 1, and the interactions have no effect on the second order coherence (cf. Fig. 3.1 and Fig. 3.3). This is because of the definition of the second order coherence parameter at an instantaneous value of time (see Eq. (3.18)). Experimentally $g^{(2)}(0)$ is measured by a Hanbury-Brown and Twiss set-up, which has a temporal resolution of about 100 ps, typically. Both below and much above the stimulation threshold this value exceeds the first order coherence time of the condensate [122], which is why the measured value of $g^{(2)}(0)$ always remains close to zero. When corrected accounting for the non monotonic dependence of the first order coherence time on the pumping power, $g^{(2)}(0)$ exhibits the decrease above threshold [125] followed in a CdTe microcavity by subsequent increase with the pumping power [122]. The decrease of $g^{(2)}(0)$ with the pumping power is reproduced by the Wigner model of Savona and Wouters [91] and by our previous [138] and present model. The non monotonic behaviour above threshold could reflect the multimode character of emission of the cavity and fluctuations of the condensate energy due to fluctuations of its occupation number $n(t)$ within the time resolution of the experimental set-up. The effect of fluctuations of the condensate occupation on the second order coherence above threshold has been studied in detail experimentally and theoretically in [142]. This effect can be described by the kinetic theory as well.

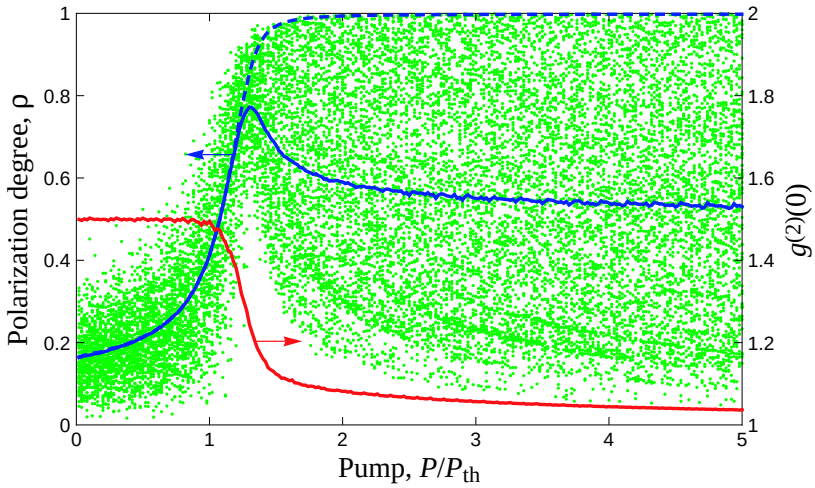

Figure 3.3: The same as Fig. 3.1 but accounting for polariton-polariton interactions. Dots show again the random values of ρ for different pulses, while the average $\langle\rho\rangle$ is shown by the blue solid line. It is seen that interactions decrease the total polarization degree with respect to the noninteracting case (dashed line). The red line shows the second-order coherence parameter.

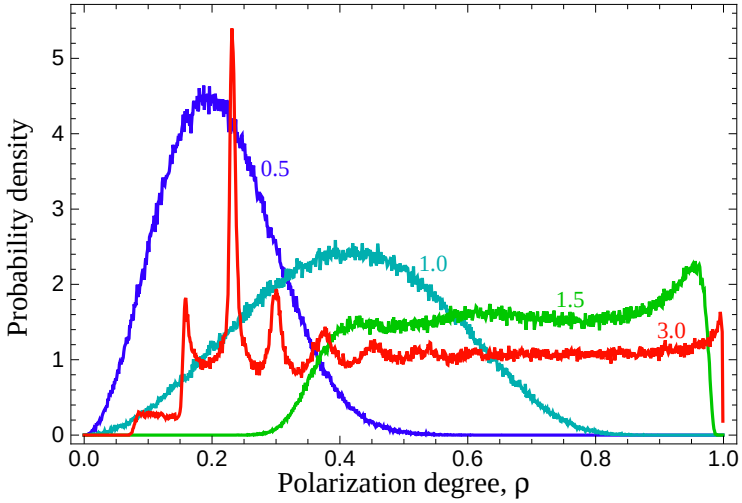

Figure 3.4: The distribution function of the total polarization degree shown in Fig. 3.3. Curves are labeled by the values of P/P_{th}.

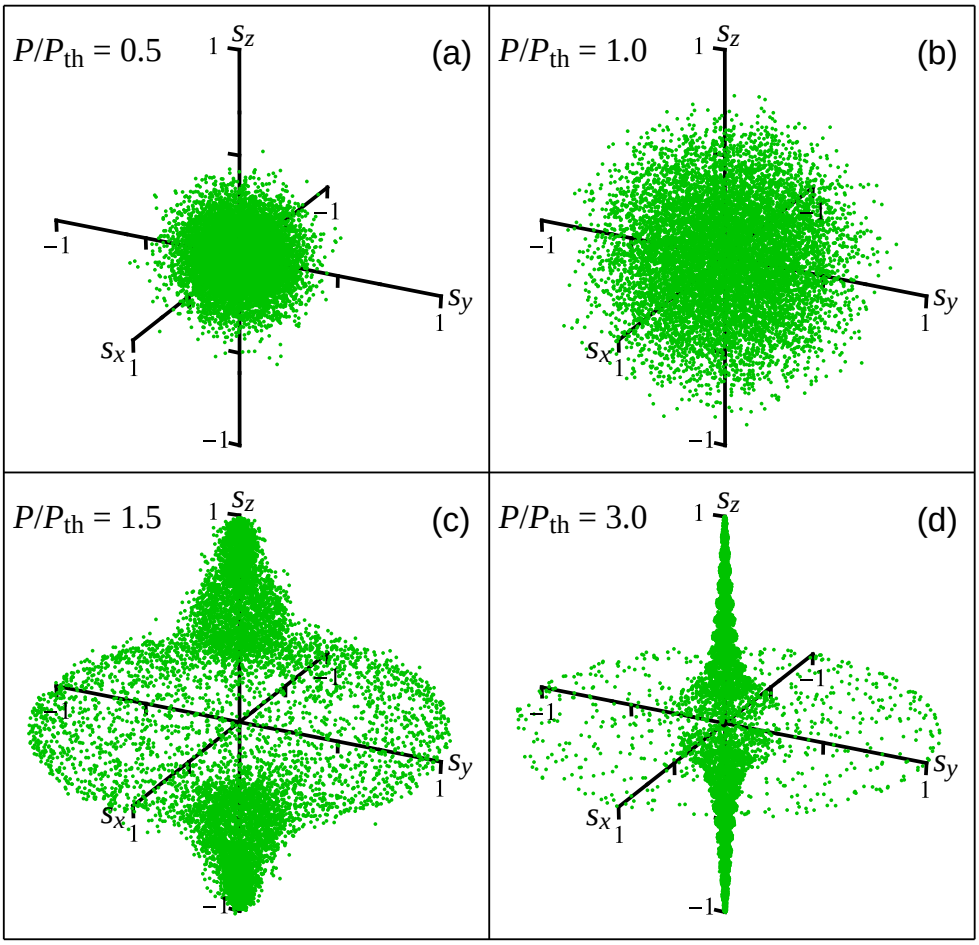

Figure 3.5: The distribution function in normalized pseudospin space, $\mathbf{s} = 2\overline{\mathbf{S}}/\overline{n}$, for different values of the excitation pump in the case of interacting polaritons. Above the threshold the formation of the Larmor rings is seen.

Combined Effects of Interactions and Polarisation Splitting

The presence of polarization splitting, described by the first term in the Hamiltonian (3.12), has a remarkable effect on the pseudospin distribution function, as shown in Fig. 3.6. The vector $\mathbf{c}$, that defines the splitting matrix (3.4) has been chosen along the $\hat{y}$-direction. One can see that the Larmor rings appearing at high pump become deformed and are accompanied by pinning of linear polarization to the $\hat{y}$-axis.

The presence of pinning seen in Fig. 3.6 is somewhat unexpected. Indeed, the pseudospin vector is initially formed with some random orientation. Then, in the absence of polariton-polariton interactions and relaxation, the pseudospin should simply precess around the $\hat{y}$-axis, and, since this precession conserves the y-component of the pseudospin vector, the distribution function should remain symmetric, i.e., without any pinning. It turns out that pinning is a combined effect of polarisation splitting and polariton interactions. The features of the precession in this case are presented in Appendix D. Physically the appearance of pinning requires the energy relaxation of polaritons. The first term in the Hamiltonian Eq. (3.12) can be written as $-\hbar\Omega(\mathbf{c}\cdot\mathbf{S})$ using the definitions of the splitting vector $\mathbf{c}$ from Eq. (3.4) and the pseudospin $\mathbf{S}$ from Eqs. (3.15). Therefore, the splitting energy is minimized for $\mathbf{S}\|\mathbf{c}$. Obviously, the relaxation process is not instantaneous, it is characterised by a time constant dependent on the spin-lattice relaxation rate. It is also shown in Appendix D that for high enough polariton-polariton interaction, one still observes the self-induced Larmor precession along with the deformed precession around the pinning $\mathbf{c}$-direction. The axis of self-induced Larmor precession, however, becomes inclined to the direction opposite to the pinning axis. This explains the deformation of the Larmor rings in the $-\hat{y}$ direction, as it is seen in Fig. 3.6.

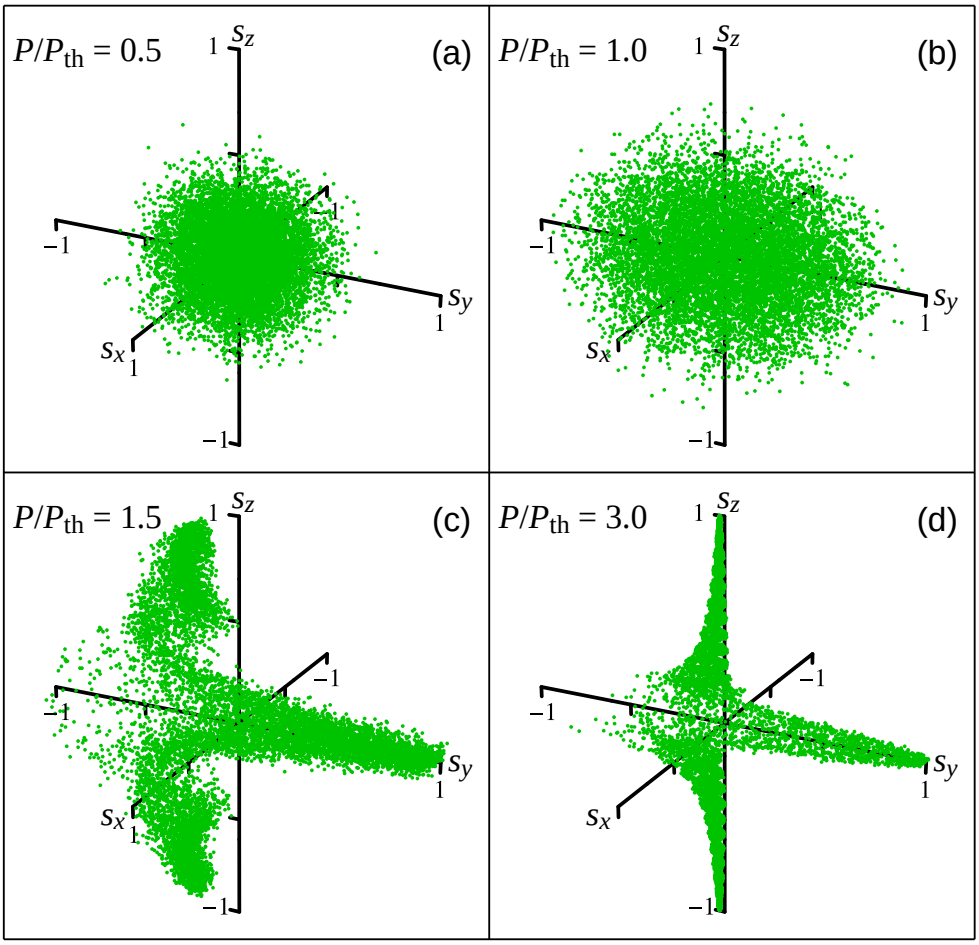

Figure 3.6: The distribution function in normalized pseudospin space, $\mathbf{s} = 2\overline{\mathbf{S}}/\overline{n}$, in the case of polarization splitting characterized by $\mathbf{c}\|\hat{y}$ with the splitting energy $\hbar\Omega = 0.08\,\mathrm{meV}$.

3.3 Relaxation of the Order Parameter

The results obtained in the previous section are valid if the lifetime of the condensate Γ_c^{-1}, that defines the duration of the luminescence signal far above the threshold, is short compared to the typical relaxation times of the order parameter. In this section we show that fast relaxation of the order parameter modifies qualitatively the polarisation properties of the polariton condensate.

The relaxation can be incorporated phenomenologically in our Eq. (3.11) by adding a relaxation term $\mathfrak{R}_\sigma$ to its right-hand side. In general this should be accompanied by an additional noise term due to the fluctuation-dissipation theorem, but this additional noise is small compared to the income noise and can be neglected if the lattice temperature is not too high. In the simplest case, the so-called model A also referred to as the Landau-Khalatnikov or the Onsager model [143], this relaxation term reads

$$\mathfrak{R}_\sigma^{\mathrm{LK}} = -\nu \frac{\delta \mathcal{H}}{\delta \psi_\sigma^*}, \tag{3.19}$$

where the parameter ν defines the relaxation rate. This term favors relaxation of the order parameter to a state with $S_z = 0$, i.e., to a linearly polarized condensate, since the polariton-polariton repulsion energy is minimized for the linear polarisation.

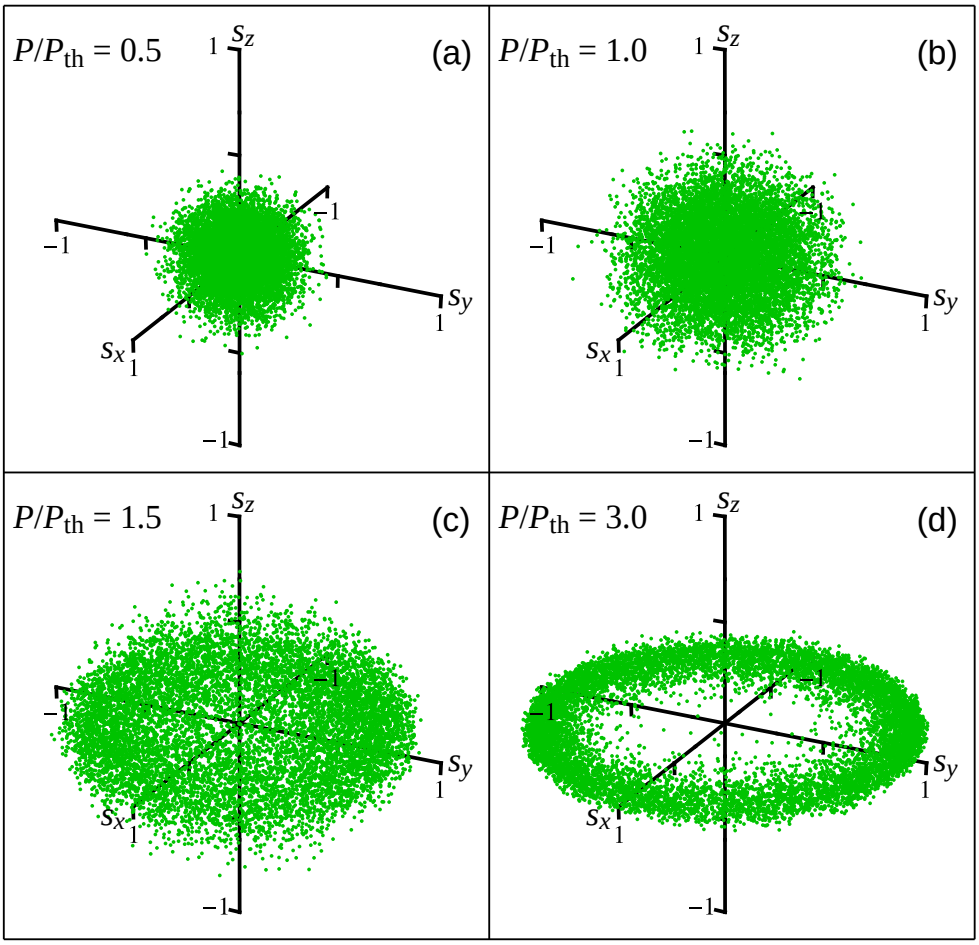

Figure 3.7: The effect of relaxation of the order parameter on the distribution function in normalized pseudospin space, $\mathbf{s} = 2\overline{\mathbf{S}}/\overline{n}$. Contrary to the case without relaxation (Fig. 3.5) a linear polarization is formed for strong pump above threshold. The relaxation parameter $\nu = 1$ meV^{-1} ps^{-1}.

The distribution functions of polaritons, normalized in the pseudospin space, calculated for different pump intensities in the absence of polarisation splitting ($\Omega = 0$) are shown in Fig. 3.7. One can see that the "Larmor rings" vanish and the circular polarisation of the condensate is rapidly lost as the pump intensity increases. The distribution of polariton condensates in pseudospin space calculated by repeating the numerical experiment with different noise realizations changes from a sphere to a torus and approaches a flat ring shape as the pump power is increased further. As a result, the condensate develops a strong spontaneous linear polarisation far above the condensation threshold. If the polarisation splitting of the ground state is present, the direction of resulting linear polarisation becomes well defined.

It should be noted that the relaxation term (3.19) does not conserve the number of polaritons in the condensate. This way the condensate depletion and leakage of polaritons from the condensate are implied by the model of Eq. (3.19). In the case when the condensate occupation is not very high and only the term linear in ψ_σ is kept in Eq. (3.19), the Landau-Khalatnikov relaxation is reduced to

$$\mathfrak{R}_\sigma^{\rm lin} = -\frac{1}{2}\gamma \sum_{\sigma'} C_{\sigma\sigma'}\psi_{\sigma'}. \tag{3.20}$$

It is easily seen that this type of relaxation is equivalent to the assumption of an anisotropy in the transparency of the distributed Bragg mirrors of the microcavity, i.e., it is equivalent to the presence of polarisation dependence of the polariton lifetime. In particular, the lifetime is $\tau_c = 1/(\Gamma_c - \gamma)$ for polarisation along $\mathbf{c}$, and $\tau_c = 1/(\Gamma_c + \gamma)$ for the perpendicular linear polarisation. Clearly this model makes sense only when the relaxation rate $\gamma < \Gamma_c$.

Probably the simplest relaxation model that conserves the number of

polaritons in the condensate is

$$\mathfrak{R}_{\sigma}^{\mathrm{cst}} = -\frac{1}{2}\gamma R_{\sigma\sigma'}\psi_{\sigma'}, \tag{3.21}$$

$$R_{\sigma\sigma'} = (\mathbf{c}\cdot\mathbf{S})\delta_{\sigma\sigma'} - SC_{\sigma\sigma'}. \tag{3.22}$$

Note that this type of relaxation is reflected in the term $-\gamma[\mathbf{S}\times[\mathbf{S}\times\mathbf{c}]]$ in the equation for the pseudospin velocity $d\mathbf{S}/dt$. If we denote θ as the angle between $\mathbf{S}$ and $\mathbf{c}$, then this angle relaxes according to the equation $d\theta/dt = -\gamma S\sin\theta$.

3.4 Room Temperature Polariton Condensation in GaN

Theoretical work as described in this Chapter provides an insight into the internal workings of strongly coupled semiconductor microcavities. However, these intrigues do not enter the rarefied world of science until experimentally realised. The first demonstration of polariton condensation at room temperature occurred in a bulk GaN microcavity in 2007 [85]. As predicted by our stochastic model the polarisation degree in this sample peaks at threshold and decreases (see Fig 1.6 and [86]) after that point. The polarisation vector is randomly oriented for each exciting pulse, evidencing the symmetry breaking nature of polariton BEC and in direct agreement with the stochastic model.

Next to the successful explanation of these bulk GaN experimental results using the kinetic model a natural continuation would be to model the polarisation degree of a planar microcavity structure with embedded QW's. A high quality GaN planar structure displaying extremely high vac-

uum Rabi splitting of $\sim$ 50meV was reported in 2008 [144]. The structure was grown by metal organic vapor phase epitaxy with a 35 pair lattice-matched $Al_{0.85}In_{0.15}N/Al_{0.2}Ga_{0.8}N$ Bragg reflector grown on a $Al_{0.2}Ga_{0.8}N$ layer. The cavity layer has an optical thickness of 3λ with a $5\lambda/2$ active region containing a 67 period GaN multiple QW structure. A 13 pair Bragg reflector is then grown on top to complete the structure. A transmission electron micrograph of the structure without the final Bragg reflector is shown in Fig. 3.8. A structure nearly identical to the completed form of the half cavity shown

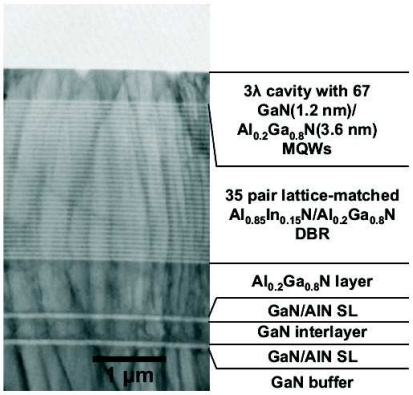

Figure 3.8: Cross-section of planar GaN half microcavity structure [144].

in Fig. 3.8 was created, with the slight difference of a 67nm thick Si_3N_4 layer before the growth of the top Bragg reflector. The purpose being to allow for small negative detunings and thereby modify the polariton dispersion (Fig. 1.4) to a form more favourable for polariton relaxation to the ground state. Polariton lasing was reported in this sample [145] at room temperature with a slightly larger vacuum Rabi splitting of 56meV. Here polariton lasing is defined as coherent light emission from a macroscopic population of polaritons occupying the lowest energy state of the lower polariton branch, Fig. 3.9. The measurement of polariton lasing is a consequence of polariton BEC but not a sufficient criterion to claim the phase transition has occurred. This is primarily due to the lack of evidence of symmetry breaking. Under the criteria defined for polariton BEC by the kinetic model, the increase in polarisation degree of the ground state emission is direct evidence of a build-

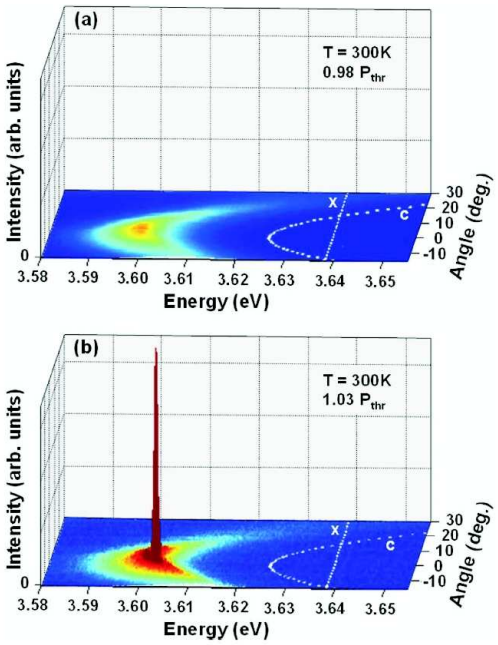

Figure 3.9: 3D plot of GaN microcavity emission intensity (a) below and (b) above threshold pumping [145].

up in the condensate order parameter. Therefore the experimentally simple technique of resolving the ground state emission in polarisation as well as intensity is enough to determine whether the phase transition has occurred. It is important that the polarisation build up of the ground state is proven to be solely due to an increase in the magnitude of the condensate order parameter and not an artifact of the polarised pumping laser. To ensure this the sample is pumped non-resonantly, 1eV above the energy of the exciton-like reservoir, by means of a pulsed 266nm Nd:YAG laser with a repetition rate of 8.52kHz and a pulse length of 500ps. This means that many scattering events must occur before the excitons relax to the polariton dispersion and the polarisation is effectively randomised. Under these pumping conditions measurements taken of the far-field emission from the polariton dispersion are shown in Fig. 3.10. As previously a macroscopic occupation of the ground state is seen above threshold while the bottleneck effect [146, 42] not seen in Fig. 3.9 is clear below threshold. Below threshold, the PL signal from the

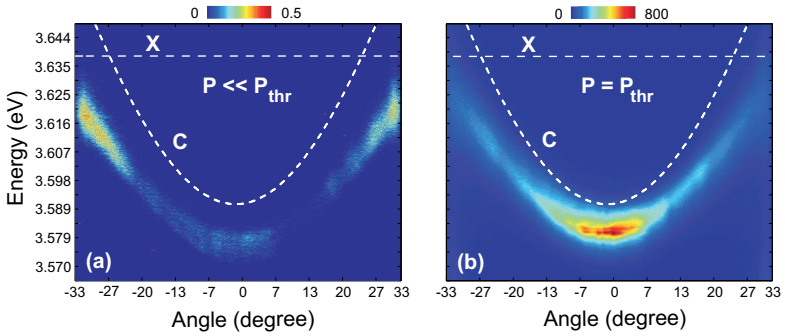

Figure 3.10: Room temperature emission of the lower polariton branch (a) far below and (b) above threshold.

sample is unpolarised. At the condensate formation threshold we observe a build-up of the linear polarisation degree up to about 85% as shown in Fig. 3.11. The linear polarisation degree, $\langle \rho_l \rangle$, is experimentally averaged

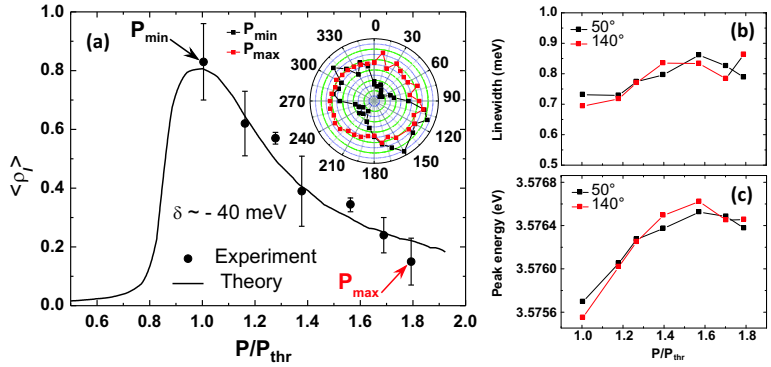

Figure 3.11: (a) Experimental pump power dependence of the linear polarisation degree above threshold (black dots) and corresponding theoretical calculation (black line). Inset: Polar intensity plot showing polarisation pinning at $P_{min} = P_{thr}$ and depinning of polarisation above threshold at P_{max}. (b)-(c) linewidth and peak energy, respectively of the ground state emission as a function of pump power.

over about 200 pulses and therefore these results demonstrate the pinning of the linear polarisation in the sample, similar to what has been previously observed in CdTe and GaAs cavities [62, 64]. This is followed by a progressive depinning of the polarisation at larger pumping intensities, manifesting itself through the decrease of $\langle \rho_l \rangle$, as shown in Fig. 3.11(a). This observation

is in contrast to what has been reported in [117] for a CdTe QW microcavity. In their experiment, the linear polarisation degree kept growing above threshold. We ascribe the difference to the different ratio of spin relaxation and lifetimes of polaritons in the two systems.

At $1.8P_{thr}$ we observe that $\langle \rho_l \rangle$ approaches zero, which means that the polarisation vector of the condensate is unpinned and randomly changes from pulse to pulse, similarly to the first display of room temperature polariton BEC [86]. Over the same range of pumping powers we observe the simultaneous progressive increase of the linewidth, Fig. 3.11(b), and the blueshift, Fig. 3.11(c), of orthogonally polarised emission peaks arising from polariton-polariton interactions as previously observed in polariton condensates [62, 64, 145].

We interpret the whole set of power-dependent experimental data in terms of the spin dependent polariton-polariton interactions [94] present in the stochastic model of polariton BEC. These act to suppress the linear polarisation. The interactions combined with static polarisation anisotropy, which favours the formation of one linear polarisation and enters our model through the splitting matrix C, Eq. (3.4), is enough to understand the experimental results. We use Eq. (3.11) and Eq. (3.14) as previously but with parameters adjusted for the specific materials and including linear relaxation, Eq. (3.20). We also modify the pump term $P(t)$ which previously entered only as an initial condition because the length of the pump pulses were much shorter than the condensate lifetime. Because of the quasi-continuous nature of the experiment $P(t)$ now takes the form of a 500ps rectangular pulse, with the threshold pumping power determined as the point at which the average condensate occupation is greater than 1. As experimental equipment is organised to measure the build up of one polarisation degree the TPDC is not equivalent to the experimental measure and the parameter to be compared is now $\langle \rho_l \rangle = \langle s_x \rangle$. Using our stochastic model the theoretical pump dependence of

$\langle\rho_l\rangle$ is shown by the solid line in Fig. 3.11 together with the experimental points.

The behaviour of the theoretical curve closely follows that of the experimental data. $\langle\rho_l\rangle$ shows a maximum at P_{thr} followed by a subsequent decrease. The maximum of $\langle\rho_l\rangle$ occurs at some macroscopic occupation of the condensate which can be deduced from the blueshift of the emission line at threshold compared to the weak excitation case. The interaction constant α_1 is a fitting parameter of the calculation. The best agreement with the data is obtained for $\alpha_1 = 5.7 \times 10^{-5}$meV. The other parameters used in the calculation are $\Gamma_c = 4.25\text{ps}^{-1}$, $\gamma = 0.03\text{ps}^{-1}$ and $\alpha_1/\alpha_2 = -0.1$. At threshold, the polariton-polariton interactions do not affect the kinetics of the condensate formation and the polarisation buildup is governed by the static anisotropy in the microcavity plane. The polarisation degree is large but less than unity due to the presence of fluctuations. A subsequent increase of P results in a rapid growth of the condensate occupation and the nonlinear interaction terms in Eq. (3.11) become more and more important. These terms lead to the self-induced Larmor precession that destroys the polarisation pinning so that above threshold polariton-polariton interactions dominate and overwhelm the pinning effect.

The self-induced Larmor precession arises due to the non-zero circular component s_z (as discussed in Appendix D) of fluctuational origin. The Larmor precession acts to suppress $\langle\rho_l\rangle$. As we measure the time integrated polarisation degree, in the extreme case where the condensate polarisation has precessed an integer number of times around the z axis, the integrated linear polarisation degree will average to zero as shown in Fig. 3.5. The distribution in pseudospin space of S_x, S_y and S_z for this microcavity is displayed in Fig. 3.12

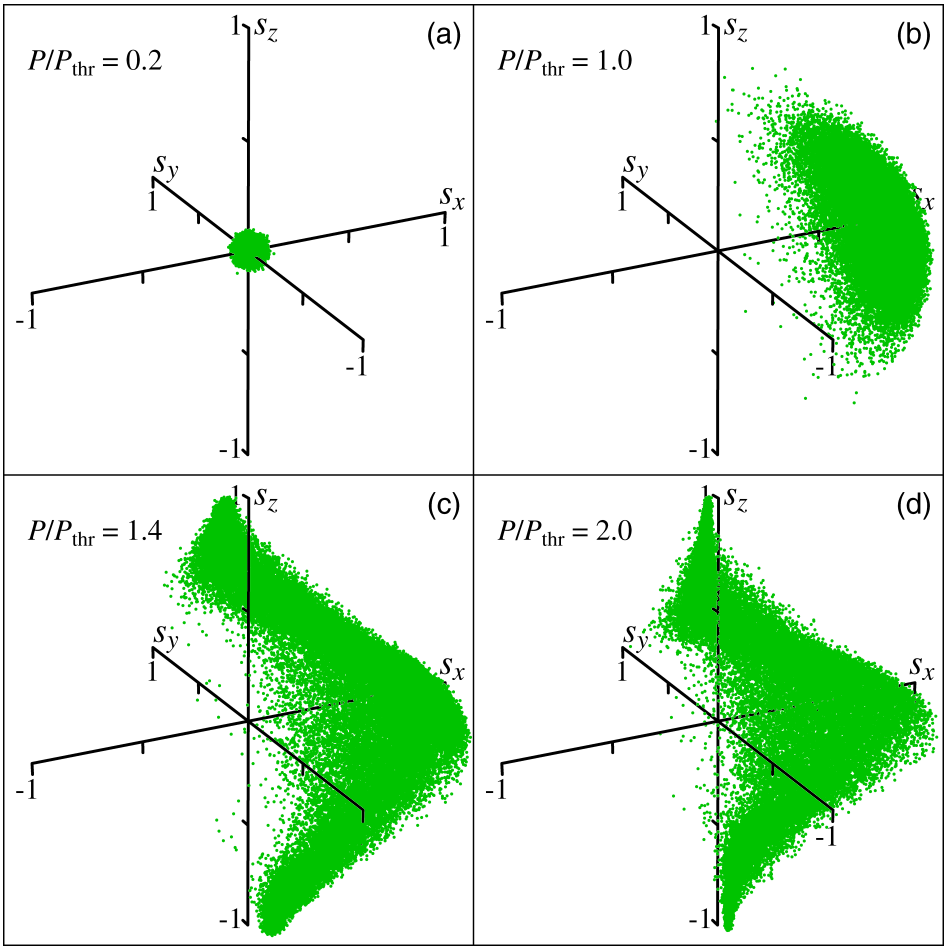

Figure 3.12: Time-integrated polarisation distribution for four different regimes. (a) far below threshold, (b) close to P_{thr}, (c) slightly above threshold and (d) far above threshold.

It is clear from this analysis that the suppression of linear polarisation holds as long as some circular component of the pseudospin is present. The polariton-phonon spin flip relaxation should equalise the occupation numbers of +1 and -1 polarisations, stop the Larmor precession effects and thus recover the linear polarisation degree so that it would again approach unity. We note the differences with earlier work [117], where the polariton decay rate was 10 times smaller. As the condensate was excited by a continuous wave laser, it did not decay with the characteristic spin relaxation time of polaritons contrary to the present experiment where the pulse duration is comparable to the typical coherence times measure in polariton condensates [142]. In addition the temperature in [117] amounted to only 20K, which can reasonably explain why in this sample the magnitude of the stochastic circular polarisation of the condensate, which is responsible for the self-induced Larmor precession and the suppression of the linear polarisation, was much weaker than in the present case.

The efficiency of the pinning at P_{thr} appears to be also detuning dependent with a non monotonic behaviour showing a minimum at $\Delta \sim -65$meV. The black line and the red line are guides for the eye showing the evolution of $\langle \rho_l \rangle$ in the strongly photon-like and in the more exciton-like region of the polariton condensate, respectively. The detuning dependence of the linear polarisation can be qualitatively understood from our model by taking into account the evolution of the polariton relaxation rate between the reservoir and the condensate on Δ [147]. The minimum of polarisation nearly corresponds to the minimum of threshold pumping [147, 148]. As the polarisation relaxation time in the condensate is expected to change very slowly with the detuning, in the case of fast polariton relaxation from the reservoir, the system has no time to relax to the lowest energy state corresponding to the pinned polarisation. This results in the decrease of $\langle \rho_l \rangle$. Finally note that in order to quantitatively reproduce the detuning dependence of the polarisation one would also need to know the dependence of detuning

on polariton-polariton interaction constants, which remains to be studied in GaN-based microcavities.

3.5 Summary

Experimental studies of polariton BEC are a new but quickly evolving field in solid state physics. The ability to demonstrate this symmetry breaking phase transition at room temperature has no doubt amplified interest in this young field and increased the rate of progress accordingly. The real world implications of a polariton laser operating at room temperature are significant due to the lack of a threshold as defined in the photonic lasing sense. Maintaining or accelerating the rate of advance requires an experimentally simple way of assuring that polariton BEC has occurred and understanding the properties of emitted light from the ground state.

The kinetic model presented in this chapter describes theoretically the build-up of the vector order parameter in the course of polariton BEC. The build-up of the order parameter manifests itself in the formation of the stochastic vector polarisation of the condensate, a relatively simple quantity to measure experimentally. This polarisation is correlated with the second order coherence of the condensate, a much more difficult quantity to measure accurately. We originally considered the pulsed regime, where the length of the exciting pulse was much shorter than the lifetime of the condensate. In the case of no polariton-polariton interactions the polarisation degree reached unity at threshold pumping and remained there for all pumping powers. In contrast, the effect of 'turning on' the interactions was a decrease in polarisation degree above threshold due to rotation of the polarisation vector around the effective field created by the spin ± 1 imbalance. With the addition of efficient spin relaxation, the polarisation dynamics of the condensate change

significantly. Energy minimisation of the system leads to a linearly polarised condensate above threshold. By the phenomenological addition of polarisation splitting of the polariton states the effects of photonic or exciton mode splitting were demonstrated. With a significant alteration in the polarisation distribution.

Experimental work on a GaN based microcavity with a quasi-pulsed pump showed the decrease in polarisation degree above threshold pumping intrinsic to the kinetic model without efficient spin relaxation. We modeled the experimental data assuming some in-plane anisotropy caused by the samples stationary disorder. The results showed that at pumping powers near threshold the anisotropy dominates, giving a high polarisation degree. Above threshold the effects of polariton-polariton interactions dominate and the self-induced Larmor precession acts to reduce the polarisation degree.

From the generalised nature of the stochastic model it would be easily possible to extend the work to further sample specific parameters. The consideration of different scattering mechanisms (so far only polariton-phonon has been calculated) could provide new insights into the condensation process. Spatial correlations as a consequence of polariton condensation are discussed in the following chapter.

Chapter 4

Josephson Coupled Polariton BEC

In this Chapter the kinetic model presented in Chapter 3 is extended to account for the spatial correlations, $g^{(1)}(\mathbf{r}, \mathbf{r}')$, which have been proposed theoretically as the criterion for the BEC phase transition [149]. In early experimental work on polariton BEC, it has been shown in the near-field emission profile that multiple condensates are formed within the microcavity sample [62, 117], Fig. 4.1. Build-up of long-range spatial coherence across the condensates is seen above threshold supporting the proposal that this is a suitable criterion for polariton BEC, while also implying a coupling mechanism between the spatially separated condensates. The disparate condensates not only demonstrate long-range spatial coherence but uniform alignment of the linear polarisation i.e., emission from each condensed region has the same polarisation vector. To account for both of these facts we propose the DC Josephson effect, [150, 92, 151] when applied as an extension to the kinetic model, can successfully account for the coupling and explain the polarisation locking and spatial coherence build-up in the system. In this sense we

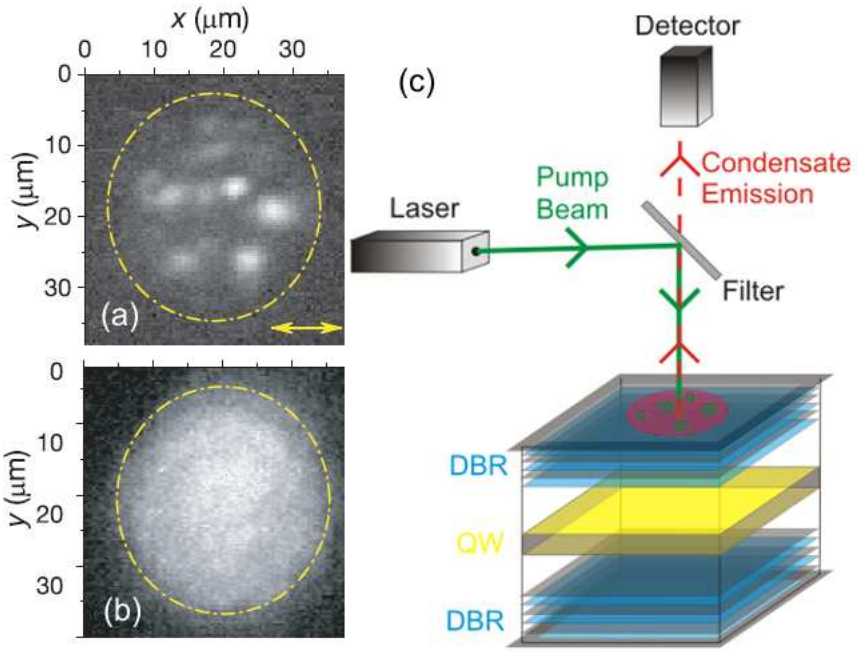

Figure 4.1: (a) and (b) show the linear polarisation of emission from the sample above and below threshold respectively from the work carried out in 2006 [62]. Below threshold the emitting spot is homogeneous and unpolarised, whereas above threshold separate regions of emission have formed, emitting with the same polarisation vector. (c) Schematic of the experimental arrangement.

argue that the measurement of a stochastic polarisation vector may be a more stringent criterion for polariton BEC in microcavities than long-range spatial coherence. Spatial coherence is a natural property of systems such as micropillars [128] and is likely a feature of localised condensates in planar microcavities once the lasing threshold is surpassed [86], making it an unsuitable criterion for defining the phase transition. The spontaneous polarisation build up defines BEC in localised condensates whereas the spatial coherence can be formed prior to the order parameter formation. Furthermore, the kinetic model can introduce the symmetry breaking effects of differing local fields for each condensate (e.g. produced by local strains at different regions of the sample) which can be used to alter the polarisation locking through changing of the field orientations.

Recently, theoretical work has been published describing the polarisation dynamics of a pair of fully correlated polariton condensates [57] and the phase correlation of Josephson coupled condensates as a function of detuning [30]. The introduction of the Josephson effect into the kinetic model is novel with respect to those works because we take into account the symmetry breaking stochastic nature of the phase transition, key to definitive display of polariton BEC. The kinetic model can also be used to demonstrate the degree of coupling between the separate condensates by examination of polarisation correlations [152], a measurement not considered in other work. The condensates are assumed to have zero detuning between them and therefore are in the steady state regime as described in [30].

This Chapter begins with a brief introduction to the Josephson effect followed by the results of its application into the kinetic model.

4.1 The Josephson Effect

The theoretical prediction of the Josephson Effect was made in 1962 [150], when Brian Josephson was a 22-year old graduate student. He predicted that two superconductors separated by a thin insulating barrier should give rise to a spontaneous DC current proportional to the difference in phase across the junction due to the finite nature of the barrier, leading to a non-negligible tunneling probability[1]. The starting point for this prediction was the incitement by his supervisor Brian Pippard to look at the tunneling experiments of Ivar Giaever [153] and the associated theory. Combining this with a lecture course from Anderson [154] led Josephson to make the leap and for his astounding discovery he was awarded the Nobel prize in 1973, no doubt

[1]The AC Josephson effect was also predicted which occurs if a DC voltage is placed across the junction.

being helped by the quick experimental realisation of these effects by Anderson [155]. The effect was later discovered for superfluid Helium [156] and interacting atomic condensates [157], showing the far reaching implications of this discovery and it's applicability to a range of systems.

In the original work of Josephson the ultimate goal was to provide a theoretical equation for the current flow between two superconductors. In the case of our kinetic model the interest lies in the effect it will have on the dynamics of the order parameter. To obtain this we begin by considering two macroscopic quantum states represented by their order parameters, $\psi_{1,2}$, separated by a finite potential barrier which allows limited tunneling between the two states. In this case the coupling is very weak and the state vector describing the coupled system can be written in the simple form

$$|\psi\rangle = \psi_1 |1\rangle + \psi_2 |2\rangle . \tag{4.1}$$

The Schrödinger equation of motion for the state vector is

$$i\hbar\partial_t |\psi\rangle = H |\psi\rangle \tag{4.2}$$

with the Hamiltonian a combination of the individual energy of the states, $H_i = E_i |i\rangle \langle i|$, $(i = 1, 2)$, and the coupling between the states,

$$H = H_1 + H_2 + H_{int}. \tag{4.3}$$

The interaction term takes the standard form

$$H_{int} = -\frac{J}{2}(|1\rangle \langle 2| + |2\rangle \langle 1|). \tag{4.4}$$

Combining the previous definitions gives the equations of motion for the two

coupled macroscopic states:

$$i\hbar\partial_t\psi_1 = E_1\psi_1 - \frac{J}{2}\psi_2,$$
$$i\hbar\partial_t\psi_2 = E_2\psi_2 - \frac{J}{2}\psi_1. \tag{4.5}$$

It is clear from this treatment how the kinetic model can be extended to include Josephson coupling between condensates. The Langevin type equation retains its form with the addition of a subscript, $i = 1, 2$, denoting which condensate is being referenced:

$$\frac{d\psi_{i\sigma}}{dt} = \frac{1}{2}\left[W(t) - \Gamma_c\right]\psi_{i\sigma} + \theta_{i\sigma}(t) - \frac{\mathrm{i}}{\hbar}\frac{\delta H}{\delta\psi^*_{i\sigma}} - \gamma R_{i\sigma}. \tag{4.6}$$

The noise correlators are similarly modified,

$$\langle\theta_{i\sigma}(t)\theta_{i'\sigma'}(t')\rangle = 0, \tag{4.7}$$
$$\langle\theta_{i\sigma}(t)\theta^*_{i'\sigma'}(t')\rangle = (1/4)W(t)\delta_{ii'}\delta_{\sigma\sigma'}\delta(t-t'), \tag{4.8}$$

where the factor $\frac{1}{2}$ is now replaced by $\frac{1}{4}$ as the income rate is spread across two condensates and therefore the noise amplitude for each is halved. Analogously to Eq. (4.4) the dynamics due to Josephson coupling are seen through a change in the Hamiltonian,

$$H = H_s + J\sum_{\sigma}(\psi^*_{1\sigma}\psi_{2\sigma} + \psi^*_{2\sigma}\psi_{1\sigma}) + \frac{1}{2}\sum_{i\sigma}\left[\alpha_1|\psi_{i\sigma}|^4 + \alpha_2|\psi_{i\sigma}|^2|\psi_{i\bar{\sigma}}|^2\right]. \tag{4.9}$$

Where H_s is the spin spitting which will be discussed later in the Chapter, J is the strength of coherent hopping between the condensates (sensitive to the condensate separation and the confining potential) and the intra-condensate interactions remain as defined in Chapter 3. A schematic of this coupling can be seen in Fig. 4.2. Income to the condensates occurs from a communal

reservoir as even though spatially separate they are both within the same excitation spot, therefore Eq. (3.14) continues to describe the time dynamics of the reservoir population.

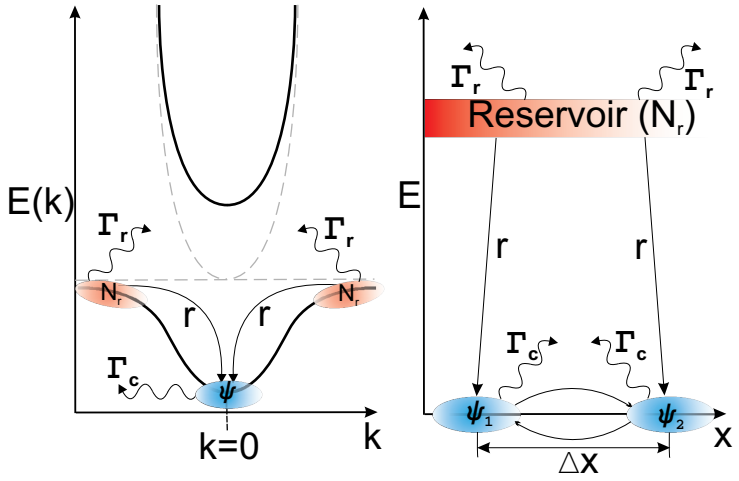

Figure 4.2: Schematic of polariton system showing the polariton dispersion in k-space (left) and the real space layout of two Josephson coupled condensates with a separation of Δx (right). The scale for E is not the same for both diagrams. Both ground state condensates are fed by a common reservoir with $N_r(t)$ polaritons on the exciton-like part of the dispersion and are Josephson coupled with coherence hopping parameter J.

4.2 Polarisation Correlation and Phase Coherence

The introduction of the Josephson coupling between two condensates is first shown in the symmetric case i.e., $H_s = 0$. With the extension to two condensates it is convenient to alter the notation for the prospect of many condensates. The condensate pseudospin (and Stokes parameters of the emitted light, which are accessible experimentally) can be defined in terms of the

Pauli matrices $\boldsymbol{\sigma}$ as

$$\mathbf{S}_i = (1/2)(\psi_i^\dagger \cdot \boldsymbol{\sigma} \cdot \psi_i), \tag{4.10}$$

where we define spinors $\psi_i = (\psi_{i+}, \psi_{i-})^{\mathrm{T}}$. In the calculations the numerical parameters used are $\Gamma_c = 0.5\,\mathrm{ps}^{-1}$, $\Gamma_r/\Gamma_c = 0.01$, $\alpha_1 = 1.8\,\mu\mathrm{eV}$, $\alpha_2/\alpha_1 = -0.1$, $\gamma = 1\,\mathrm{meV}^{-1}\mathrm{ps}^{-1}$, $J = 10\hbar\Gamma_r$ and $r = 10^{-4}\,\mathrm{ps}^{-1}$. The value of J varies in large limits as the distance between two condensates changes. It ranges from zero (corresponding to the infinitely remote condensates) to about 1 meV, which is the characteristic localisation energy of a condensate of exciton polaritons. We have taken $J = 0.03$meV, which is two orders of magnitude less than the localisation energy. The corresponding tunneling time between two condensates is about 20 ps, which is an order of magnitude longer than the exciton-polariton life-time. This is a characteristic value for the weak coupling regime of two condensates corresponding to a spatial separation on the order of several micrometers.

The most convenient way to evidence locking of random polarisations generated by the two localized condensates is by direct measurement of the two-emitter polarisation correlator,

$$S_{corr}(t) = \sqrt{\left| \left\langle \frac{(\mathbf{S}_1(t)\mathbf{S}_2(t))}{|S_1(t)||S_2(t)|} \right\rangle \right|} \tag{4.11}$$

where the denominator represents normalization by the condensate populations. $S_{corr}(t)$ changes between 0 for uncorrelated polarisations and 1 for full correlation. It can be calculated for different values of P/P_{th}, where P_{th} is the threshold pump determined by the income and outcome rate of polaritons i.e. $\int P_{th} dt = \Gamma_c/r$. The results of these calculations are shown in Fig. 4.3 with the time resolved, ensemble averaged, population of the condensates (the population of each condensate is virtually identical as relaxation from the reservoir is equally probable). During the condensate formation, the polarisations and phases $\phi_{i\sigma} = \arg(\psi_{i\sigma})$ of the condensates are stochastically

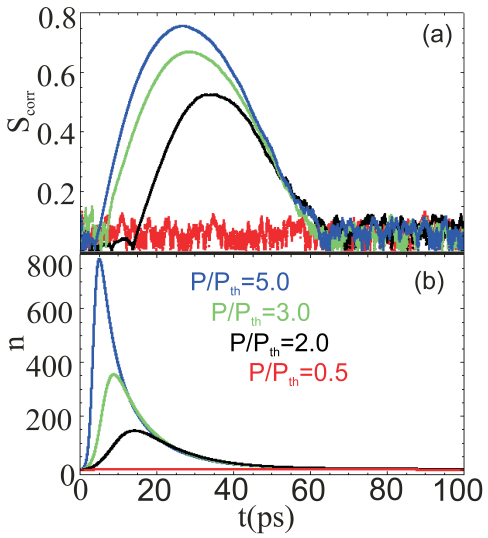

Figure 4.3: Below and above threshold time dynamics of the (a) polarisation correlator defined by Eq. (4.11), and (b) condensate occupation. The polarisation correlations are seen as long as the condensates are macroscopically occupied. The maximum degree of correlation is dependent on the condensate occupation.

chosen. The relationship between the two phases is an important quantity as correlations would evidence the build up of spatial coherence. To explore this relationship we look at the phase difference between the components of the order parameter, $\phi_{2\sigma} - \phi_{1\sigma}$. The probability density for this quantity is shown in Fig. 4.4 at 6 different times above threshold pumping.

When the condensate occupation is less than 1 the probability density as shown in Fig. 4.4 is that of the difference between two uniform random variables spanning the interval $-\pi$ to π, proof of which is in Appendix E. During the period of significant population (as can be seen in Fig. 4.3 (b)) the condensates have the greatest probability of assuming phase differences of π or $-\pi$, which are equivalent. We believe this phase difference is due to the rotation of the order parameter from the Josephson coupling. Because we are dealing with a stochastic process either condensate 1 or 2 will breach threshold occupation first and as the Josephson coupling enters our system as

an imaginary term this acts to shift the phase of the later forming condensate. This shift is by a factor $\pi/2$. Once the later forming condensate becomes macroscopically occupied it acts in the same way on the initially formed condensate and we see a total phase difference of π or $-\pi$. It can be seen from Fig. 4.4 that once the condensate occupation has decayed below 1 (for $t > 60\,\mathrm{ps}$) the distribution reverts to the same form as at $t = 1\,\mathrm{ps}$. A figure identical to Fig. 4.4 is obtained for the minus circularly polarized components of the condensates.

Below threshold no correlations are seen between the condensates, also the total polarisation degree of the condensates, which is directly proportional to their order parameters, is close to zero. There is no macroscopic population of the condensate as can be seen in Fig. 4.3 and therefore no Josephson current between them.

Above threshold the condensates populate macroscopically with a narrowing of the emission peak with increasing pump power. The polarisation degree approaches 1 (see Chapter 3) indicating a spontaneous symmetry breaking, the "smoking gun" for BEC. The polarisation correlator increases with increasing pump to a maximum value of $S_{corr}(t) \approx 0.75$. This evidences the polarisation locking of the two condensates due to the DC Josephson effect. Importantly, the lifetime of the correlation is roughly constant regardless of pump power, in opposition to the condensate occupations. This indicates that any macroscopic population of the condensates is enough for a significant polarisation locking effect between them. The spatial coherence builds up in a similar way, as evidenced by the results in Fig. 4.4. This shows that the spatial coherence and spontaneous polarisation both carry information on the order parameter of BEC. In systems of large size the build up of spatial coherence and of spontaneous polarisation equally characterize the BEC threshold. However, in small systems like pillar microcavities, phase correlations are present both below and above threshold, so that the sponta-

neous polarisation remains the only direct measure of the order parameter.

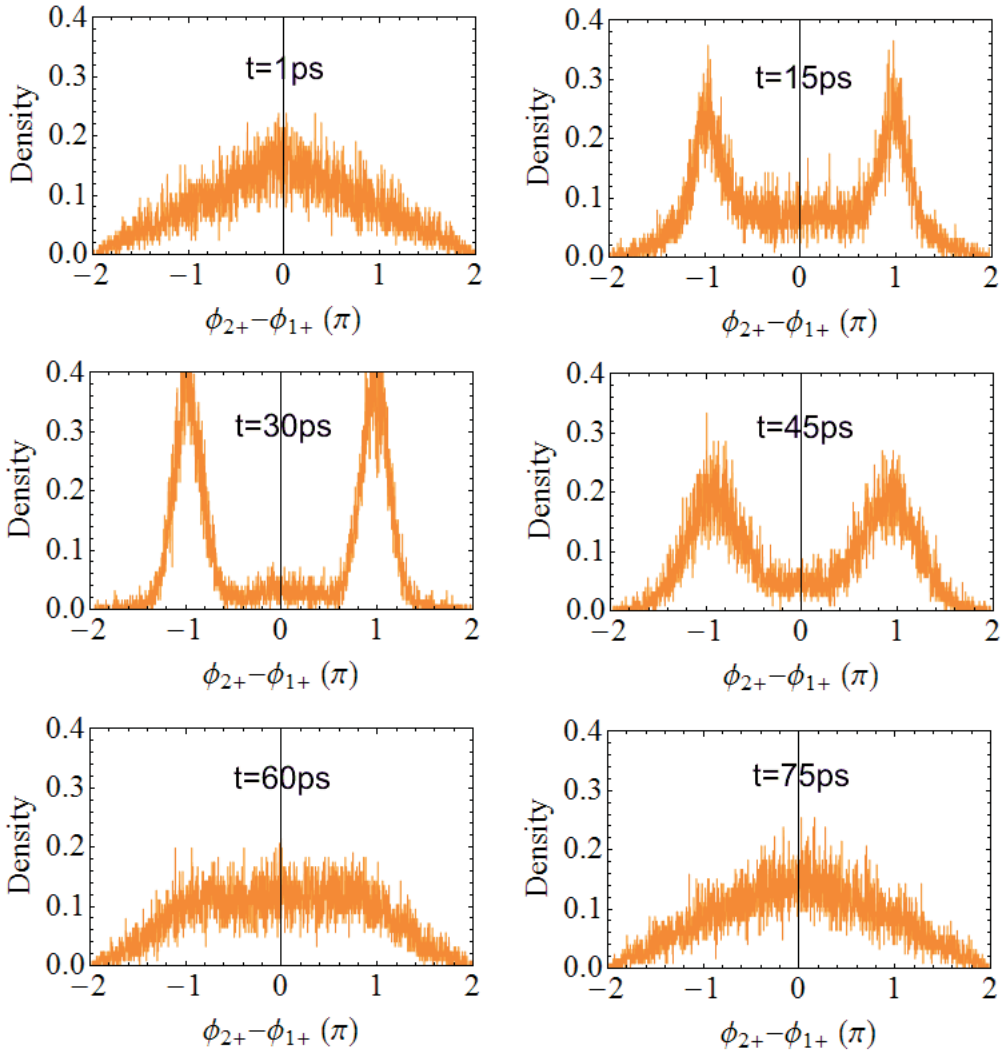

Figure 4.4: Probability density of phase difference between the two condensates at times before, during and after macroscopic occupation. For all times $P/P_{th} = 3.0$.

4.3 Introducing Effective Magnetic Fields

In experimental microcavity samples local strain effects and inhomogeneous photonic disorder produce effective magnetic fields acting upon the pseudospins of polaritons. An effective magnetic field of these origins splits the linearly polarized states of the condensate. If the two condensates experience the same splitting frequency Ω, but the fields are oriented differently, the splitting Hamiltonian is given by

$$H_s = -\hbar\Omega\left[(\mathbf{c}_1\mathbf{S}_1) + (\mathbf{c}_2\mathbf{S}_2)\right], \tag{4.12}$$

where unit vectors $\mathbf{c}_{1,2}$ define orientations of the fields.

The introduction of the local fields modifies the distribution function of the condensate polarisation as seen in Fig. 4.5. In this figure, points show the time-averaged values of the Stokes vector of the condensates for different realizations of the Langevin noise, corresponding to different excitation pulses. Here the splitting favors polarisations in the positive x- and y-directions for condensate 1 and 2, respectively. The splitting leads to a bias in the time integrated values of the polarisation and results in frustration of polarisation locking. As expected this produces a reduction in the polarisation correlation. The fields also introduce a bias in the phase relationship between the two condensates. $\phi_{2\sigma} - \phi_{1\sigma}$ becomes locked to either π or $-\pi$ depending on the pinning, which indicates that an antisymmetric solution for two Josephson coupled condensates corresponds to the minimum energy.

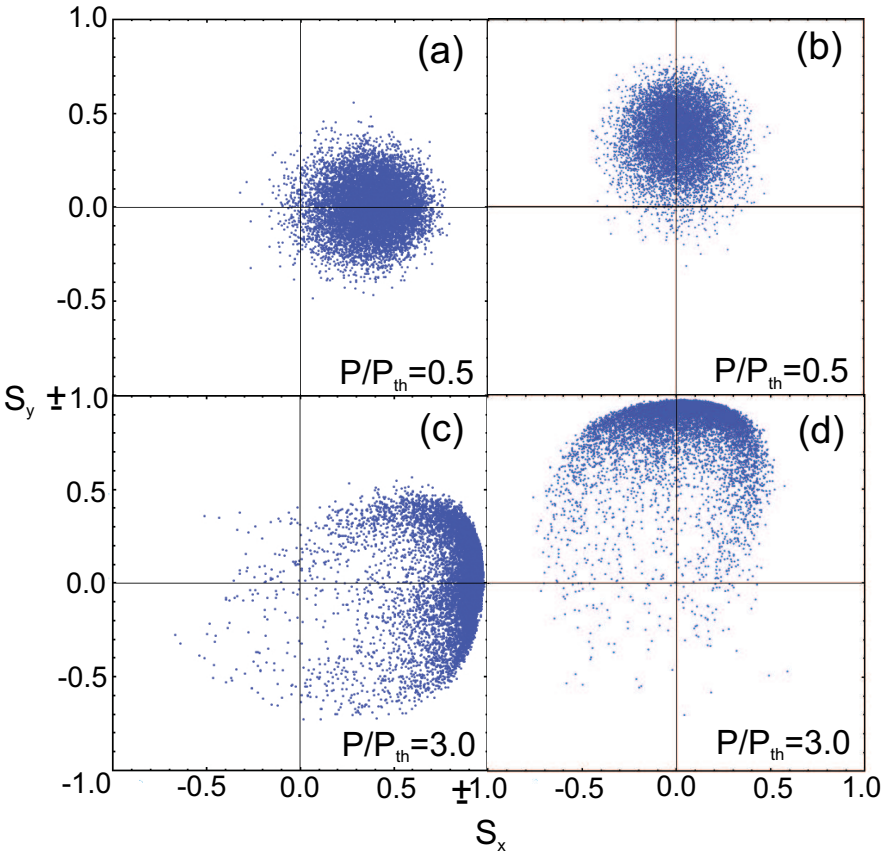

Figure 4.5: (a), (c) Time integrated polarisation for condensate 1 below and well above threshold, respectively, where polarisation is pinned to positive S_x. (b), (d) Corresponding results for condensate 2 where polarisation is pinned to positive S_y. The magnitude of applied effective fields is $\Omega = 1\text{ps}^{-1}$.

4.4 Slow Energy Relaxation of Condensate

We now consider the case where energy relaxation is slow and can be neglected over the lifetime of the condensate. To describe this regime we remove the final term of Eq. (4.6). Here the polarisation correlation is not observed below or above threshold. This can be illustrated by considering the states 1 and 2 when the polaritons are condensed. If there is no tunneling between the states ($J = 0$) then the order parameters are uncorrelated, $\langle \psi_1^\dagger \cdot \psi_2 \rangle = 0$. One can show that any linear combinations of ψ_1 and ψ_2, $\zeta_1 = u_{11}\psi_1 + u_{12}\psi_2$ and $\zeta_2 = u_{21}\psi_1 + u_{22}\psi_2$, are also uncorrelated provided the u-coefficients form a unitary matrix [2].

If Josephson tunneling is turned on, $J \neq 0$, the result is unchanged. In particular, the symmetric and antisymmetric states, $(\psi_1 \pm \psi_2)/\sqrt{2}$ are uncoupled and therefore uncorrelated. The unitary transformations of these states, in particular, ψ_1 and ψ_2 are also uncorrelated. Physically it means that any combination of the condensates wave functions can be spontaneously formed. The role of relaxation is to bring the system into a particular state that minimizes the Hamiltonian energy, e.g., into the anti-symmetric $(\psi_1 - \psi_2)/\sqrt{2}$ state. No correlations are seen when the system randomly occupies symmetric and antisymmetric states, but they appear if the system relaxes into e.g. an anti-symmetric state. This theoretical argument is corroborated by numerical results.

[2] This statement becomes transparent if one defines the quantum mechanical internal product of two states as the statistical average of the two.

4.5 Summary

The definitive criterion for polariton BEC remains an issue of dispute. With the kinetic model we showed that the build up of the condensate macroscopic wavefunction is directly linked to a build up in the polarisation degree of emission. This is not enough for definitive proof of polariton BEC. Using the stochastic nature of the symmetry breaking phase transition we demonstrated that a randomly oriented condensate polarisation is a clear indicator for polariton BEC. Experimentally it was observed that condensate emission is fragmented within the emission spot but long-range spatial coherence and aligned polarisation vectors occur across condensates. By introducing the DC Josephson effect into the kinetic model, both the polarisation locking and spatial coherence can be explained. They manifest themselves as an increase in the polarisation correlator and correlation in the phase alignment respectively. Significant effects are seen at all times when the condensates are macroscopically occupied.

On the scale on which these events occur the polariton environment is in general inhomogeneous (as is clear from condensate fragmentation). In samples with spatially separated condensates it is expected that due to differing local strains each condensate may see differently oriented local fields. We take into account this effect and see the frustration of correlations due to pinning. We also show that energy relaxation is a necessary condition for correlations to exist. The results demonstrate that the build up of a common vector polarisation can be considered a criterion for appearance of a macroscopically coherent state in a system of localised polariton condensates. This criterion is as strict as the appearance of spatial coherence in a large size system and becomes more rigorous in the case of strongly localised condensates. Extension of the model to further condensates, coupled in different structures is an interesting future possibility.

Chapter 5

Conclusions

The field of polariton physics is an established but quickly evolving discipline. Considering the first experimental realisation of strong coupling in a semiconductor microcavity occurred only 18 years ago, the number of interesting physical effects demonstrated in this system is exceptional. From definitive demonstration of the bosonic nature of polaritons it was a brief gap before this was translated into the experimental realisation of polariton BEC. Room temperature polariton BEC is now a not uncommon occurrence (a feat unachievable in any other medium), polariton superfluids are regularly manipulated and polariton superconductivity could be just around the corner. It is almost a case of pick an effect and it can be done with polaritons. Even with this rapid progress (or perhaps as a result of it) the theoretical underpinnings of polariton dynamics are still a point of debate, with numerous models in a state of contention or cooperation depending on which experiment they are being applied to. In this thesis, the polarisation properties of polaritons have been studied theoretically in an attempt to provide a practical insight into what is seen experimentally and shine some light on what underlies these breakthroughs.

Many attempts have been made to fully understand polariton-polariton scattering, but the quasiparticles composite nature makes this process highly nontrivial. The route considered in Chapter 2 begins with the scattering processes available to the fermionic exciton constituents and builds upon this with the photonic possibilities. To pin down specific results it is necessary to restrict the experimental geometry; in this case to a realistically sized elastic circle. For this case (i.e., small transferred momentum,q), the direct scattering matrix element is approximately proportional to q^3 and the exchange interaction virtually constant. The polarisation sensitive nature of polariton-polariton interactions is enough to produce effects such as depolarisation, polarisation conversion and spin currents in this relatively simple experimental geometry. These effects are tunable and the understanding gained from this approach translates into the ability to design and tune the cavity to see specific effects just using the scattering polarisation dependence.

In the low density regime it is appropriate to consider polaritons as good bosons with the interaction strength calculated phenomenologically on a case by case basis. Chapter 3, although ostensibly introducing a new model for the BEC of polaritons, provides insight into the effect of polariton-polariton interactions on the polarisation of condensate emission. The condensate order parameter was modeled using a stochastic Langevin type equation, in keeping with the phase breaking nature of polariton BEC. This formalism showed that a build up in the condensate polarisation degree is directly linked with an increase in the magnitude of the condensate order parameter. Interactions act to reduce the polarisation degree once the population is large enough for Larmor precession to dominate the polarisation dynamics. Stochastic choice of polarisation vector and a decrease of polarisation degree above threshold have been seen experimentally and the stochastic model successfully interprets these results with realistic parameters. In the case of efficient spin relaxation it was shown that a linearly polarised condensate is formed, agreeing with a number of other theoretical and experimental works.

The obvious extension to the stochastic model (which characterises a localised state) is the introduction of spatial dependence. In keeping with experimental results, this was implemented in Chapter 4 as a Josephson coupling between spatially separate localised condensates. The presence of this simple and intuitive coupling mechanism produced both polarisation and phase correlations between the condensates, providing a clear explanation for the polarisation locking and spatial coherence seen experimentally. Introducing local fields to the condensates modifies these correlations, inhibiting or amplifying them depending on the correlation between the pinning directions.

It is possible to summarise the main original results of this thesis as follows:

- Calculation of the small q dependence of direct and exchange matrix elements in polariton-polariton scattering.
- The prediction of depolarisation and spin currents on the elastic circle purely from the polariton scattering polarisation dependence.
- The proposal that the stochastic choice of polarisation vector characterises the BEC phase transition.
- The prediction of a decrease in polarisation degree due to polariton-polariton interactions, which was evidenced experimentally.
- The proposal of Josephson coupling as a mechanism for the build up of long range order in systems of localised polariton condensates.
- The demonstration that build up of a common vector polarisation is a more stringent condition for the appearance of a macroscopically coherent state in strongly localised condensates than spatial coherence.

Appendix A

Direct Scattering Term

The interaction term for direct scattering from state $i \rightarrow m$ and $j \rightarrow n$ is given by

$$\xi^{\mathrm{dir}}_{\mathrm{ij,mn}} = \frac{e^2}{4\pi\epsilon_0\epsilon_{\mathrm{r}}} X_i X_j X_m X_n \int \mathrm{d}\mathbf{R}_{e_1}\mathrm{d}\mathbf{R}_{e_2}\mathrm{d}\mathbf{R}_{h_1}\mathrm{d}\mathbf{R}_{h_2}\phi^*_m(\mathbf{R}_{e_1},\mathbf{R}_{h_1})\phi^*_n(\mathbf{R}_{e_2},\mathbf{R}_{h_2})\times \left(\sum_{\substack{\alpha_l,\beta_{l'} \\ l\neq l'}} V_{\alpha_l,\beta_{l'}}\right)\phi_i(\mathbf{R}_{e_1},\mathbf{R}_{h_1})\phi_j(\mathbf{R}_{e_2},\mathbf{R}_{h_2}). \tag{A.1}$$

Where the X are the exciton Hopfield coefficients for each state, $\mathbf{R}_\alpha$ are 3-dimensional vectors defined by the in-plane vectors $\mathbf{r}_\alpha$ and the coordinate z_α along the growth direction: $\mathbf{R}_\alpha \equiv (\mathbf{r}_\alpha, z_\alpha)$ The potentials $V_{\alpha\beta}$, $\alpha,\beta = e_l, h_{l'}$, $l, l' = 1, 2$ are given by

$$V_{\alpha\beta} = \pm\frac{1}{|\mathbf{R}_\alpha - \mathbf{R}_\beta|}, \tag{A.2}$$

with the minus sign for electron-hole attraction and the plus sign for for electron-electron and hole-hole repulsions. The exciton wavefunctions are

decomposed as the product of the plane wave describing the in-plane motion of the center of mass, the 2D relative wavefunction and the electron and hole envelope functions normal to the quantum well plane:

$$\phi_\nu(\mathbf{R}_{e_l},\mathbf{R}_{h_l}) = \frac{1}{\sqrt{S}}\exp(i\mathbf{k}_\nu\cdot\mathbf{R}_{X_l})\sqrt{\frac{8}{\pi a_B^2}}\exp\left(\frac{-2|\mathbf{r}_{e_l}-\mathbf{r}_{h_l}|}{a_B}\right)\times U_e(z_{e_l})U_h(z_{h_l}), \tag{A.3}$$

where $\mathbf{k}$ is the center of mass momentum, U are the envelope functions and $\mathbf{R}_{X_l}$ is the exction center of mass coordinate

$$\mathbf{R}_{X_l} = \frac{m_e\mathbf{r}_{e_l}+m_h\mathbf{r}_{h_l}}{m_e+m_h} = \gamma_e\mathbf{r}_{e_l}+\gamma_h\mathbf{r}_{h_l}. \tag{A.4}$$

Using these relations, Eq. (A.1) can be rewritten as

$$\xi = \sum_{\substack{\alpha_l,\beta_{l'}\\ l\neq l'}} \xi^{\mathrm{dir}}_{\alpha_l,\beta_l}, \tag{A.5}$$

where the function $\xi^{\mathrm{dir}}_{\alpha_l,\beta_l}$, is given by:

$$\begin{aligned}\xi^{\mathrm{dir}}_{\alpha_l,\beta_l} = \pm\int \mathrm{d}\mathbf{r}_{e_1}\mathrm{d}\mathbf{r}_{e_2}\mathrm{d}\mathbf{r}_{h_1}\mathrm{d}\mathbf{r}_{h_1}\Bigg[&\exp\left(\frac{-4|\mathbf{r}_{e_1}-\mathbf{r}_{h_1}|}{a_B}\right)\exp\left(\frac{-4|\mathbf{r}_{e_2}-\mathbf{r}_{h_2}|}{a_B}\right)\\ &\times\exp(-i\mathbf{k}_m\cdot\mathbf{R}_{X_1})\exp(-i\mathbf{k}_n\cdot\mathbf{R}_{X_2})\exp(i\mathbf{k}_i\cdot\mathbf{R}_{X_1})\exp(i\mathbf{k}_j\cdot\mathbf{R}_{X_2})\\ &\times\int_0^w \mathrm{d}z_{e_1}\mathrm{d}z_{e_2}\mathrm{d}z_{h_1}\mathrm{d}z_{h_2}\frac{U_e^2(z_{e_1})U_e^2(z_{e_2})U_h^2(z_{h_1})U_h^2(z_{h_2})}{\sqrt{|\mathbf{r}_{\alpha_l}-\mathbf{r}_{\beta_{l'}}|^2+(z_{\alpha_l}-z_{\beta_{l'}})^2}}\Bigg],\end{aligned} \tag{A.6}$$

where $l\neq l'$ and again the sign depends on the repulsive or attractive nature of the Coulomb interactions. Beginning with the repulsive term, $\xi^{\mathrm{dir}}_{e_1e_2}$ a quasi 2D effective Coulomb potential can be defined as

$$\int_0^w \mathrm{d}z_{e_1}\mathrm{d}z_{e_2}\mathrm{d}z_{h_1}\mathrm{d}z_{h_2}\frac{U_e^2(z_{e_1})U_e^2(z_{e_2})}{\sqrt{|\mathbf{r}_{\alpha_l}-\mathbf{r}_{\beta_{l'}}|^2+(z_{\alpha_l}-z_{\beta_{l'}})^2}} \tag{A.7}$$

to account for the finite carrier wavefunctions extent in the growth direction. The integral of the numerator leaves a trivial prefactor which is left aside for

now. Substituting $\mathbf{q} = \mathbf{k}_3 - \mathbf{k}_1$ the above equation then reduces to

$$V(\mathbf{q}) = f(\mathbf{q}, w) V_{2D}(\mathbf{q}), \tag{A.8}$$

in Fourier space, where the form factor $f(\mathbf{q}, w)$, with w the well width, can be written as

$$f(\mathbf{q}, w) = \frac{2}{w} \left[\frac{1}{q} + \frac{1}{2} \frac{qw^2}{q^2 w^2 + 4\pi^2} + (e^{-qw} - 1) \frac{1}{w} \left(\frac{1}{q} - \frac{qw^2}{q^2 w^2 + 4\pi^2} \right)^2 \right], \tag{A.9}$$

in the case of an infinitely deep QW and $V_{2D}(\mathbf{q})$ is the Fourier transform of the ideal 2D Coulomb potential, $V_{2D}(\mathbf{q}) \propto 1/q$. From these relations and conservation of momentum and energy it is possible to arrive at the form

$$\xi^{\mathrm{dir}}_{e_1 e_2} = f(\mathbf{q}, w) V_{2D}(\mathbf{q}) \tilde{\psi}^2(\gamma_h \mathbf{q}), \tag{A.10}$$

where $\tilde{\psi}^2(\gamma_h \mathbf{q})$ is the Fourier transform of the relative motion part of the 2D excitonic wavefunction

$$\tilde{\psi}^2(\gamma_h \mathbf{q}) = \left(1 + \frac{\gamma_h q^2 a_B^2}{16} \right)^{-3/2}. \tag{A.11}$$

A similar process results in the direct term for the hole-hole interaction

$$\xi^{\mathrm{dir}}_{h_1 h_2} = f(\mathbf{q}, w) V_{2D}(\mathbf{q}) \tilde{\psi}^2(\gamma_e \mathbf{q}). \tag{A.12}$$

As expected carrying out the same calculations for the attractive interactions (electron-hole) follows a similar process giving

$$\xi^{\mathrm{dir}}_{e_1 h_2} = \xi^{\mathrm{dir}}_{e_2 h_1} = -f(\mathbf{q}, w) V_{2D}(\mathbf{q}) \tilde{\psi}(\gamma_e \mathbf{q}) \tilde{\psi}(\gamma_h \mathbf{q}). \tag{A.13}$$

Summing the contributions from repulsive and attractive interactions

$$\xi^{\mathrm{dir}} = f(\mathbf{q}, q) V_{2D}(\mathbf{q}) \left(\tilde{\psi}(\gamma_e \mathbf{q}) - \tilde{\psi}(\gamma_h \mathbf{q}) \right)^2. \tag{A.14}$$

Appendix B

Langevin Equation

The master equation for a system is a differential equation describing the transition probability between states. In quantum mechanics the state occupation statistics are naturally defined in terms of the density matrix $\hat{\varrho}$. By assuming that polaritons leave and enter the condensate one at a time, the master equation for polariton BEC into one spatially localised state is given by

$$\frac{d\hat{\varrho}}{dt} = \frac{\mathrm{i}}{\hbar}[\hat{\varrho}, \hat{H}] - \frac{1}{2}\sum_{\sigma=\pm 1}\{W(t)(\hat{a}_\sigma \hat{a}_\sigma^\dagger \hat{\varrho} + \hat{\varrho}\hat{a}_\sigma \hat{a}_\sigma^\dagger - 2\hat{a}_\sigma^\dagger \hat{\varrho}\hat{a}_\sigma) + \Gamma_c(\hat{a}_\sigma^\dagger \hat{a}_\sigma \hat{\varrho} + \hat{\varrho}\hat{a}_\sigma^\dagger \hat{a}_\sigma - 2\hat{a}_\sigma \hat{\varrho}\hat{a}_\sigma^\dagger)\}. \quad \text{(B.1)}$$

where the relevant quantities are defined in Chapter 3. The first term characterises the density matrix evolution under the action of the Hamiltonian $\hat{H}$, while the second term has two components. The first part can be thought of as the product of the transition rate to the condensate, $W(t)$, and the probability of such a transition occurring. Equivalently the second term defines escape from the condensate.

The Hamiltonian $\hat{H}$ can be decomposed into two components, the ground state energy of the system and the interaction dynamics

$$\hat{H} = \hat{H}_0 + \hat{V}, \tag{B.2}$$

ignoring the polarisation degree of freedom the interaction contribution is simply

$$\hat{V} = V_0 \hat{a}^{\dagger 2} \hat{a}^2, \tag{B.3}$$

where V_0 is the interaction strength between polaritons. It is beneficial to derive the order parameter dynamics with just this term as the technique is similar for all terms. Under the assumption of purely self-interaction effects we can write

$$\frac{d\hat{\varrho}}{dt} = \frac{i}{\hbar}\left[\hat{\varrho}, \hat{V}\right] = \frac{i}{2}\frac{V_0}{\hbar}\left[\hat{\varrho}, \hat{a}^{\dagger 2}\hat{a}^2\right]. \tag{B.4}$$

It is convenient to write the density matrix in the Glauber-Surdarshan representation [158]

$$\hat{\varrho} = \int \mathcal{P}(\psi, \psi^*) \left|\psi\right\rangle\!\left\langle\psi\right| d^2\psi, \tag{B.5}$$

here $\mathcal{P}$ is the quasi-probability distribution. We define the coherent state as

$$\left|\psi\right\rangle = e^{\psi\hat{a}^\dagger - \psi^*\hat{a}} \left|0\right\rangle = e^{-\frac{1}{2}\psi\psi^*} e^{\psi\hat{a}^\dagger} \left|0\right\rangle \equiv e^{-\frac{1}{2}\psi\psi^*} \left|\psi\right\rangle \tag{B.6}$$

so that without normalisation $\left|\psi\right\rangle = e^{\psi\hat{a}^\dagger}\left|0\right\rangle$. Producing the following relations

$$\hat{a}\left|\psi\right\rangle = \psi\left|\psi\right\rangle, \tag{B.7a}$$

$$\hat{a}^\dagger\left|\psi\right\rangle = e^{-\frac{1}{2}\psi\psi^*}\hat{a}^\dagger\left|\psi\right\rangle = e^{-\frac{1}{2}\psi\psi^*}\frac{\partial}{\partial\psi}\left|\psi\right\rangle. \tag{B.7b}$$

Using Eq. (B.7), Eq. (B.4) can be rewritten

$$\frac{\partial\hat{\varrho}}{\partial t} = \frac{i}{2}\frac{V_0}{\hbar}\int e^{-\psi\psi^*}\mathcal{P}\left\{\psi^{*2}\frac{\partial^2}{\partial\psi^{*2}} - \psi^2\frac{\partial^2}{\partial\psi^2}\right\}\left|\psi\right\rangle\!\left\langle\psi\right| d^2\psi, \tag{B.8}$$

integrating by parts and substituting for $\hat{\varrho}$

$$\begin{aligned}
&\int \frac{\partial \mathcal{P}}{\partial t} |\psi\rangle\langle\psi| d^2\psi = \\
&= \frac{i}{2}\frac{V_0}{\hbar} \int |\psi\rangle\langle\psi| \left\{ \frac{\partial^2}{\partial \psi^{*2}} \left(\psi^{*2} e^{-\psi\psi^*} \mathcal{P} \right) - \frac{\partial^2}{\partial \psi^2} \left(\psi^2 e^{-\psi\psi^*} \mathcal{P} \right) \right\} d^2\psi \\
&= \frac{i}{2}\frac{V_0}{\hbar} \int |\psi\rangle\langle\psi| \left\{ 4 \left(\psi^* \frac{\partial \mathcal{P}}{\partial \psi^*} - \psi \frac{\partial \mathcal{P}}{\partial \psi} \right) \right. \\
&\qquad\qquad + \left(\psi^{*2} \frac{\partial^2 \mathcal{P}}{\partial \psi^{*2}} - \psi^2 \frac{\partial \mathcal{P}}{\partial \psi^2} \right) \\
&\qquad\qquad \left. - 2|\psi|^2 \left(\psi^* \frac{\partial \mathcal{P}}{\partial \psi^*} - \psi \frac{\partial \mathcal{P}}{\partial \psi} \right) \right\} d^2\psi \\
&= \frac{i}{2}\frac{V_0}{\hbar} \int |\psi\rangle\langle\psi| \left\{ 2 \left[\frac{\partial}{\partial \psi} \left(\psi^2 \psi^* \mathcal{P} \right) - \frac{\partial}{\partial \psi^*} \left(\psi \psi^{*2} \mathcal{P} \right) \right] \right. \\
&\qquad\qquad \left. + \left[\frac{\partial^2}{\partial \psi^{*2}} \left(\psi^{*2} \mathcal{P} \right) - \frac{\partial^2}{\partial \psi^2} \left(\psi^2 \mathcal{P} \right) \right] \right\} d^2\psi.
\end{aligned} \tag{B.9}$$

Which leads directly to the Fokker-Planck equation

$$\begin{aligned}
\frac{\partial \mathcal{P}}{\partial t} = \frac{i}{2}\frac{V_0}{\hbar} \Bigg\{ & 2 \left[\frac{\partial}{\partial \psi} \left(\psi^2 \psi^* \mathcal{P} \right) - \frac{\partial}{\partial \psi^*} \left(\psi \psi^{*2} \mathcal{P} \right) \right] \\
& + \left[\frac{\partial^2}{\partial \psi^{*2}} \left(\psi^{*2} \mathcal{P} \right) - \frac{\partial^2}{\partial \psi^2} \left(\psi^2 \mathcal{P} \right) \right] \Bigg\}.
\end{aligned} \tag{B.10}$$

It is possible to gain further physical insight by substituting ψ with it's complex expansion, $\psi = x + iy$, and the associated differentials

$$\frac{\partial}{\partial \psi} = \frac{1}{2} \left(\frac{\partial}{\partial x} - i \frac{\partial}{\partial y} \right), \tag{B.11}$$

$$\frac{\partial}{\partial \psi^*} = \frac{1}{2} \left(\frac{\partial}{\partial x} + i \frac{\partial}{\partial y} \right). \tag{B.12}$$

We start with the first term of Eq. (B.10), known as the drift term, containing

the first order differentials. Substituting Eq's. (B.11) we obtain

$$\frac{\partial \mathcal{P}}{\partial t} = \frac{i}{2}\frac{V_0}{\hbar}\Bigg\{ \left(\frac{\partial}{\partial x} - i\frac{\partial}{\partial y}\right)\left[\left(x^2+y^2\right)(x+iy)\,\mathcal{P}\right] - \left(\frac{\partial}{\partial x} + i\frac{\partial}{\partial y}\right)\left[\left(x^2+y^2\right)(x-iy)\,\mathcal{P}\right]\Bigg\} \quad \text{(B.13)}$$

which can be rearranged to

$$\frac{\partial \mathcal{P}}{\partial t} = -\frac{V_0}{\hbar}\frac{\partial}{\partial x}\left[\left(x^2+y^2\right) y\mathcal{P}\right] + \frac{V_0}{\hbar}\frac{\partial}{\partial y}\left[\left(x^2+y^2\right) x\mathcal{P}\right]. \quad \text{(B.14)}$$

From this representation the drift coefficients for the real and complex plane are clear,

$$v_x = \dot{x} = \frac{V_0}{\hbar}\left(x^2+y^2\right) y, \quad \text{(B.15)}$$

$$v_y = \dot{y} = -\frac{V_0}{\hbar}\left(x^2+y^2\right) x, \quad \text{(B.16)}$$

or equivalently

$$i\dot{\psi} = \frac{V_0}{\hbar}\left|\psi\right|^2\psi. \quad \text{(B.17)}$$

Beginning with only the polariton-polariton interaction term from the Hamiltonian, Eq. (B.3), the kinetic model has provided the same result as the Gross-Pitaevskii [38] equation for the interaction dynamics [133] as Eq. (B.17) can be rewritten

$$i\hbar\frac{\partial \psi}{\partial t} = \frac{\partial H_{p-p}}{\partial \psi^*}, \quad \text{(B.18)}$$

with $H_{p-p} = \frac{1}{2}V_0\psi^{*2}\psi^2$. A similar analysis can be carried out for the second term of Eq. (B.10) leading to the anomalous negative diffusion term discussed in Chapter 3, which becomes negligible for large occupations.

Returning to Eq. (3.2) a similar technique can be employed to derive a Fokker-Planck equation for the quasi-probability distribution starting with the second term i.e., the income and outgoing of particles from the conden-

sate. We obtain an equation of the same form as Eq. (B.10),

$$\frac{\partial \mathcal{P}}{\partial t} = \frac{1}{2}\left[\Gamma_c - W(t)\right]\left[\frac{\partial(\psi\mathcal{P})}{\partial\psi} + \frac{\partial(\psi^*\mathcal{P})}{\partial\psi^*}\right] + W(t)\frac{\partial^2\mathcal{P}}{\partial\psi\partial\psi^*}. \tag{B.19}$$

The last term in Eq. (B.19) describes the diffusion of ψ in the complex plane. The rate of diffusion is proportional to the income rate of polaritons, $W(t)$, therefore as long as particles are entering the condensate there will be fluctuations in the order parameter. It is possible to switch between Fokker-Planck type equations, which represent the time dynamics of the probability distribution of a stochastic process and Langevin type equations which directly model the dynamics of the process. The choice depends on which is more useful for the current application. In this case direct modeling of the order parameter is required and so Eq. (B.19) can be transformed to

$$\frac{d\psi}{dt} = -\frac{1}{2}\left[\Gamma_c - W(t)\right]\psi + \theta(t), \tag{B.20}$$

where $\theta(t)$ is random complex white noise with the correlators

$$\langle\theta(t)\theta(t')\rangle = 0, \tag{B.21}$$

$$\langle\theta(t)\theta^*(t')\rangle = \frac{1}{2}W(t)\delta(t-t'). \tag{B.22}$$

Combining the order parameter dynamics of Eq. (B.20) and Eq. (B.18) produces

$$\frac{d\psi}{dt} = \frac{1}{2}\left[W(t) - \Gamma_c\right]\psi + \theta(t) - \frac{i}{\hbar}\frac{\partial H_{p-p}}{\partial\psi^*}. \tag{B.23}$$

Applying the same derivation technique with a two component order parameter and the complete interaction Hamiltonian Eq. (3.12) produces Eq. (3.11), of which Eq. (B.23) is the spin-less equivalent.

Appendix C

Second Order Coherence

Coherence measurements for light require taking a series of two-time readings with a fixed time delay τ. The statistical average of the product of each pair of readings is the correlation function. The degree of first order temporal coherence is a measure of the electric field correlation,

$$g^{(1)}(\tau) = \frac{\langle E^*(t)E(t+\tau)\rangle}{\langle E^*(t)E^*(t)\rangle}, \tag{C.1}$$

where the quantity takes values between 0 and 1 due to the normalisation. Equivalently, the degree of second-order temporal coherence is a measure of intensity correlation,

$$g^{(2)}(\tau) = \frac{\langle I^*(t)I(t+\tau)\rangle}{I^2} = \frac{\langle E^*(t)E^*(t+\tau)E(t+\tau)E(t)\rangle}{\langle E^*(t)E(t)\rangle^2}, \tag{C.2}$$

where $I = \langle I(t)\rangle$. The allowed range for $g^{(2)}(\tau)$ is not as straightforward and is determined by two inequalities, both based on Cauchy's. Two intensity

measurements at times t and $t+\tau$ must satisfy

$$2I(t)I(t+\tau) \leq I(t)^2 + I(t+\tau)^2. \tag{C.3}$$

It is clear from Eq. (C.3) the following inequality must hold,

$$\left(\frac{I(t) + I(t+\tau) + \ldots + I(t+N\tau)}{N}\right)^2 \leq \frac{I(t)^2 + I(t+\tau)^2 + \ldots + I(t+N\tau)^2}{N} \tag{C.4}$$

for N intensity measurements. In terms of correlation functions,

$$I^2 \equiv \langle I(t)\rangle^2 \leq \left\langle I(t)^2\right\rangle, \tag{C.5}$$

from which for the case of $\tau = 0$ i.e., zero time delay, a lower bound for $g^{(2)}$ is obtained from Eq. (C.2)

$$g^{(2)}(0) \geq 1. \tag{C.6}$$

This derivation is applicable to the classical case, whereas for a single photon emitter, a strictly quantum device, $g^{(2)}(0) = 0$. Establishing an upper limit in generality for zero time is not possible and therefore the complete range is given by

$$\infty \geq g^{(2)}(0) \geq 1, \tag{C.7}$$

with the extension to $\tau > 0$ reducing the restrictions further to just positivity

$$\infty \geq g^{(2)}(\tau) \geq 0. \tag{C.8}$$

Far below threshold pumping emission from the polariton condensate is thermal in nature. Thermal light is a statistical ensemble of light beams with all possible amplitudes and phases. The probability distribution is defined by the random walk undergone by the amplitude and phase, resulting in

$$P[I(t)] = \frac{1}{I} e^{\frac{-I(t)}{I}}, \tag{C.9}$$

with statistical moments

$$\langle I(t)^r \rangle = \frac{1}{I} \int_0^\infty I(t)^r e^{\frac{-I(t)}{I}} dI(t) = r! I^r. \tag{C.10}$$

Using Eq. (C.10) for a single component thermal light source the zero time degree of second order coherence always assumes the value

$$g^{(2)}(0) = \frac{\langle I(t)^2 \rangle}{I^2} = 2. \tag{C.11}$$

Due to the two component nature of the condensate order parameter, specification of $g^{(2)}(0)$ requires extension to two distinct beams. The result is four degrees of second order coherence defined as

$$g^{(2)}_{\sigma,\sigma'}(t, t+\tau) = \frac{\langle I_\sigma(t) I_{\sigma'}(t+\tau) \rangle}{\langle I_\sigma(t) \rangle \langle I_{\sigma'}(t+\tau) \rangle}, \tag{C.12}$$

where $\sigma = \sigma'$ refers to same polarisation correlations and $\sigma \neq \sigma'$ correlations across polarisations. Condensate emission can be considered as a linear superposition of the two polarisations

$$\begin{aligned} I(t) &= I_{+1}(t) + I_{-1}(t) \\ &= |\psi_+(t)|^2 + |\psi_-(t)|^2 \\ &= n(t). \end{aligned} \tag{C.13}$$

Substituting Eq. (C.13) into Eq. (C.2)

$$g^{(2)}_{\pm}(\tau) = \frac{\langle (I_+(t) + I_-(t))(I_+(t+\tau) + I_-(t+\tau)) \rangle}{(I_+(t) + I_-(t))^2}, \tag{C.14}$$

which expands to

$$g^{(2)}_{\pm}(\tau) = \frac{\langle I_+(t)I_+(t+\tau)\rangle}{(I_+ + I_-)^2} + \frac{\langle I_-(t)I_-(t+\tau)\rangle}{(I_+ + I_-)^2} + \frac{\langle I_+(t)I_-(t+\tau)\rangle}{(I_+ + I_-)^2} + \frac{\langle I_-(t)I_+(t+\tau)\rangle}{(I_+ + I_-)^2}. \tag{C.15}$$

From Eq. (C.12)

$$g^{(2)}_{\pm}(\tau) = \frac{I_+^2 g^{(2)}_{+,+}(\tau) + I_-^2 g^{(2)}_{-,-}(\tau) + 2I_+I_-}{(I_+ + I_-)^2}. \tag{C.16}$$

Under the reasonable assumption of equal intensities and degrees of second order coherence for each polarisation, i.e., $g^{(2)}_{+,+}(\tau) = g^{(2)}_{-,-}(\tau)$ and $I_+ = I_-$, Eq. (C.16) simplifies to

$$g^{(2)}_{\pm}(\tau) = \frac{1}{2}\left(1 + g^{(2)}_{+,+}(\tau)\right). \tag{C.17}$$

From the earlier result, Eq. (C.11), it is therefore the case that for unpolarised thermal light in the limit $\tau = 0$

$$g^{(2)}_{\pm}(0) = \frac{3}{2}. \tag{C.18}$$

Appendix D

Pseudospin Dynamics

Here we discuss the dynamics of the pseudospin vector **S** in the region of high excitation densities, i.e., for the pump far above the stimulation threshold.

It is necessary to point out that, in general, there is no closed equation for the pseudospin vector. Such an equation cannot be obtained from Eq. (3.11) and definitions (3.15) because of the noise term in (3.11) that cannot be transformed into a term depending solely on **S**. Physically the absence of a closed equation for **S** is related to the fact that the pseudospin vector misses the information about the phase of the condensate and therefore does not provide the complete description of the system.

However, at high pump densities, i.e., far above the threshold, the relative fluctuations of the order parameter are small and the noise term can be omitted. Also, if we are interested in the dynamics of the order parameter on time scales where the condensate occupation does not change significantly, it is possible to neglect the (first) pump-decay term in (3.11) as well. Then

the order parameter evolves according to the Gross-Pitaevskii equation

$$\mathrm{i}\hbar\frac{d\psi_\sigma}{dt} = \frac{\delta\mathcal{H}}{\delta\psi_\sigma^*} = -\frac{1}{2}\hbar\Omega\sum_{\sigma'} C_{\sigma\sigma'}\psi_{\sigma'} + \left[\alpha_1|\psi_\sigma|^2\psi_\sigma + \alpha_2|\psi_{-\sigma}|^2\psi_\sigma\right]. \qquad \text{(D.1)}$$

This equation can be transformed to the equation for the pseudospin vector (3.15). Namely,

$$\frac{d\mathbf{S}}{dt} = \Omega[\mathbf{S}\times\mathbf{c}] + 2\frac{(\alpha_1-\alpha_2)}{\hbar}(\hat{\mathbf{z}}\cdot\mathbf{S})[\hat{\mathbf{z}}\times\mathbf{S}], \qquad \text{(D.2)}$$

where we used the definition of the 3D vector $\mathbf{c}$ from Eq. (3.4).

For low condensate occupation the nonlinear interaction term can be neglected and this equation describes the precession of the pseudospin vector $\mathbf{S}$ around the pinning direction $\mathbf{c}$. On the contrary, for large condensate occupation n the first term in (D.2) can be neglected and the self-induced Larmor precession around the $\hat{z}$-axis appears due to the polariton-polariton interaction. The angular velocity of this precession depends on the value of S_z, which is the reason for the appearance of the Larmor rings discussed in Chapter 3.

In the general case Eq. (D.2) also describes a periodic motion of the pseudospin. The value of $|\mathbf{S}|$ is conserved and the end of the vector $\mathbf{S}$ draws closed trajectories on the Poincaré sphere. To describe the experimentally relevant case of linearly polarized pinning we choose the pining direction $\mathbf{c}\|\hat{\mathbf{y}}$, as in subsection 3.2. Then, introducing the unit vector $\mathbf{s} = 2\mathbf{S}/n$ we have

$$\frac{1}{\Omega}\frac{ds_x}{dt} = -s_z - \lambda s_z s_y, \qquad \text{(D.3a)}$$

$$\frac{1}{\Omega}\frac{ds_y}{dt} = \lambda s_z s_x, \qquad \text{(D.3b)}$$

$$\frac{1}{\Omega}\frac{ds_z}{dt} = s_x, \qquad \text{(D.3c)}$$

where

$$\lambda = \frac{(\alpha_1 - \alpha_2)n}{\hbar\Omega}. \tag{D.4}$$

The solutions to Eqs. (D.3) can be expressed in terms of Jacobi's elliptic functions,

$$s_z = A\,\mathrm{cn}(\omega t, k^2), \tag{D.5a}$$

$$s_y = a + (1/2)\lambda s_z^2, \tag{D.5b}$$

$$s_x = -\omega A\,\mathrm{sn}(\omega t, k^2)\,\mathrm{dn}(\omega t, k^2), \tag{D.5c}$$

where the frequency ω, the elliptic modulus k, and the amplitude A can be found from

$$(\omega/\Omega)^4 = 1 + 2a\lambda + \lambda^2, \tag{D.6}$$

$$A^2 = \frac{2(1-a^2)}{(1+a\lambda) + \sqrt{1+2a\lambda+\lambda^2}}, \tag{D.7}$$

$$k^2 = \frac{1}{2}\left[1 - \frac{(1+a\lambda)}{\sqrt{1+2a\lambda+\lambda^2}}\right]. \tag{D.8}$$

The number a in above equations is a free parameter that is defined by the initial condition. For the weak interaction case, when $0 < \lambda < 1$, one has $-1 < a < 1$ and all the pseudospin trajectories cross the equatorial plane of the Poincaré sphere, so that one has a deformed precession around **c**-axis. When $\lambda > 1$, the parameter a can be smaller than -1, namely, $-(1+\lambda^2)/2\lambda < a < 1$. The trajectories for $a < -1$ never reach the equator of the Poincaré sphere and they describe the precession analogous to the self-induced Larmor precession[1]. The precession axis, however, is inclined with respect to the $\hat{z}$-direction (see Fig. D.1).

[1]Note that for the case $\lambda > 1$ and $a < -1$ the solution for s_z is numerically better calculated from the expression $s_z = A\,\mathrm{dn}(k\omega t, k^{-2})$, which is equivalent to Eq. (D.5a)

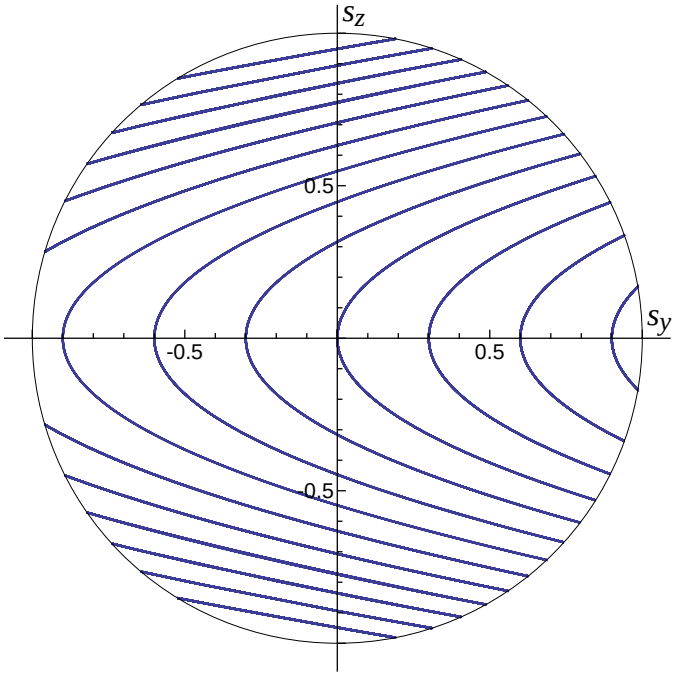

Figure D.1: Showing the projections on the yz-plane of several trajectories drawn by the end of the pseudospin vector on the Poincaré sphere for the case of combined precession discussed in Appendix. The trajectories are defined by the parameter a ranging from -2.7 to 0.9 in increments of 0.3. The interaction parameter $\lambda = 6$.

Appendix E

Difference of Independent Random Variables

When we are looking at the phase difference of the two Josephson coupled condensates it is important to show that the distribution obtained below threshold is that of the difference of two uniformly distributed independent variables. We start with the general case of two independent continuous random variables, X and Y, with probability density functions f_X and f_Y respectively. The cumulative distribution function of $X - Y$, F_{X-Y} is obtained as follows:

$$\begin{aligned} F_{X-Y}(a) &= P\{X - Y \leq a\} \\ &= \iint\limits_{x-y\leq a} f_X(x) f_Y(y)\,\mathrm{d}x\,\mathrm{d}y \\ &= \int_{-\infty}^{\infty}\int_{-\infty}^{a+y} f_X(x) f_Y(y)\,\mathrm{d}x\,\mathrm{d}y \\ &= \int_{-\infty}^{\infty}\int_{-\infty}^{a+y} f_X(x)\,\mathrm{d}x\, f_Y(y)\,\mathrm{d}y \end{aligned}$$

$$= \int_{-\infty}^{\infty} F_X(a+y) f_Y(y)\, dy \tag{E.1}$$

The probability density function f_{X-Y} of $X-Y$ is reached by differentiation of Eq. (E.1),

$$\begin{aligned} f_{X-Y}(a) &= \frac{\mathrm{d}}{\mathrm{d}a} \int_{-\infty}^{\infty} F_X(a+y) f_Y(y)\, \mathrm{d}y \\ &= \int_{-\infty}^{\infty} \frac{\mathrm{d}}{\mathrm{d}a} F_X(a+y) f_Y(y)\, \mathrm{d}y \\ &= \int_{-\infty}^{\infty} f_X(a+y) f_Y(y)\, \mathrm{d}y \end{aligned} \tag{E.2}$$

This can be applied to our specific case of the phase difference in the $\sigma = +1$ component of condensate 1 and 2 i.e., ϕ_{1+} and ϕ_{2+} respectively. We assume that below threshold they are independent uniform random variables distributed on $[-\pi, \pi]$,

$$f_{\phi_{1+}} = f_{\phi_{2+}} = \begin{cases} \frac{1}{2\pi} & -\pi < a < \pi \\ 0 & \text{otherwise} \end{cases} \tag{E.3}$$

From Eq. (E.2) we obtain

$$f_{\phi_{2+}-\phi_{1+}}(a) = \int_{-\pi}^{\pi} f_{\phi_{1+}}(a + \Phi_{2+})\, \mathrm{d}\Phi_{2+}. \tag{E.4}$$

For $-2\pi \leq a \leq 0$, this yields

$$f_{\phi_{2+}-\phi_{1+}}(a) = \frac{1}{4\pi^2} \int_{-(a+\pi)}^{\pi} \mathrm{d}\Phi_{2+} = \frac{1}{4\pi^2}(2\pi + a). \tag{E.5}$$

Similarly for $0 < a \leq 2\pi$ we get

$$f_{\phi_{2+}-\phi_{1+}}(a) = \frac{1}{4\pi^2} \int_{-\pi}^{\pi-a} \mathrm{d}\Phi_{2+} = \frac{1}{4\pi^2}(2\pi - a). \tag{E.6}$$

Combining these produces the distribution function for $\phi_{1+} - \phi_{2+}$,

$$f_{\phi_{2+}-\phi_{1+}}(a) = \frac{1}{4\pi^2} \begin{cases} 2\pi + a & -2\pi \leq a \leq 0 \\ 2\pi - a & 0 < a \leq 2\pi \\ 0 & \text{otherwise} \end{cases} \tag{E.7}$$

Plotting this result we obtain Fig. E.1. Which matches the theoretical results for $t = 1$ps shown in Fig. 4.4 and confirms that below threshold the condensate phases can be considered as uniformly distributed random variables as expected from the symmetry breaking nature of the phase transition.

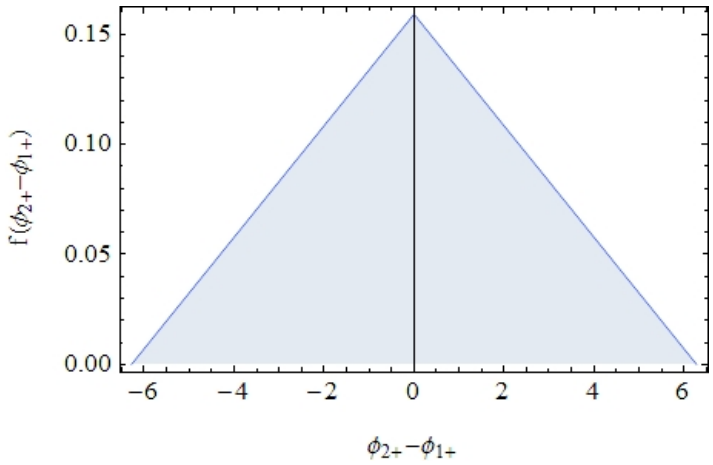

Figure E.1: Distribution function of the difference of two uncorrelated uniform random variables.

Bibliography

[1] R. Dingle, W. Wiegmann, and C. H. Henry, "Quantum states of confined carriers in very thin $Al_xGa_{1-x}As$-GaAs-$Al_xGa_{1-x}As$ heterostructures", *Physical Review Letters*, vol. **33**, pp. 827, (1974).

[2] J. Cibert, P. M. Petroff, G. J. Dolan, S. J. Pearton, A. C. Gossard, and J. H. English, "Optically detected carrier confinement to one and zero dimension in GaAs quantum well wires and boxes", *Applied Physics Letters*, vol. **49**, pp. 1275, (1986).

[3] M. A. Reed, J. N. Randall, R. J. Aggarwal, R. J. Matyi, T. M. Moore, and A. E. Wetsel, "Observation of discrete electronic states in a zero-dimensional semiconductor nanostructure", *Physical Review Letters*, vol. **60**, pp. 535, (1988).

[4] J. N. Holonyak and S. F. Bevacqua, "Coherent (visible) light emission from $Ga(As_{1-x}P_x)$ junctions", *Applied Physics Letters*, vol. **1**, pp. 82, (1962).

[5] R. D. Dupuis, P. D. Dapkus, J. N. Holonyak, E. A. Rezek, and R. Chin, "Room-temperature laser operation of quantum-well $Ga_{1-x}Al_xAs$-GaAs laser diodes grown by metalorganic chemical vapor deposition", *Applied Physics Letters*, vol. **32**, pp. 295, (1978).

[6] H. Soda, K. Iga, C. Kitahara, and Y. Suematsu, "GaInAsP/InP surface emitting injection-lasers", *Japanese Journal of Applied Physics*, vol. **18**, pp. 2329, (1979).

[7] J. Frenkel, "On the transformation of light into heat in solids. I", *Physical Review*, vol. **37**, pp. 17, (1931).

[8] G. H. Wannier, "The structure of electronic excitation levels in insulating crystals", *Physical Review*, vol. **52**, pp. 191, (1937).

[9] N. F. Mott, "Conduction in polar crystals. II. The conduction band and ultra-violet absorption of alkali-halide crystals", *Transcripts of the Faraday Society*, vol. **34**, (1938).

[10] J. J. Hopfield, "Theory of the contribution of excitons to the complex dielectric constant of crystals", *Physical Review*, vol. **112**, pp. 1555, (1958).

[11] Y. Zhu, D. J. Gauthier, S. E. Morin, Q. Wu, H. J. Carmichael, and T. W. Mossberg, "Vacuum Rabi splitting as a feature of linear-dispersion theory: Analysis and experimental observations", *Physical Review Letters*, vol. **64**, pp. 2499, (1990).

[12] A. Kavokin, J. J. Baumberg, G. Malpuech, and F. P. Laussy, *Microcavities*, Oxford University Press, Oxford, (2007).

[13] A. Kavokin and B. Gil, "GaN microcavities: Giant Rabi splitting and optical anisotropy", *Applied Physics Letters*, vol. **72**, pp. 2880, (1998).

[14] C. Weisbuch, M. Nishioka, A. Ishikawa, and Y. Arakawa, "Observation of the coupled exciton-photon mode splitting in a semiconductor quantum microcavity", *Physical Review Letters*, vol. **69**, pp. 3314, (1992).

[15] P. G. Savvidis, J. J. Baumberg, R. M. Stevenson, M. S. Skolnick, D. M. Whittaker, and J. S. Roberts, "Angle-resonant stimulated polariton amplifier", *Physical Review Letters*, vol. **84**, pp. 1547, (2000).

[16] R. Huang, F. Tassone, and Y. Yamamoto, "Stimulated scattering of excitons into microcavity polaritons", *Microelectronic Engineering*, vol. **47**, pp. 325, (1999).

[17] A. Imamoglu, R. J. Ram, S. Pau, and Y. Yamamoto, "Nonequilibrium condensates and lasers without inversion: Exciton-polariton lasers", *Physical Review A*, vol. **53**, pp. 4250, (1996).

[18] M. Kira, F. Jahnke, S. W. Koch, J. D. Berger, D. V. Wick, T. R. Nelson, G. Khitrova, and H. M. Gibbs, "Quantum theory of nonlinear semiconductor microcavity luminescence explaining "Boser" experiments", *Physical Review Letters*, vol. **79**, pp. 5170, (1997).

[19] F. Tassone and Y. Yamamoto, "Exciton-exciton scattering dynamics in a semiconductor microcavity and stimulated scattering into polaritons", *Physical Review B*, vol. **59**, pp. 10830, (1999).

[20] P. Senellart and J. Bloch, "Nonlinear emission of microcavity polaritons in the low density regime", *Physical Review Letters*, vol. **82**, pp. 1233, (1999).

[21] F. Quochi, G. Bongiovanni, A. Mura, J. L. Staehli, B. Deveaud, R. P. Stanley, U. Oesterle, and R. Houdré, "Strongly driven semiconductor microcavities: From the polariton doublet to an ac stark triplet", *Physical Review Letters*, vol. **80**, pp. 4733, (1998).

[22] F. Quochi, C. Ciuti, G. Bongiovanni, A. Mura, M. Saba, U. Oesterle, M. A. Dupertuis, J. L. Staehli, and B. Deveaud, "Strong coherent gain from semiconductor microcavities in the regime of excitonic saturation", *Physical Review B*, vol. **59**, pp. R15594, (1999).

[23] C. Ciuti, P. Schwendimann, and A. Quattropani, "Parametric luminescence of microcavity polaritons", *Physical Review B*, vol. **63**, pp. 041303, (2001).

[24] I. A. Shelykh, A. V. Kavokin, Y. G. Rubo, T. C. H. Liew, and G. Malpuech, "Polariton polarization-sensitive phenomena in planar semiconductor microcavities", *Semiconductor Science and Technology*, vol. **25**, pp. 013001, (2010).

[25] T. C. H. Liew and V. Savona, "Single photons from coupled quantum modes", *Physical Review Letters*, vol. **104**, pp. 183601, (2010).

[26] E. del Valle, D. Sanvitto, A. Amo, F. P. Laussy, R. André, C. Tejedor, and L. Via, "Dynamics of the formation and decay of coherence in a polariton condensate", *Physical Review Letters*, vol. **103**, pp. 096404, (2009).

[27] J. Keeling, "Polarized polariton condensates and coupled xy models", *Physical Review B*, vol. **78**, pp. 205316, (2008).

[28] F. M. Marchetti, M. H. Szymańska, J. M. J. Keeling, J. Kasprzak, R. Andr, P. B. Littlewood, and L. Si Dang, "Phase diagram for condensation of microcavity polaritons: From theory to practice", *Physical Review B*, vol. **77**, pp. 235313, (2008).

[29] A. Verger, I. Carusotto, and C. Ciuti, "Quantum Monte Carlo study of ring-shaped polariton parametric luminescence in a semiconductor microcavity", *Physical Review B*, vol. **76**, pp. 115324, (2007).

[30] M. Wouters, "Synchronized and desynchronized phases of coupled nonequilibrium exciton-polariton condensates", *Physical Review B*, vol. **77**, pp. 121302, (2008).

[31] M. Maragkou, A. J. D. Grundy, E. Wertz, A. Lemaître, I. Sagnes, P. Senellart, J. Bloch, and P. G. Lagoudakis, "Spontaneous nonground state polariton condensation in pillar microcavities", *Physical Review B*, vol. **81**, pp. 081307, (2010).

[32] K. G. Lagoudakis, T. Ostatnicky, A. V. Kavokin, Y. G. Rubo, R. Andre, and B. Deveaud-Pledran, "Observation of half-quantum vortices in an exciton-polariton condensate", *Science*, vol. **326**, pp. 974, (2009).

[33] D. Bajoni, D. Gerace, M. Galli, J. Bloch, R. Braive, I. Sagnes, A. Miard, A. Lemaître, M. Patrini, and L. C. Andreani, "Exciton polaritons in two-dimensional photonic crystals", *Physical Review B*, vol. **80**, pp. 201308, (2009).

[34] T. Byrnes, P. Recher, and Y. Yamamoto, "Mott transitions of exciton polaritons and indirect excitons in a periodic potential", *Physical Review B*, vol. **81**, pp. 205312, (2010).

[35] C. Xiong, P. R. Edwards, G. Christmann, E. Gu, M. D. Dawson, J. J. Baumberg, R. W. Martin, and I. M. Watson, "High-reflectivity GaN/air vertical distributed bragg reflectors fabricated by wet etching of sacrificial AlInN layers", *Semiconductor Science and Technology*, vol. **25**, pp. 032001, (2010).

[36] J. Levrat, R. Butté, T. Christian, M. Glauser, E. Feltin, J. F. Carlin, N. Grandjean, D. Read, A. V. Kavokin, and Y. G. Rubo, "Pinning and depinning of the polarization of exciton-polariton condensates at room temperature", *Physical Review Letters*, vol. **104**, pp. 166402, (2010).

[37] A. Kavokin and G. Malpuech, *Cavity Polaritons*, Elsevier, Amsterdam, (2003).

[38] L. Pitaevakii and S. Stringari, "The ideal Bose gas", in *Bose-Einstein Condensation*. Oxford University Press, Oxford, —2003—.

[39] J. M. Kosterlitz and D. J. Thouless, "Ordering, metastability and phase transitions in two-dimensional systems", *Journal of Physics C: Solid State Phys*, vol. **6**, (1972).

[40] D. S. Fisher and P. C. Hohenberg, "Dilute Bose gas in two dimensions", *Physical Review B*, vol. **37**, pp. 4936, (1988).

[41] P. G. Savvidis, C. Ciuti, J. J. Baumberg, D. M. Whittaker, M. S. Skolnick, and J. S. Roberts, "Off-branch polaritons and multiple scattering in semiconductor microcavities", *Physical Review B*, vol. **64**, pp. 075311, (2001).

[42] A. I. Tartakovskii, M. Emam-Ismail, R. M. Stevenson, M. S. Skolnick, V. N. Astratov, D. M. Whittaker, J. J. Baumberg, and J. S. Roberts, "Relaxation bottleneck and its suppression in semiconductor microcavities", *Physical Review B*, vol. **62**, pp. R2283, (2000).

[43] R. M. Stevenson, V. N. Astratov, M. S. Skolnick, D. M. Whittaker, M. Emam-Ismail, A. I. Tartakovskii, P. G. Savvidis, J. J. Baumberg, and J. S. Roberts, "Continuous wave observation of massive polariton redistribution by stimulated scattering in semiconductor microcavities", *Physical Review Letters*, vol. **85**, pp. 3680, (2000).

[44] J. J. Baumberg, P. G. Savvidis, R. M. Stevenson, A. I. Tartakovskii, M. S. Skolnick, D. M. Whittaker, and J. S. Roberts, "Parametric oscillation in a vertical microcavity: A polariton condensate or micro-optical parametric oscillation", *Physical Review B*, vol. **62**, pp. R16247, (2000).

[45] M. Saba, C. Ciuti, J. Bloch, V. Thierry-Mieg, R. André, L. S. Dang, S. Kundermann, A. Mura, G. Bongiovanni, J. L. Staehli, and B. Deveaud, "High-temperature ultrafast polariton parametric amplification in semiconductor microcavities", *Nature*, vol. **414**, pp. 731, (2001).

[46] A. I. Tartakovskii, D. N. Krizhanovskii, D. A. Kurysh, V. D. Kulakovskii, M. S. Skolnick, and J. S. Roberts, "Polariton parametric scattering processes in semiconductor microcavities observed in continuous wave experiments", *Physical Review B*, vol. **65**, pp. 081308, (2002).

[47] P. Kapitza, "Viscosity of liquid helium below the lambda-point", *Nature*, vol. **141**, pp. 74, (1938).

[48] J. F. Allen and A. D. Misener, "Flow of liquid helium II", *Nature*, vol. **141**, pp. 75, (1938).

[49] M. H. Anderson, J. R. Ensher, M. R. Matthews, C. E. Wieman, and E. A. Cornell, "Observation of Bose-Einstein condensation in a dilute atomic vapor", *Science*, vol. **269**, pp. 198, (1995).

[50] K. B. Davis, M. O. Mewes, M. R. Andrews, N. J. van Druten, D. S. Durfee, D. M. Kurn, and W. Ketterle, "Bose-Einstein condensation in a gas of sodium atoms", *Physical Review Letters*, vol. **75**, pp. 3969, (1995).

[51] A. L. Ivanov, P. B. Littlewood, and H. Haug, "Bose-Einstein statistics in thermalization and photoluminescence of quantum-well excitons", *Physical Review B*, vol. **59**, pp. 5032, (1999).

[52] L. V. Butov, A. L. Ivanov, A. Imamoglu, P. B. Littlewood, A. A. Shashkin, V. T. Dolgopolov, K. L. Campman, and A. C. Gossard, "Stimulated scattering of indirect excitons in coupled quantum wells: Signature of a degenerate Bose-gas of excitons", *Physical Review Letters*, vol. **86**, pp. 5608, (2001).

[53] L. V. Butov, C. W. Lai, A. L. Ivanov, A. C. Gossard, and D. S. Chemla, "Towards Bose-Einstein condensation of excitons in potential traps", *Nature*, vol. **417**, pp. 47, (2002).

[54] C. Monney, E. F. Schwier, M. G. Garnier, N. Mariotti, C. Didiot, H. Beck, P. Aebi, H. Cercellier, J. Marcus, C. Battaglia, H. Berger, and A. N. Titov, "Temperature-dependent photoemission on 1T-TiSe2: Interpretation within the exciton condensate phase model", *Physical Review B*, vol. **81**, pp. 9, (2010).

[55] Y. Barlas, R. Cote, J. Lambert, and A. H. MacDonald, "Anomalous exciton condensation in graphene bilayers", *Physical Review Letters*, vol. **104**, pp. 4, (2010).

[56] H. Stolz and D. Semkat, "Unique signatures for Bose-Einstein condensation in the decay luminescence lineshape of weakly interacting excitons in a potential trap", *Physical Review B*, vol. **81**, pp. 081302, (2010).

[57] I. A. Shelykh, D. D. Solnyshkov, G. Pavlovic, and G. Malpuech, "Josephson effects in condensates of excitons and exciton polaritons", *Physical Review B*, vol. **78**, pp. 4, (2008).

[58] G. Malpuech, A. Di Carlo, A. Kavokin, J. J. Baumberg, M. Zamfirescu, and P. Lugli, "Room-temperature polariton lasers based on GaN microcavities", *Applied Physics Letters*, vol. **81**, pp. 412, (2002).

[59] P. G. Savvidis and P. G. Lagoudakis, "Teaching polaritons new tricks", *Semiconductor Science and Technology*, vol. **18**, pp. S311, (2003).

[60] M. H. Szymańska and P. B. Littlewood, "The crossover between lasing and polariton condensation in optical microcavities", *Solid State Communications*, vol. **124**, pp. 103, (2002).

[61] D. Porras, C. Ciuti, J. J. Baumberg, and C. Tejedor, "Polariton dynamics and bose-Einstein condensation in semiconductor microcavities", *Physical Review B*, vol. **66**, pp. 85304, (2002).

[62] J. Kasprzak, M. Richard, S. Kundermann, A. Baas, P. Jeambrun, J. M. J. Keeling, R. André, J. L. Staehli, V. Savona, P. B. Littlewood, B. Deveaud, and L. S. Dang, "Bose-Einstein condensation of exciton polaritons", *Nature*, vol. **443**, pp. 409, (2006).

[63] D. Hui, D. Press, S. Gotzinger, G. S. Solomon, R. Hey, K. H. Ploog, and Y. Yamamoto, "Quantum degenerate exciton-polaritons in thermal equilibrium", *Physical Review Letters*, vol. **97**, pp. 146402, (2006).

[64] R. Balili, V. Hartwell, D. Snoke, L. Pfeiffer, and K. West, "Bose-Einstein condensation of microcavity polaritons in a trap", *Science*, vol. **316**, pp. 1007, (2007).

[65] D. N. Krizhanovskii, D. M. Whittaker, R. A. Bradley, K. Guda, D. Sarkar, D. Sanvitto, L. Vina, E. Cerda, P. Santos, K. Biermann, R. Hey, and M. S. Skolnick, "Effect of interactions on vortices in a nonequilibrium polariton condensate", *Physical Review Letters*, vol. **104**, pp. 4, (2010).

[66] G. Nardin, K. G. Lagoudakis, M. Wouters, M. Richard, A. Baas, R. André, L. S. Dang, B. Pietka, and B. Deveaud-Pledran, "Dynamics of long-range ordering in an exciton-polariton condensate", *Physical Review Letters*, vol. **103**, pp. 4, (2009).

[67] E. Wertz, L. Ferrier, D. D. Solnyshkov, P. Senellart, D. Bajoni, A. Miard, A. Lemaître, G. Malpuech, and J. Bloch, "Spontaneous formation of a polariton condensate in a planar GaAs microcavity", *Applied Physics Letters*, vol. **95**, pp. 3, (2009).

[68] S. Utsunomiya, L. Tian, G. Roumpos, C. W. Lai, N. Kumada, T. Fujisawa, M. Kuwata-Gonokami, A. Loffler, S. Hofling, A. Forchel, and Y. Yamamoto, "Observation of Bogoliubov excitations in exciton-polariton condensates", *Nature Physics*, vol. **4**, pp. 700, (2008).

[69] J. Kasprzak, D. D. Solnyshkov, R. André, L. S. Dang, and G. Malpuech, "Formation of an exciton polariton condensate: Thermodynamic versus kinetic regimes", *Physical Review Letters*, vol. **101**, pp. 146404, (2008).

[70] M. H. Szymańska, J. Keeling, and P. B. Littlewood, "Nonequilibrium quantum condensation in an incoherently pumped dissipative system", *Physical Review Letters*, vol. **96**, pp. 230602, (2006).

[71] A. Kavokin, G. Malpuech, and F. P. Laussy, "Polariton laser and polariton superfluidity in microcavities", *Physics Letters A*, vol. **306**, pp. 187, (2003).

[72] G. Malpuech, Y. G. Rubo, F. P. Laussy, P. Bigenwald, and A. V. Kavokin, "Polariton laser: thermodynamics and quantum kinetic theory", *Semiconductor Science and Technology*, vol. **18**, pp. S395, (2003).

[73] F. M. Marchetti, J. Keeling, M. H. Szymańska, and P. B. Littlewood, "Thermodynamics and excitations of condensed polaritons in disordered microcavities", *Physical Review Letters*, vol. **96**, pp. 066405, (2006).

[74] M. Wouters and I. Carusotto, "Excitations in a nonequilibrium Bose-Einstein condensate of exciton polaritons", *Physical Review Letters*, vol. **99**, pp. 140402, (2007).

[75] G. Malpuech, D. D. Solnyshkov, H. Ouerdane, M. M. Glazov, and I. Shelykh, "Bose glass and superfluid phases of cavity polaritons", *Physical Review Letters*, vol. **98**, pp. 206402, (2007).

[76] A. Amo, D. Sanvitto, F. P. Laussy, D. Ballarini, E. d. Valle, M. D. Martin, A. Lemaître, J. Bloch, D. N. Krizhanovskii, M. S. Skolnick, C. Tejedor, and L. Vina, "Collective fluid dynamics of a polariton condensate in a semiconductor microcavity", *Nature*, vol. **457**, pp. 291, (2009).

[77] A. Amo, D. Sanvitto, and L. Vina, "Collective dynamics of excitons and polaritons in semiconductor nanostructures", *Semiconductor Science and Technology*, vol. **25**, pp. 043001, (2010).

[78] D. Sanvitto, A. Amo, F. P. Laussy, A. Lemaître, J. Bloch, C. Tejedor, and L. Vina, "Polariton condensates put in motion", *Nanotechnology*, vol. **21**, pp. 134025, (2010).

[79] M. Wouters and V. Savona, "Superfluidity of a nonequilibrium Bose-Einstein condensate of polaritons", *Physical Review B*, vol. **81**, pp. 054508, (2010).

[80] K. G. Lagoudakis, M. Wouters, M. Richard, A. Baas, I. Carusotto, R. André, L. Dang, and B. Deveaud-Pledran, "Quantized vortices in an exciton-polariton condensate", *Nature Physics*, vol. **4**, pp. 706, (2008).

[81] D. Sanvitto, F. M. Marchetti, M. H. Szymańska, G. Tosi, M. Baudisch, F. P. Laussy, D. N. Krizhanovskii, M. S. Skolnick, L. Marrucci, A. Lemaître, J. Bloch, C. Tejedor, and L. Vina, "Persistent currents and quantized vortices in a polariton superfluid", *Nature Physics*, vol. **advance online publication**, (2010).

[82] H. Flayac, I. A. Shelykh, D. D. Solnyshkov, and G. Malpuech, "Topological stability of the half-vortices in spinor exciton-polariton condensates", *Physical Review B*, vol. **81**, pp. 045318, (2010).

[83] Y. G. Rubo, "Half vortices in exciton polariton condensates", *Physical Review Letters*, vol. **99**, pp. 106401, (2007).

[84] F. P. Laussy, A. V. Kavokin, and I. A. Shelykh, "Exciton-polariton mediated superconductivity", *Physical Review Letters*, vol. **104**, pp. 106402, (2010).

[85] S. Christopoulos, G. B. H. Vön Högersthal, A. J. D. Grundy, P. G. Lagoudakis, A. V. Kavokin, J. J. Baumberg, G. Christmann, R. Butté, E. Feltin, J. F. Carlin, and N. Grandjean, "Room-temperature polariton lasing in semiconductor microcavities", *Physical Review Letters*, vol. **98**, pp. 126405, (2007).

[86] J. J. Baumberg, A. V. Kavokin, S. Christopoulos, A. J. D. Grundy, R. Butté, G. Christmann, D. D. Solnyshkov, G. Malpuech, G. Baldassarri Höger von Högersthal, E. Feltin, J. F. Carlin, and N. Grandjean, "Spontaneous polarization buildup in a room-temperature polariton laser", *Physical Review Letters*, vol. **101**, pp. 136409, (2008).

[87] D. Bajoni, P. Senellart, E. Wertz, I. Sagnes, A. Miard, A. Lematre, and J. Bloch, "Polariton laser using single micropillar GaAs-GaAlAs semiconductor cavities", *Physical Review Letters*, vol. **100**, pp. 047401, (2008).

[88] L. V. Butov, "Solid-state physics: A polariton laser", *Nature*, vol. **447**, pp. 540, (2007).

[89] F. P. Laussy, G. Malpuech, A. Kavokin, and P. Bigenwald, "Spontaneous coherence buildup in a polariton laser", *Physical Review Letters*, vol. **93**, pp. 016402, (2004).

[90] T. D. Doan, H. T. Cao, D. B. T. Thoai, and H. Haug, "Coherence of condensed microcavity polaritons calculated within Boltzmann-Master equations", *Physical Review B*, vol. **78**, pp. 205306, (2008).

[91] M. Wouters and V. Savona, "Stochastic classical field model for polariton condensates", *Physical Review B*, vol. **79**, pp. 165302, (2009).

[92] B. D. Josephson, "The discovery of tunnelling supercurrents", *Reviews of Modern Physics*, vol. **46**, pp. 251, (1974).

[93] D. D. Solnyshkov, R. Johne, I. A. Shelykh, and G. Malpuech, "Chaotic Josephson oscillations of exciton-polaritons and their applications", *Physical Review B*, vol. **80**, pp. 235303, (2009).

[94] D. N. Krizhanovskii, D. Sanvitto, I. A. Shelykh, M. M. Glazov, G. Malpuech, D. D. Solnyshkov, A. Kavokin, S. Ceccarelli, M. S. Skolnick, and J. S. Roberts, "Rotation of the plane of polarization of light in a semiconductor microcavity", *Physical Review B*, vol. **73**, pp. 73303, (2006).

[95] E. L. Ivchenko, *Optical Spectroscopy of Semiconductor Nanostructures*, Alpha Science, England, (2005).

[96] M. M. Glazov, H. Ouerdane, L. Pilozzi, G. Malpuech, A. V. Kavokin, and A. D'Andrea, "Polariton-polariton scattering in microcavities: A microscopic theory", *Physical Review B*, vol. **80**, pp. 155306, (2009).

[97] R. J. Elliott, "Theory of the effect of spin-orbit coupling on magnetic resonance in some semiconductors", *Physical Review*, vol. **96**, pp. 266, (1954).

[98] M. I. Dyakonov and V. I. Perel, "Current-induced spin orientation of electrons in semiconductors", *Physics Letters A*, vol. **35**, pp. 459, (1971).

[99] G. Dresselhaus, "Spin-orbit coupling effects in zinc blende structures", *Physical Review*, vol. **100**, pp. 580, (1955).

[100] M. Z. Maialle, E. A. de Andrada e Silva, and L. J. Sham, "Exciton spin dynamics in quantum wells", *Physical Review B*, vol. **47**, pp. 15776, (1993).

[101] R. I. Dzhioev, H. M. Gibbs, E. L. Ivchenko, G. Khitrova, V. L. Korenev, M. N. Tkachuk, and B. P. Zakharchenya, "Determination of interface preference by observation of linear-to-circular polarization conversion under optical orientation of excitons in type-II GaAs/AlAs superlattices", *Physical Review B*, vol. **56**, pp. 13405, (1997).

[102] K. V. Kavokin, I. A. Shelykh, A. V. Kavokin, G. Malpuech, and P. Bigenwald, "Quantum theory of spin dynamics of exciton-polaritons in microcavities", *Physical Review Letters*, vol. **92**, pp. 017401, (2004).

[103] M. Combescot and O. Betbeder-Matibet, "Many-body effects between unbosonized excitons", *Solid State Communications*, vol. **134**, pp. 11, (2005).

[104] M. Combescot, O. Betbeder-Matibet, and R. Combescot, "Exciton-exciton scattering: composite boson versus elementary boson", *Physical Review B*, vol. **75**, pp. 174305, (2007).

[105] M. Combescot, M. A. Dupertuis, and O. Betbeder-Matibet, "Polariton-polariton scattering: Exact results through a novel approach", *Europhysics Letters*, vol. **79**, pp. 17001, (2007).

[106] T. Ostatnicky, D. Read, and A. V. Kavokin, "Polarization and depolarization in scattering of cavity polaritons", *Physical Review B*, vol. **80**, pp. 115328, (2009).

[107] C. Ciuti, P. Schwendimann, B. Deveaud, and A. Quattropani, "Theory of the angle-resonant polariton amplifier", *Physical Review B*, vol. **62**, pp. R4825, (2000).

[108] C. Diederichs, J. Tignon, G. Dasbach, C. Ciuti, A. Lemaître, J. Bloch, P. Roussignol, and C. Delalande, "Parametric oscillation in vertical triple microcavities", *Nature*, vol. **440**, pp. 904, (2006).

[109] W. Langbein and J. M. Hvam, "Elastic scattering dynamics of cavity polaritons: evidence for time-energy uncertainty and polariton localization", *Physical Review Letters*, vol. **88**, pp. 047401, (2002).

[110] M. Romanelli, C. Leyder, J. P. Karr, E. Giacobino, and A. Bramati, "Four wave mixing oscillation in a semiconductor microcavity: Generation of two correlated polariton populations", *Physical Review Letters*, vol. **98**, pp. 106401, (2007).

[111] C. Leyder, T. C. H. Liew, A. V. Kavokin, I. A. Shelykh, M. Romanelli, J. P. Karr, E. Giacobino, and A. Bramati, "Interference of coherent polariton beams in microcavities: Polarization-controlled optical gates", *Physical Review Letters*, vol. **99**, pp. 196402, (2007).

[112] C. Ciuti, V. Savona, C. Piermarocchi, A. Quattropani, and P. Schwendimann, "Role of the exchange of carriers in elastic exciton-exciton scattering in quantum wells", *Physical Review B*, vol. **58**, pp. 7926, (1998).

[113] M. Combescot, O. Betbeder-Matibet, and F. Dubin, "The many-body physics of composite bosons", *Physics Reports*, vol. **463**, pp. 215, (2008).

[114] S. Okumura and T. Ogawa, "Boson representation of two-exciton correlations: An exact treatment of composite-particle effects", *Physical Review B*, vol. **65**, pp. 035105, (2001).

[115] C. Schindler and R. Zimmermann, "Analysis of the exciton-exciton interaction in semiconductor quantum wells", *Physical Review B*, vol. **78**, pp. 045313, (2008).

[116] I. A. Shelykh, R. Johne, D. D. Solnyshkov, A. V. Kavokin, N. A. Gippius, and G. Malpuech, "Quantum kinetic equations for interacting bosons and their application for polariton parametric oscillators", *Physical Review B*, vol. **76**, pp. 155308, (2007).

[117] J. Kasprzak, R. André, L. S. Dang, I. A. Shelykh, A. V. Kavokin, Y. G. Rubo, K. V. Kavokin, and G. Malpuech, "Build up and pinning of linear polarization in the Bose condensates of exciton polaritons", *Physical Review B*, vol. **75**, pp. 5, (2007).

[118] S. Schumacher, N. H. Kwong, and R. Binder, "Influence of exciton-exciton correlations on the polarization characteristics of polariton amplification in semiconductor microcavities", *Physical Review B*, vol. **76**, pp. 245324, (2007).

[119] P. Renucci, T. Amand, X. Marie, P. Senellart, J. Bloch, B. Sermage, and K. V. Kavokin, "Microcavity polariton spin quantum beats without a magnetic field: A manifestation of Coulomb exchange in dense and polarized polariton systems", *Physical Review B*, vol. **72**, pp. 075317, (2005).

[120] A. Kavokin, G. Malpuech, and M. Glazov, "Optical spin Hall effect", *Physical Review Letters*, vol. **95**, pp. 136601, (2005).

[121] C. Leyder, M. Romanelli, J. P. Karr, E. Giacobino, T. C. H. Liew, M. M. Glazov, A. V. Kavokin, G. Malpuech, and A. Bramati, "Observation of the optical spin Hall effect", *Nature Physics*, vol. **3**, pp. 628, (2007).

[122] J. Kasprzak, M. Richard, A. Baas, B. Deveaud, R. André, J. P. Poizat, and L. S. Dang, "Second-order time correlations within a polariton Bose-Einstein condensate in a CdTe microcavity", *Physical Review Letters*, vol. **100**, pp. 067402, (2008).

[123] E. M. Lifshitz and L. P. Pitaevskii, *Statistical Physics, Part 2*, Pergamon Press, New York, (1980).

[124] O. Penrose and L. Onsager, "Bose-Einstein condensation and liquid helium", *Physical Review*, vol. **104**, pp. 576, (1956).

[125] H. Deng, G. Weihs, C. Santori, J. Bloch, and Y. Yamamoto, "Condensation of semiconductor microcavity exciton polaritons", *Science*, vol. **298**, pp. 199, (2002).

[126] F. P. Laussy, I. A. Shelykh, G. Malpuech, and A. Kavokin, "Effects of Bose-Einstein condensation of exciton polaritons in microcavities on the polarization of emitted light", *Physical Review B*, vol. **73**, pp. 35315, (2006).

[127] I. A. Shelykh, Y. G. Rubo, G. Malpuech, D. D. Solnyshkov, and A. Kavokin, "Polarization and propagation of polariton condensates", *Physical Review Letters*, vol. **97**, pp. 066402, (2006).

[128] D. Bajoni, E. Peter, P. Senellart, J. L. Smirr, I. Sagnes, A. Lemaître, and J. Bloch, "Polariton parametric luminescence in a single micropillar", *Applied Physics Letters*, vol. **90**, pp. 051107, (2007).

[129] D. N. Krizhanovskii, D. Sanvitto, A. P. D. Love, M. S. Skolnick, D. M. Whittaker, and J. S. Roberts, "Dominant effect of polariton-polariton

interactions on the coherence of the microcavity optical parametric oscillator", *Physical Review Letters*, vol. **97**, pp. 097402, (2006).

[130] D. Sanvitto, D. N. Krizhanovskii, D. M. Whittaker, S. Ceccarelli, M. S. Skolnick, and J. S. Roberts, "Spatial structure and stability of the macroscopically occupied polariton state in the microcavity optical parametric oscillator", *Physical Review B*, vol. **73**, pp. 241308, (2006).

[131] G. Malpuech, A. Kavokin, A. Di Carlo, and J. J. Baumberg, "Polariton lasing by exciton-electron scattering in semiconductor microcavities", *Physical Review B*, vol. **65**, pp. 153310, (2002).

[132] I. Carusotto and C. Ciuti, "Probing microcavity polariton superfluidity through resonant Rayleigh scattering", *Physical Review Letters*, vol. **93**, pp. 166401, (2004).

[133] T. C. H. Liew and I. A. Shelykh, "Polarization phenomena in resonantly pumped disordered semiconductor microcavities", *Physical Review B*, vol. **80**, pp. 161303, (2009).

[134] T. C. H. Liew, A. V. Kavokin, and I. A. Shelykh, "Optical circuits based on polariton neurons in semiconductor microcavities", *Physical Review Letters*, vol. **101**, pp. 016402, (2008).

[135] I. Shelykh, K. V. Kavokin, A. V. Kavokin, G. Malpuech, P. Bigenwald, H. Deng, G. Weihs, and Y. Yamamoto, "Semiconductor microcavity as a spin-dependent optoelectronic device", *Physical Review B*, vol. **70**, pp. 35320, (2004).

[136] D. Porras and C. Tejedor, "Linewidth of a polariton laser: Theoretical analysis of self-interaction effects", *Physical Review B*, vol. **67**, pp. 161310, (2003).

[137] Y. G. Rubo, F. P. Laussy, G. Malpuech, A. Kavokin, and P. Bigenwald, "Dynamical theory of polariton amplifiers", *Physical Review Letters*, vol. **91**, pp. 156403, (2003).

[138] Y. G. Rubo, "Kinetics of the polariton condensate formation in a microcavity", *Physica Status Solidi A*, vol. **201**, pp. 641, (2004).

[139] L. Mandel and E. Wolf, *Optical Coherence and Quantum Optics*, Cambridge University press, Cambridge, (1995).

[140] N. G. van Kampen, *Stochastic Processes in physics and chemistry*, North-Holland, Amsterdam, (2007).

[141] D. R. Kincaid and E. W. Cheney, *Numerical Analysis*, Brooks Cole, (1991).

[142] A. P. D. Love, D. N. Krizhanovskii, D. M. Whittaker, R. Bouchekioua, D. Sanvitto, S. A. Rizeiqi, R. Bradley, M. S. Skolnick, P. R. Eastham, R. André, and L. S. Dang, "Intrinsic decoherence mechanisms in the microcavity polariton condensate", *Physical Review Letters*, vol. **101**, pp. 067404, (2008).

[143] P. C. Hohenberg and B. I. Halperin, "Theory of dynamic critical phenomena", *Reviews of Modern Physics*, vol. **49**, pp. 435, (1977).

[144] G. Christmann, R. Butté, E. Feltin, A. Mouti, P. A. Stadelmann, A. Castiglia, J.-F. Carlin, and N. Grandjean, "Large vacuum Rabi splitting in a multiple quantum well GaN-based microcavity in the strong-coupling regime", *Physical Review B*, vol. **77**, pp. 085310, (2008).

[145] G. Christmann, R. Butté, E. Feltin, J.-F. Carlin, and N. Grandjean, "Room temperature polariton lasing in a GaN/AlGaN multiple quantum well microcavity", *Applied Physics Letters*, vol. **93**, pp. 051102, (2008).

[146] F. Tassone, C. Piermarocchi, V. Savona, A. Quattropani, and P. Schwendimann, "Bottleneck effects in the relaxation and photoluminescence of microcavity polaritons", *Physical Review B*, vol. **56**, pp. 7554, (1997).

[147] R. Butté, J. Levrat, G. Christmann, E. Feltin, J. F. Carlin, and N. Grandjean, "Phase diagram of a polariton laser from cryogenic to room temperature", *Physical Review B*, vol. **80**, pp. 233301, (2009).

[148] J. Levrat, R. Butté, E. Feltin, J.-F. Carlin, N. Grandjean, D. Solnyshkov, and G. Malpuech, "Condensation phase diagram of cavity polaritons in GaN-based microcavities: Experiment and theory", *Physical Review B*, vol. **81**, pp. 125305, (2010).

[149] D. Sarchi and V. Savona, "Long-range order in the Bose-Einstein condensation of polaritons", *Physical Review B*, vol. **75**, pp. 115326, (2007).

[150] B. D. Josephson, "Possible new effects in superconductive tunnelling", *Physics Letters*, vol. **1**, pp. 251, (1962).

[151] J. M. Rowell, P. W. Anderson, and D. E. Thomas, "Image of the phonon spectrum in the tunneling characteristic between superconductors", *Physical Review Letters*, vol. **10**, pp. 334, (1963).

[152] D. Read, Y. G. Rubo, and A. V. Kavokin, "Josephson coupling of Bose-Einstein condensates of exciton-polaritons in semiconductor microcavities", *Physical Review B*, vol. **81**, pp. 235315, (2010).

[153] I. Giaever, "Energy gap in superconductors measured by electron tunneling", *Physical Review Letters*, vol. **5**, pp. 147, (1960).

[154] P. W. Anderson, "More is different", *Science*, vol. **177**, pp. 393, (1972).

[155] P. W. Anderson and J. M. Rowell, "Probable observation of the Josephson superconducting tunneling effect", *Physical Review Letters*, vol. **10**, pp. 230, (1963).

[156] S. V. Pereverzev, A. Loshak, S. Backhaus, J. C. Davis, and R. E. Packard, "Quantum oscillations between two weakly coupled reservoirs of superfluid 3He", *Nature*, vol. **388**, pp. 449, (1997).

[157] M. Albiez, R. Gati, J. Flling, S. Hunsmann, M. Cristiani, and M. Oberthaler, "Direct observation of tunneling and nonlinear self-trapping in a single bosonic Josephson junction", *Physical Review Letters*, vol. **95**, pp. 010402, (2005).

[158] E. C. G. Sudarshan, "Equivalence of semiclassical and quantum mechanical descriptions of statistical light beams", *Physical Review Letters*, vol. **10**, pp. 277, (1963).